DUAL-BAND REFLECTARRAYS USING MICROSTRIP RING ELEMENTS AND THEIR APPLICATIONS WITH VARIOUS FEEDING ARRANGEMENTS

A Dissertation

by

CHUL MIN HAN

Submitted to the Office of Graduate Studies of
Texas A&M University
in partial fulfillment of the requirements for the degree of

DOCTOR OF PHILOSOPHY

August 2006

Major Subject: Electrical Engineering

DUAL-BAND REFLECTARRAYS USING MICROSTRIP RING ELEMENTS AND THEIR APPLICATIONS WITH VARIOUS FEEDING ARRANGEMENTS

A Dissertation

by

CHUL MIN HAN

Submitted to the Office of Graduate Studies of
Texas A&M University
in partial fulfillment of the requirements for the degree of

DOCTOR OF PHILOSOPHY

Approved by:

Chair of Committee,	Kai Chang
Committee Members,	Robert D. Nevels
	Chin B. Su
	Thomas Wilheit
Head of Department,	Costas N. Georgiades

August 2006

Major Subject: Electrical Engineering

ABSTRACT

Dual-Band Reflectarrays Using Microstrip Ring Elements and Their Applications with Various Feeding Arrangements. (August 2006)

Chul Min Han, B.S., Korea University

Chair of Advisory Committee: Dr. Kai Chang

In recent years there has been a growing demand for reduced mass, small launch volume, and, at the same time, high-gain large-aperture antenna systems in modern space-borne applications. This dissertation introduces new techniques for dual-band reflectarray antennas to meet these requirements. A series of developments is presented to show the dual-band capability of the reflectarray.

A novel microstrip ring structure has been developed to achieve circular polarization (CP). A C/Ka dual-band front-fed reflectarray antenna has been designed to demonstrate the dual-band circular polarized operation. The proposed ring structure provides many advantages of compact size, more freedom in the selection of element spacing, less blockage between circuit layers, and broader CP bandwidth as compared to the patches.

An X/Ka dual-band offset-fed reflectarray is made of thin membranes, with their thickness equal to 0.0508 mm in both layers. Several degrading effects of thin substrates are discussed. To overcome these problems, a new configuration is developed by inserting empty spaces of the proper thickness below both the X and Ka band membranes. More than 50 % efficiencies are achieved at both frequency ranges, and the

proposed scheme is expected to be a good candidate to meet the demand for future inflatable antenna systems.

An X/Ka dual-band microstrip reflectarray with circular polarization has also been constructed using thin membranes and a Cassegrain offset-fed configuration. It is believed that this is the first Cassegrain reflectarray ever developed. This antenna has a 0.75-meter-diameter aperture and uses a metallic sub-reflector and angular-rotated annular ring elements. It achieved a measured 3 dB gain bandwidth of 700 MHz at X-band and 1.5 GHz at Ka-band, as well as a CP bandwidth (3 dB axial ratio) of more than 700 MHz at X-band and more than 2 GHz at Ka-band. The measured peak efficiencies are 49.8 % at X-band and 48. 2 % at Ka-band.

In summary, this dissertation presents a series of new research developments to support the dual-band operation of the reflectarray antenna. The results of this work are currently being implemented onto a 3-meter reflectarray with inflatable structures at the Jet Propulsion Laboratory and are planned for other applications such as an 8-meter inflatable reflectarray in the near future.

To my wife Yongsuk,
whose encouragement, love, and support have made all of this possible.

ACKNOWLEDGMENTS

Thank you, Lord for the blessings you have given me. Your mercy and love is with me guiding my life. Thank you for everything you have done.

I would like to express my deepest gratitude to Dr. Kai Chang for his support and guidance throughout my graduate studies and research at Texas A&M University. I also appreciate Dr. Robert D. Nevels, Dr. Chin B. Su, Dr. Thomas Wilheit and Dr. Ugur Cilingiroglu for serving as members on my dissertation committee and for their helpful comments.

I would like to thank Mr. Ming-yi Li for his technical assistance. I gratefully acknowledge all my friends and members of the Electromagnetics and Microwave Laboratory for their technical assistance, incentives and valuable discussions. I would also like to give special thanks to Dr. John Huang at the Jet Propulsion Laboratory for his support of my research and helpful comments.

I would like to thank my parents and all my brothers and sisters for their constant love, encouragement, and support. I also thank my two sons, Seulchan and Gaon, for their love. Finally, my sincere thanks are given to my lovely wife, Yongsuk, for all her patience, love, and support during my graduate studies.

TABLE OF CONTENTS

Page

CHAPTER Page

LIST OF FIGURES

FIGURE Page

FIGURE Page

FIGURE Page

FIGURE Page

FIGURE Page

LIST OF TABLES

TABLE Page

CHAPTER I

INTRODUCTION

The conventional high-gain antenna most often used is a reflector antenna [1]. It has been widely used for decades in radars, telecommunications, direct broadcast, radio astronomy, and deep-space explorations. The reflector antenna shown in Figure 1 is simple in geometry and mature in design methodology. It features high-gain characteristic over wide frequency ranges and can accommodate high levels of power. However, the reflector antenna has a curved structure leading to manufacturing difficulty. It is heavy and its bulky size makes it occupy more space than a planar antenna. Without the mechanical movement, the main beam has only limited scan angle.

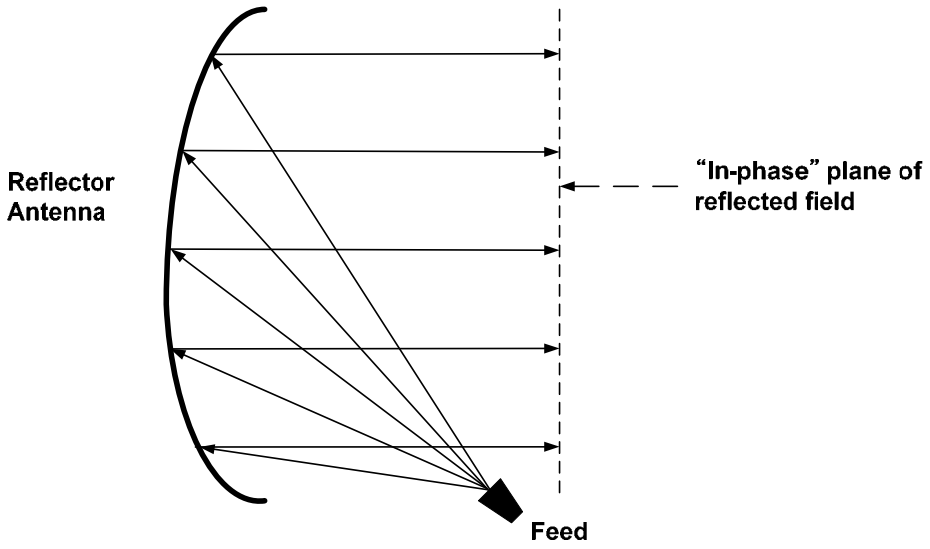

Fig. 1. Reflector antenna with an offset feed configuration.

The journal model for this dissertation is *IEEE Transactions on Antennas and Propagations*.

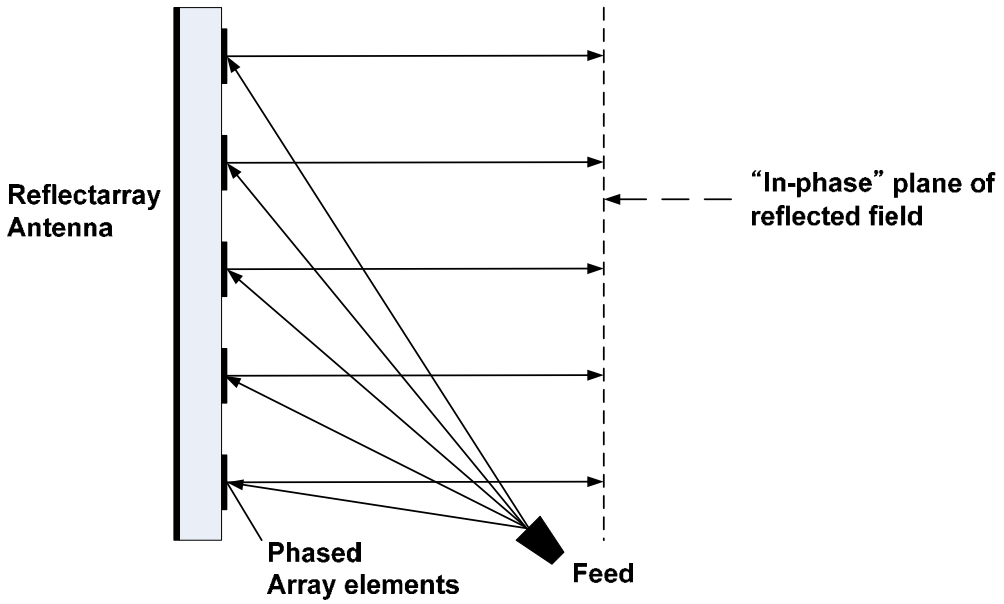

Fig. 2. A reflectarray antenna.

As an alternative, a flat reflector called a microstrip reflectarray [2-20] has emerged as a future candidate for high-gain antenna. A reflectarray antenna consists of a flat reflecting surface and a illuminating feed as shown in Figure 2. A large reflectarray antenna is made of thousands of antenna elements printed on a flat surface and illuminated by a feed horn located above this surface. It is a low-cost, low profile high gain antennas with the beam scanning capability of a phased array antenna if it is integrated with solid-state control devices. Because the feed horn illuminates many isolated microstrip array elements on a thin reflecting surface eliminating the use of the conventional transmission feeding lines, it also features low insertion loss of the parabolic reflector.

The key feature of a reflectarray antenna design is the adjustment of the reflected phase of the microstrip array elements. When a plane wave from a transmitter reaches the flat reflectarray aperture, the operation of a reflectarray antenna can be explained as collimating the incident plane wave into the feed horn by suitable phase variations across

the surface of the reflectarray.

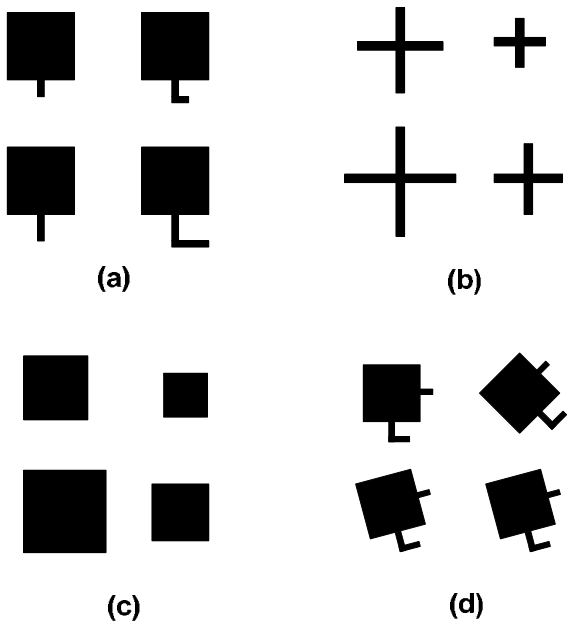

Fig. 3. Various reflectarray elements: (a) identical patches with different-length delay lines; (b) variable-size dipoles; (c) variable-size patches; (d) variable angular rotations [2].

As shown in Figure 3, there are several methods to achieve a planar phase front depending on the array element and the type of polarization. For a linearly polarized case, the most common approach is to use identical microstrip patches with different-length transmission delay lines attached to the patches for phase compensation [3-6]. Other approaches use different size of patches [7-12], dipoles or circular rings [13-14] to produce a cophasal far field beam. For a circularly polarized reflectarray, an efficient way of producing phase variations is to use variable angular rotations reported in 1998 by Huang and Pogorzelski [15] using identical patches with different delay lines.

The microstrip reflectarray has several applications due to its low-profile, small mass

characteristic [16]. The flat reflectarray can be surface-mounted on a building's side wall or rooftop as a Ku-band Direct Broadcast Satellite (DBS) antenna because it takes less space, or it can be mounted on the rooftop of a large vehicle for satellite reception. The reflectarray antenna can also be used in space application due to its flat reflecting surface. For space application, the reflectarray and the solar array panels can be combined into one large panel saving space efficiently. Another important application of the microstrip reflectarray is a Ka-band circularly polarized reflectarray for NASA's future spacecraft communication antenna application. For large-aperture spacecraft antenna applications, the reflectarray's flat surface allows the antenna to be constructed as an inflatable structure with relative ease in maintaining its surface tolerance in comparison to a curved parabolic surface.

With all the above characteristics, there is one distinct disadvantage associated with the reflectarray antenna and it is its inherent narrow bandwidth [17-18] due to different path lengths or the differential spatial phase delays. It is caused by the path length differences between the feed to the center elements and the feed to the edge elements. In other words, the phase change of these path length differences versus the change of frequency can be a large portion of a wavelength and thus cause performance degradation. This narrow bandwidth generally cannot exceed beyond ten percent depending on its element design, aperture size, focal length, etc.

While narrow in bandwidth, microstrip reflectarray antennas are well-suited for dual-frequency operation in a stacked configuration [19-20]. This dessertation introduces dual-band reflectarray antennas for future spacecraft antenna applications. A series of developments are presented to show the dual-band capability of the reflectarray with

different feeding arrangements. The dissertation consists of four major chapters.

Chapter II presents a novel microstrip ring structure developed to achieve circular polarization (CP) with excellent axial ratio [21-23]. The ring antenna element has a major advantage over patches in the case of multi-layer multi- frequency applications. It allows other non-resonant frequencies to pass through them with little blockage. It also has the advantages of compact size, more freedom in the selection of element spacing and broader CP bandwidth as compared to the patches. A front-fed 0.5 m dual layer dual frequency printed reflectarray has been realized with variable angular rotations to achieve far field phase coherence. The tested results show that the designed ring structure is suitable for both the single and dual layer applications with good efficiency and CP performance.

Chapter III presents an X/Ka dual-band offset-fed reflectarray. The reflectarray designed is made of thin membranes with their thickness equal to 0.0508 mm (2 mils) at both layers [24]. Several degrading effects of thin substrates are discussed. To overcome these problems, a new configuration is developed by inserting empty spaces of the proper thickness below both the X and Ka band membranes. A 0.5 m offset-fed X/Ka-band dual frequency reflectarray has been designed and tested. An offset feed scheme is applied to reduce relatively high sidelobes with main beam scanned off broadside. More than 50 % efficiencies are achieved at both frequency ranges and the proposed scheme is expected to be a good candidate to meet the demand in future inflatable antenna systems.

Chapter IV presents an X/Ka dual-band microstrip reflectarray with circular polarization using thin membranes and Cassegrain offset-fed configuration. It is believed that this is the first Cassegrain reflectarray ever been developed [25-26]. This antenna has a 0.75-meter-diameter aperture and uses metallic sub-reflector and angular-rotated annular

ring elements. Two 4 by 4 circularly polarized microstrip patch arrays are designed as feed networks at both the X-band and Ka-band in this study. The complete system achieved a measured 3 dB gain bandwidth of 700 MHz at X-band and 1.5 GHz at Ka-band, as well as a CP bandwidth (3 dB axial ratio) of more than 700 MHz at X-band and more than 2 GHz at Ka-band. The measured peak efficiencies are 49.8 % at X-band and 48. 2 % at Ka-band.

Chapter V summarizes the research accomplishments in this dissertation, and presents recommendations for further research.

CHAPTER II

FRONT-FED C/KA DUAL-BAND REFLECTARRAY ANTENNA*

1. Introduction

The major objective of this study is to accomplish analysis, design, and hardware development for a C/Ka dual-frequency shared aperture reflectarray antenna. This antenna technology is to be developed for the JPL/NASA Inter-Planetary Network & Information System Directorate (IPN-ISD) and is intended to enhance the capabilities of future deep-space spacecraft telecom high-gain antenna systems.

In this study, the novel microstrip ring structure has been developed for broadband performance combined with variable rotation to achieve the proper phasing between the elements. Ring antennas have a major advantage over patches in the case of multi-frequency reflectarrays. In multi-frequency reflectarrays, the rings allow other nonresonant frequencies to pass through between layers with little blockage. This is extremely important in the case where multi-frequency reflectarrays implement a stacked configuration. The ring antennas also have potential advantages of compact size and broader CP bandwidth as compared to the patches.

Some of the previous reflectarray work has achieved very good efficiency performance. In 1995, Chang and Huang developed a linearly polarized (LP) 0.75 m reflectarray using variable length delay line to obtain 70 % efficiency and a peak gain of 35

---

dB at *X*-band [8]. In 1995, Targonski and Pozar developed an LP 0.23 m reflectarray using variable patch sizes to achieve 31 % efficiency at 27 GHz [9]. This efficiency was lower due to difficulties in the patch fabrication tolerances at such high frequencies. In 1998, Huang and Pogorzelski developed a circularly polarized (CP) 0.5 m reflectarray using patches with variable rotations to obtain 69 % efficiency and 42.75 dB gain at 31.5 GHz [15]. This reflectarray is electrically the largest ever built. Using attached transmission lines differing by a quarter wavelength, [15] concluded that the desired reflected CP component is advanced or delayed in phase by 2ψ degrees due to the element rotation by ψ degrees, while eliminating the other unwanted CP component. Although [15] used two delay lines to achieve circular polarization, matching the line impedance to the input impedance of the square patch is not easy since the input impedance of the square patch is usually more than 200 ohm and it yields an extremely thin line width at Ka-band frequency causing high loss, and serious reliability and fabrication problems. Also, the footprint of open stub lengths can limit element spacing as each element is rotated.

In this study, the same angular rotation technique has been applied to simple ring structures with gaps to achieve circular polarization with superior axial ratio and broader bandwidth. Fundamentally, ring elements with gaps are capable of responding to the excitation of each of the two orthogonal component fields with a different phase response of 180^{o} degree in order to operate as a CP.

The photograph of the reflectarray is shown in Figure 4 with its dual layer topology shown in Figure 5. The reflectarray antenna is fabricated on Rogers Duroid 5870 substrate with ε_r = 2.33 and 0.508 mm thickness for both layers. Two different sized ring structures are arrayed in each layer with lower frequency operating on the top layer. The top layer is

placed 7 mm above the bottom layer with the aid of foam and its thickness is chosen to be less than 0.25 free space wavelengths at 7.1 GHz. The element spacing within each array is 0.5 free space wavelengths for both layers to give sufficient room between array elements so that the mutual coupling is minimized [27]. Counter-clockwise rotations are applied to the array elements to achieve the right-hand circular polarization for both layers.

Fig. 4. A photo of the reflectarray with microstrip rings of variable rotations and a CP feed horn.

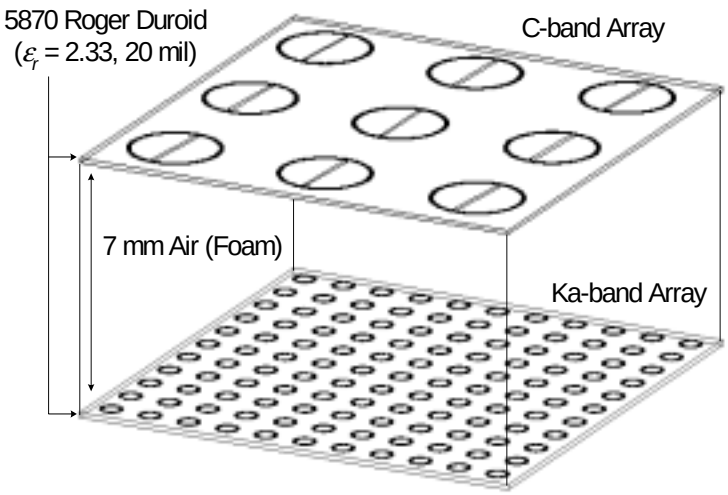

Fig. 5. Dual-band reflectarray topology.

2. Reflecting antenna array analysis

A. Principle of operation

For deep-space applications, microstrip reflectarrays must be capable of operation in both the E-plane and H-plane so that the signal received is independent of the orientation of the receiving antenna. Dual or circularly polarized reflectarrays are used in these cases. For a circularly polarized reflectarray, Huang and Pogorzelski [15] proposed the angular rotation technique to attain the phase delay needed so that a far field cophasal beam appears in a specified direction. The brief theory of rotation technique is reviewed here to help understand the principle of operation.

Let's consider the square patch with two open-circuit terminated delay lines as shown in Figure 6. Assuming the reflectarray is illuminated by a right CP wave propagating in the negative z direction, the incident wave may be expressed as

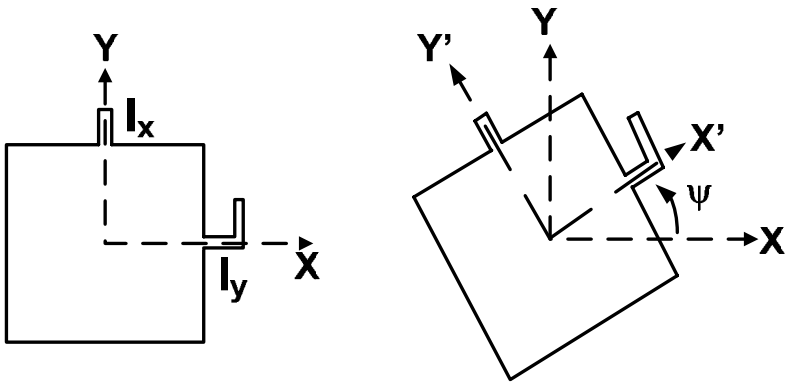

(a) (b)

Fig. 6. Circularly polarized patch element: (a) reference element with 0^o phase shift; (b) ψ degree rotated element with 2ψ degree phase shift.

$$\vec{E}^{inc} = (\hat{u}_x - j\hat{u}_y)ae^{-jkz}e^{-j\omega t} \quad (1)$$

Then, the reflected wave may be written as

$$\vec{E}^{ref} = (\hat{u}_x e^{2jkl_x} - j\hat{u}_y e^{2jkl_y})ae^{+jkz}e^{-j\omega t} \quad (2)$$

where the same signs arise from the reflection coefficients of +1 at the open-circuit terminations. "*a*" is the amplitude and no attenuation is assumed in the patch and transmission lines. When $l_x = l_y$, the reflected wave is a left CP wave upon reflection owing to the change of the direction of propagation. If one delay line is longer than the other by 90^o, for example when $kl_y = kl_x + \pi/2$, then the reflected wave will be

$$\vec{E}^{ref} = e^{2jkl_x}(\hat{u}_x + j\hat{u}_y)ae^{+jkz}e^{-j\omega t} \quad (3)$$

which is a right CP wave, the same as the incident wave. Now let the antenna element be rotated by ψ degree in the counter-clockwise direction to align with the axes of a new coordinate system. Then the excitation of the two orthogonal component fields can be determined by projecting the $\hat{u}_x$ and $\hat{u}_y$ field components onto the $\hat{u}_x'$ and $\hat{u}_y'$ axes at $z = 0$. That is

$$\vec{E}^{inc} = [(\hat{u}_x'\cos\psi - \hat{u}_y'\sin\psi) - j(\hat{u}_x'\sin\psi + \hat{u}_y'\cos\psi)]ae^{-jkz}e^{-j\omega t}$$

$$= (\hat{u}_x \, ' e^{-j\psi} - j\hat{u}_y \, ' e^{-j\psi}) a e^{-jkz} e^{-j\omega t} \quad (4)$$

The reflected wave now becomes

$$\vec{E}^{ref} = (\hat{u}_x \, ' e^{2jkl_x \, '} - j\hat{u}_y \, ' e^{2jkl_y \, '}) a e^{-j\psi} e^{+jkz} e^{-j\omega t} \quad (5)$$

Finally re-expressing above reflected fields in terms of the original *x* and *y* field components yields

$$\vec{E}^{ref} = \frac{1}{2}[(e^{2jkl_x} - e^{2jkl_y})(\hat{u}_x + j\hat{u}_y) e^{-2j\psi} + (e^{2jkl_x} + e^{2jkl_y})(\hat{u}_x - j\hat{u}_y)] a e^{+jkz} e^{-j\omega t} \quad (6)$$

Note that the reflected wave has both left and right CP components, and only the right CP component is dependent upon the angular rotation angle of the element. By choosing the transmission lines to differ by a quarter wavelength, the left CP component is eliminated and the right CP component becomes

$$\vec{E}^{ref} = (\hat{u}_x + j\hat{u}_y) e^{-2j\psi} a e^{+jkz} e^{-j\omega t} \quad (7)$$

Thus the reflected right CP component is advanced in phase by 2ψ degrees due to the element rotation by ψ degrees in the counter-clockwise direction. If a left CP incident wave illuminates the reflectarray, the reflected left CP component experiences a phase delay of 2ψ due to the counter-clockwise element rotation.

The above circumstance for a square patch with lines differing by a quarter wavelength can further be generalized to an arbitrary shape satisfying a corresponding condition for a circular polarization. Fundamentally, the antenna element must be able to respond to the excitation of each of the two orthogonal component fields with a different phase response of 180^{o} degree.

B. Phase requirement of array elements

The analysis presented here is derived by comparing the configurations of a parabolic reflector and a flat microstrip reflectarray. It is known from geometrical optics that if a beam of parallel rays is incident upon a parabolic reflector, the radiation will converge at a spot which is known as the focal point. Figure 7 shows the block diagram of a flat reflectarray with its virtual parabolic surface. In Figure 7, an incident plane wave strikes the parabolic reflector's metal surface and bounces to a focal point a distance f above the center of the parabolic reflector. A feed horn is generally placed at the focal point to transmit and collect the energy.

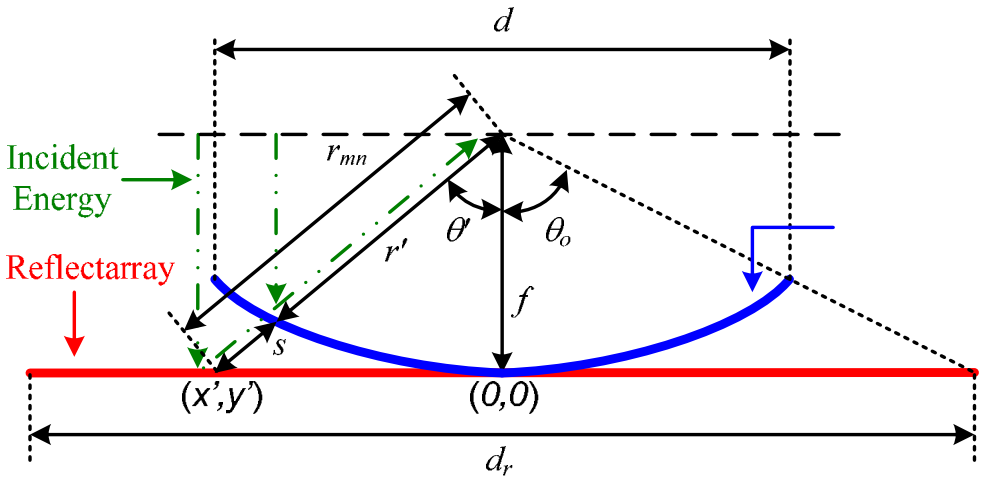

Fig. 7. Center fed reflectarray block diagram.

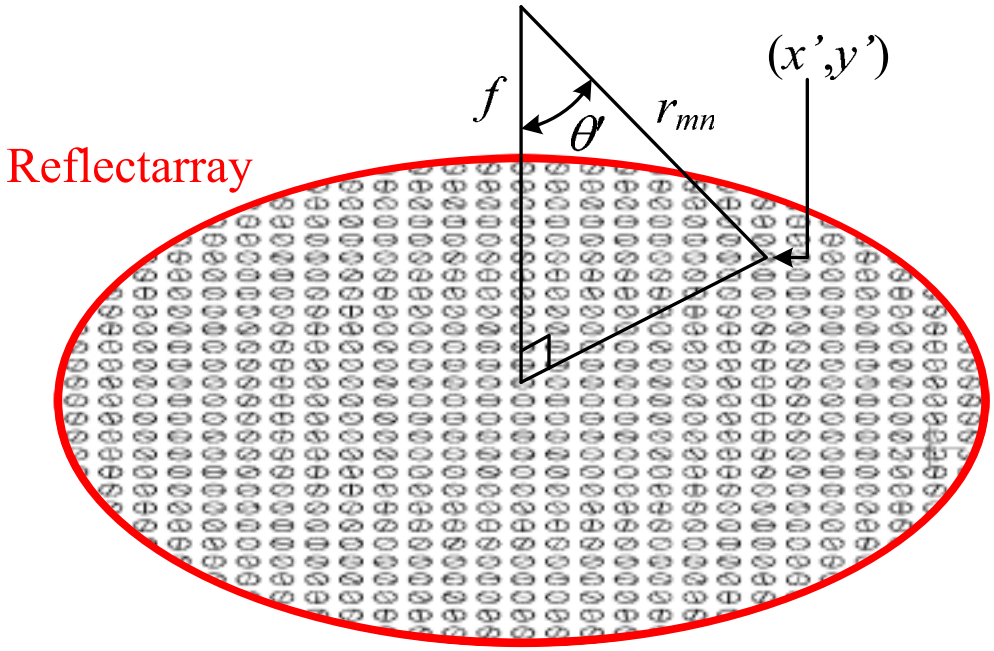

Fig. 8 Element location and rotation.

Referring to Figure 7 and specifying the reflector's dimension *d*, the largest angle from the center of the parabolic reflector to its edge is [28]

$$\theta_o = \tan^{-1}\left(\frac{\left|0.5\frac{f}{d}\right|}{\left(\frac{f}{d}\right)^2 - \frac{1}{16}}\right) \tag{8}$$

From Equation (8), the diameter of the reflectarray can be determined by

$$d_r = 2f\tan(\theta_o) \tag{9}$$

The reflectarray shown in Figure 8 uses a flat panel of microstrip ring antennas to

focus the energy. Each ring antenna in the reflectarray is located at a position (*x'*,*y'*) from the center of the array (0,0). The distance between the focal point and any antenna element is denoted as r_{mn}. The angle θ' is the angle between the path connecting the focal point and the array's center and the path connecting the focal point and the antenna element. It is defined as

$$\theta' = \tan^{-1}\left(\frac{\sqrt{x'^2 + y'^2}}{f}\right) \tag{10}$$

The distance from the focal point to any point on the surface of the parabolic reflector is [28]

$$r' = \frac{2f}{1+\cos\theta'} \tag{11}$$

For any angle θ', the ray trace from the reference plane to the reflectarray to the focal point is ($s + s\cos\theta$') longer than the corresponding ray trace from the reference plane to the parabolic dish to the focal point. This additional path length must be accounted for in the reflecting antenna array's design in order to create a parabolic phase front across the array's surface. This path length in radians is

$$\Delta l = \frac{2\pi f_o}{c}\left(s + s\cos\theta'\right) \tag{12}$$

where f_o is the resonant frequency of the array and c is the speed of light. The distance s is equal to

$$s = \frac{f}{\cos\theta'} - r' \tag{13}$$

To compensate for the additional Δl path lengths, the CP antenna arrays are rotated. The centermost element has zero rotation since Δl is zero at (0,0). As the elements are placed moving away from (0,0), the variable rotation increases as shown in Figure 9. The variable rotation ψ in radians for a circularly polarized radiator that is necessary to compensate for Δl is

$$\psi = \frac{\Delta l}{2} \times \frac{2\pi}{\lambda_o} \tag{14}$$

degrees in the counterclockwise direction to compensate for these additional path delays. The MATLAB code to evaluate the required rotation angles is attached in Appendix A.

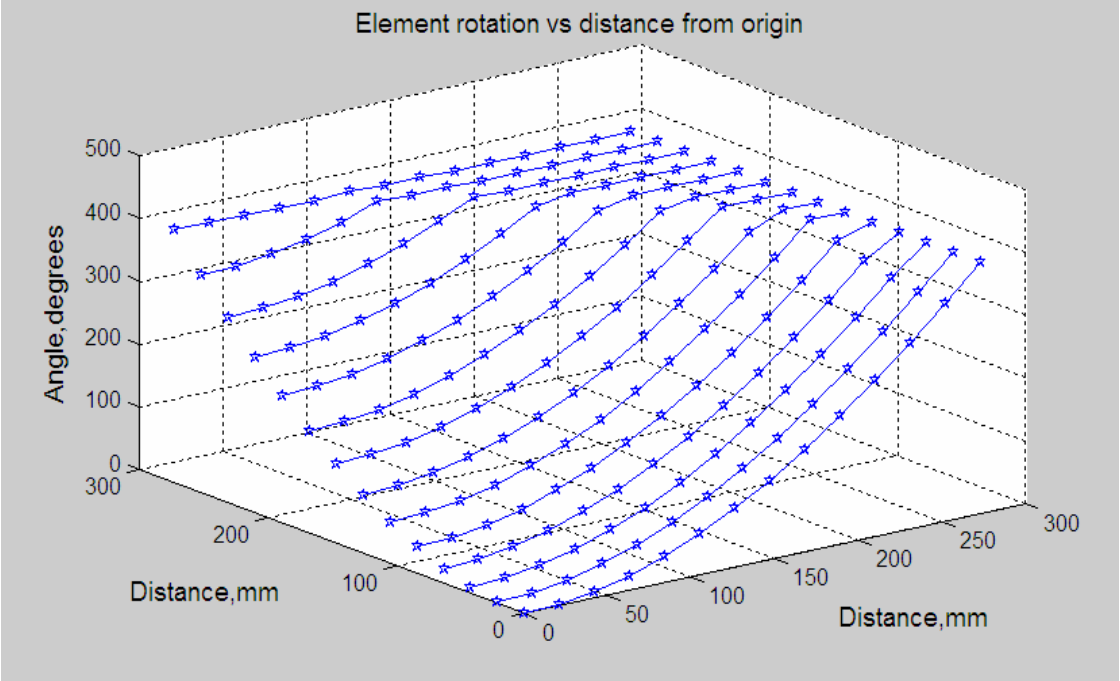

(a)

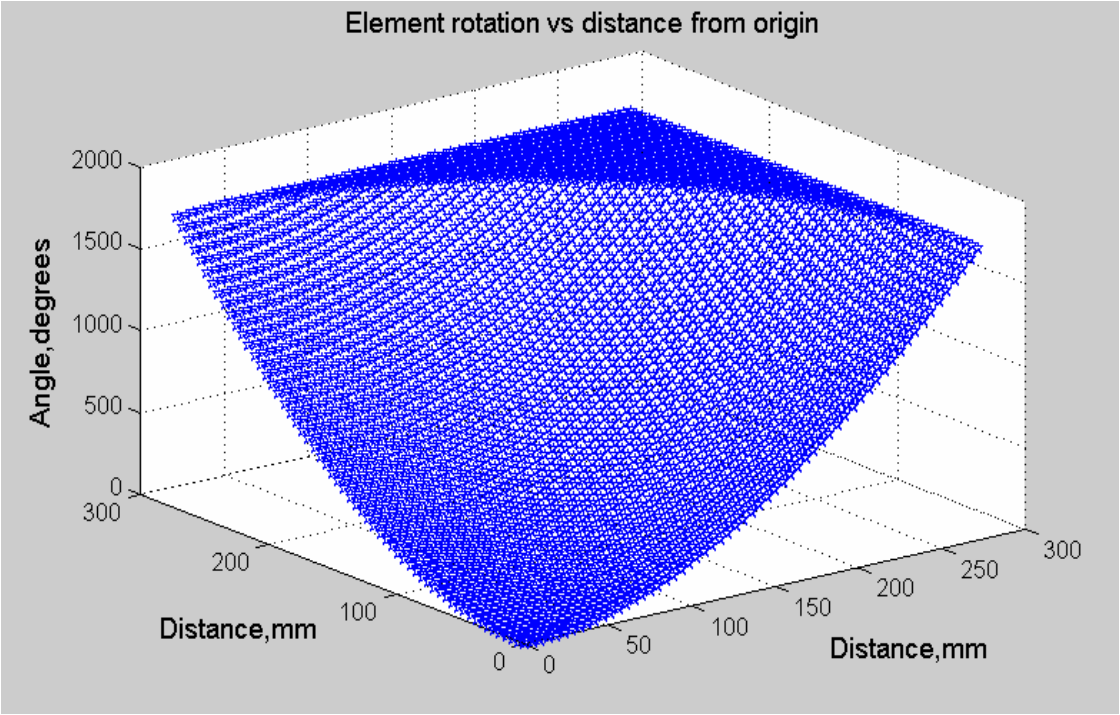

(b)

Fig. 9. Required rotation angles simulated in Matlab: (a) C-band; (b) Ka-band.

3. Circularly polarized antenna element design

A. Element design

Many different microstrip element shapes have been simulated with the aid of Zeland's IE3D and Ansoft's HFSS simulator to achieve circular polarization. Although the microstrip patch element with two delay lines is a good candidate for a CP operation, the phase delay lines have to be very thin in order to match the input impedance of the square patch. Moreover, to operate as a dual-band reflectarray, the top layer needs to be transparent to the bottom layer at Ka-band. Since the ring element uses less metallization than an equivalent patch element, it allows more incident energy to pass through between the layers.

In this study, a simple ring structure with gaps is used to develop a dual layer CP reflectarray. A ring structure without any gaps can resonate to the excitation of two orthogonal field components [29]. To obtain circular polarization, however, additional gaps are needed in the ring structure so that the reflected phase response to the excitation of each of the two orthogonal component fields differs by 180^{o} at the desired resonant frequency. In other words, adding gaps in the ring enables the direction of propagation to be reversed so that the reflected wave has same polarization as the incident wave.

Figure 10 shows the element configurations at 7.1 GHz and 32 GHz. The ring element is simulated using the H-wall waveguide approach [30]. This approach assumes that a uniform plane wave with a vertically polarized electric field is normally incident on an infinite array of periodic structure. A perfect magnetic conductor and a perfect electric conductor form the four waveguide side walls. Two simulations are performed using

Ansoft High Frequency Structure Simulator (HFSS) [31] with orthogonal polarizations to determine the reflected phase and combined to extract the CP performance [32]. Figure 11 compares the simulated result of the ring element at 32 GHz with that of square patch element with two delay lines for the right-hand CP design. Increased CP bandwidth and left-hand CP suppression are observed for the ring element. The gap sizes are limited to 0.3 mm and 0.28 mm, respectively, due to the tolerances of fabrication in Texas A&M facilities but would ideally be smaller.

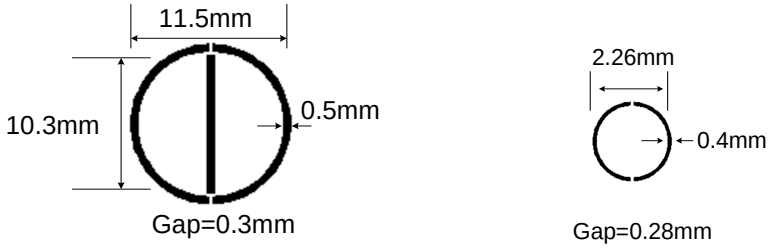

(a) (b)

Fig. 10 Ring antenna elements: (a) C-band; (b) Ka-band.

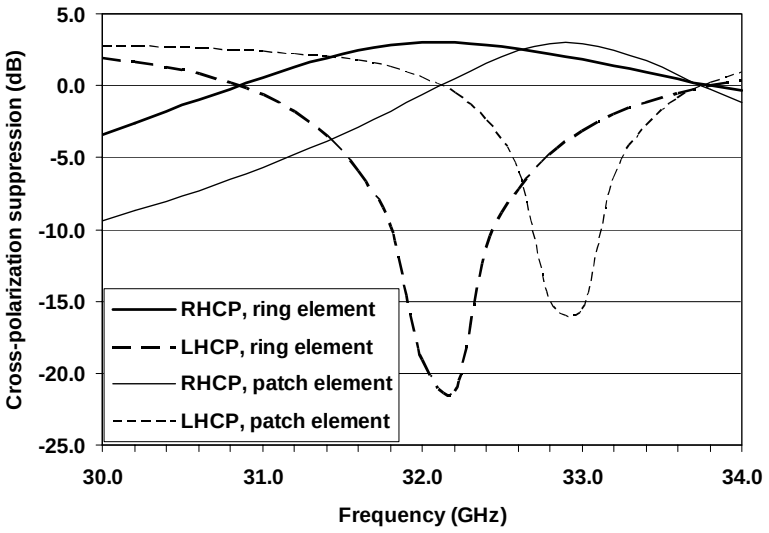

Fig. 11. Comparison of cross-polarization suppression in dB at 32 GHz.

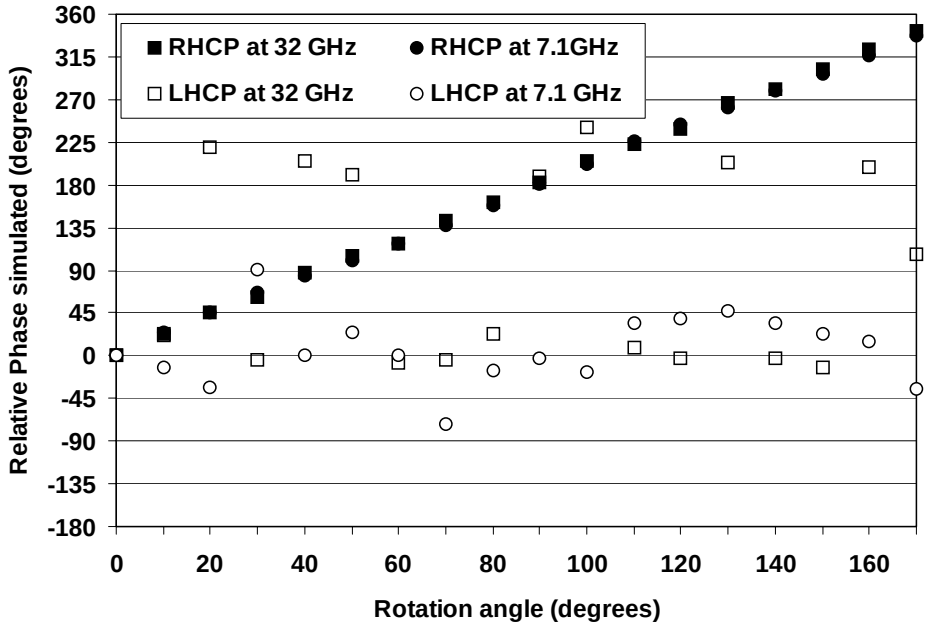

Fig. 12. Relative phase variations at a focal point referenced to zero rotation when the ring element is rotated in the counter-clockwise direction.

17 rotations with a right CP incident wave are simulated using HFSS for the rotation angles shown in Figure 12. The analysis results show good agreement with the theoretical values given in [15]. It also shows that the reflected phase of the right-hand CP component is advanced in phase by rotating each element in the counter-clockwise direction. The reflected phase of the left-hand CP component, however, is randomly distributed regardless of rotation angles.

B. Array simulation

To examine the interference effects of the top C-band layer on the bottom Ka-band reflectarray, 7 by 7 arrays at 32 GHz are simulated using HFSS combined with 2 by 2

arrays at 7.1GHz in the top layer. The results show that the peak gain degrades about 1 dB in the dual layer compared to the single layer as shown in Figure 13. This 1 dB gain drop corresponds to an efficiency drop of about 10 % at 32 GHz.

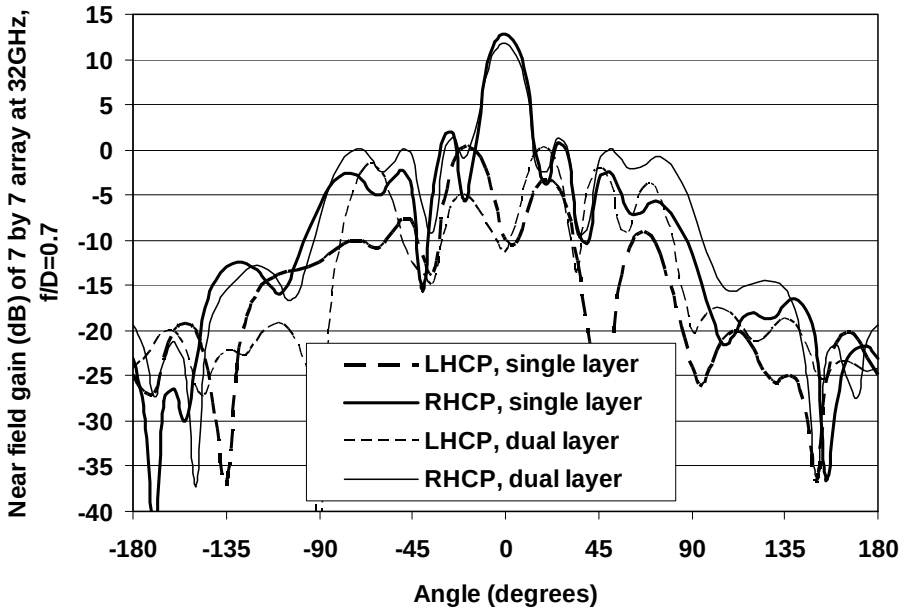

Fig. 13. 7 by 7 arrays simulated result at 32 GHz with and without the top layer of 2 by 2 arrays.

4. Experiments

A. C-band measurements for dual layer reflectarray

A 0.5 m diameter C-band right-hand CP planar reflectarray has been fabricated on the top layer using 437 ring elements. The feed horn is placed at 350 mm above the center of the reflectarray, which corresponds to a focal ratio of 0.7. The ring elements are separated by 0.5 free space wavelengths at 7.1 GHz or 21 mm in both orthogonal directions. This spacing provides a distance of approximately 0.25 free space wavelengths at 7.1 GHz between the edges of adjacent ring elements.

The preliminary measurements (I) are performed in the anechoic chamber at Texas A&M University using a circularly polarized corrugated horn as the feed antenna and a linearly polarized standard horn as the transmit antenna. The measured phase and magnitude information are used to determine the axial ratio of the CP reflectarray [32]. Final measurements (II) are conducted in the outdoor range at the Jet Propulsion Laboratory (JPL) using circularly polarized corrugated horns for both the feed and transmit antennas.

Figure 14 shows typical radiation patterns measured at A&M and JPL respectively. Although the phase measurement done at A&M is not completely accurate, the extracted CP gain patterns are quite similar with the patterns obtained at JPL. The peak gain is 28.2 dB (I) at 7.3 GHz and 27.8 dB (II) at 7.4GHz. The corresponding efficiency is 46% (I) and 40 % (II). Both main beams have a beam width of 5°. The peak sidelobe level is greater than 17.3 dB (I) and 13.1 dB (II) down from the main beam and the left-hand cross polarization level is 21 dB (I) and 27.8 dB (II) below the peak right-hand CP gain.

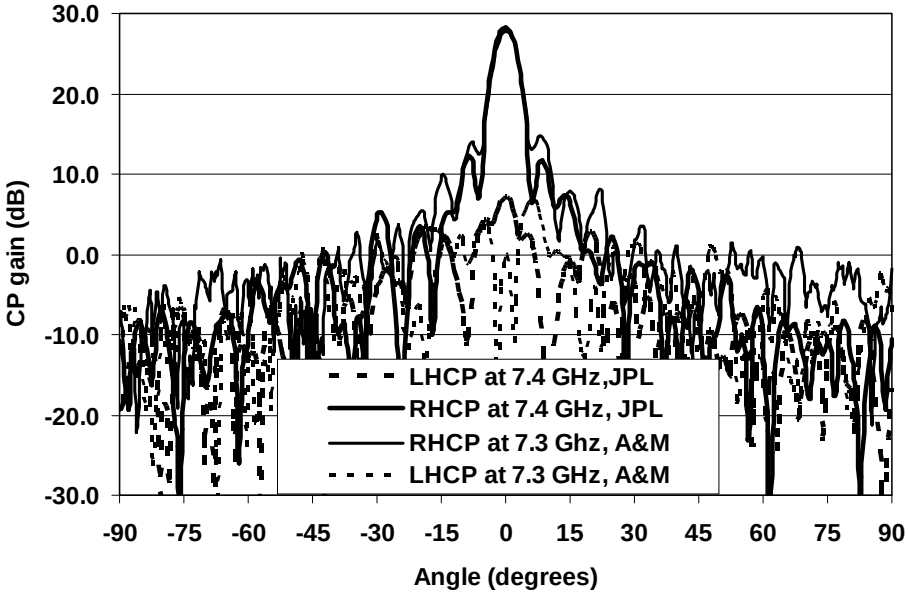

Fig. 14. Measured CP gains for a C band reflectarray.

The relatively large sidelobe level is, for the most part, caused by the feed horn blockage located at the broadside direction of the reflectarray aperture. For the C band measurements, the radiation patterns for the dual layer are not degraded compared to the single layer case. The CP gain variations versus frequency are shown in Figure 15. The peak gain occurs at 7.3 GHz (I) and at 7.4 GHz (II). In the measurements at JPL, the co-polarized gain keeps increasing, but the patterns are only tested from 6.6 GHz to 7.4 GHz. Also, both the CP horn and amplifier used in JPL operated from 8 GHz and made the cross-polarization level unstable over frequency ranges tested.

The aperture efficiencies versus frequency are shown in Figure 16. The highest efficiency is 46 % (I) at 7.3 GHz and 40 % at 7.4 GHz (II). Greater than 40 % efficiency is observed between 7.1GHz and 7.4GHz in the measurements at A&M. Again, the efficiency measured at JPL is unstable due to the operating range of the amplifier used.

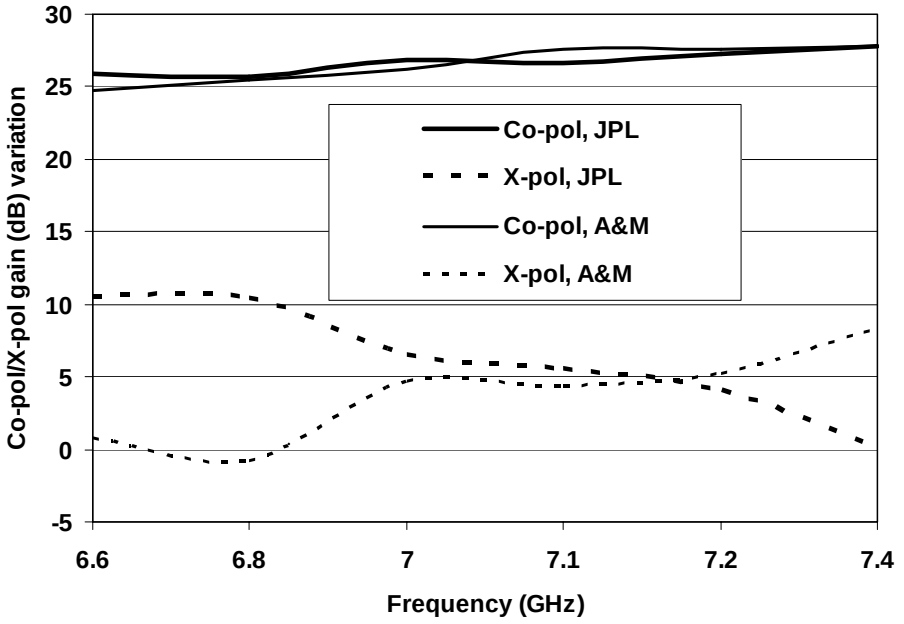

Fig. 15. Measured gain variations versus frequency at C-band for a dual layer.

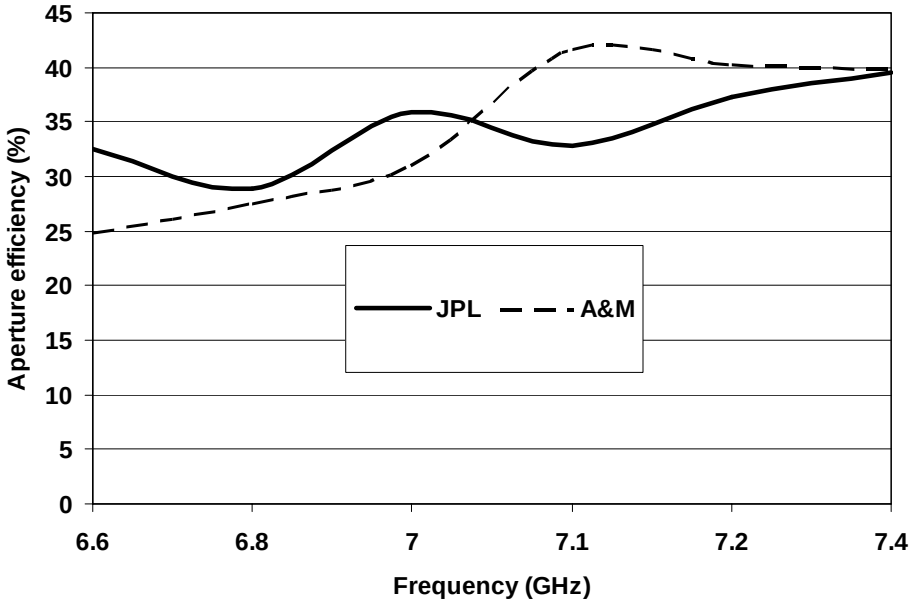

Fig. 16. Aperture efficiencies versus frequency for a dual layer.

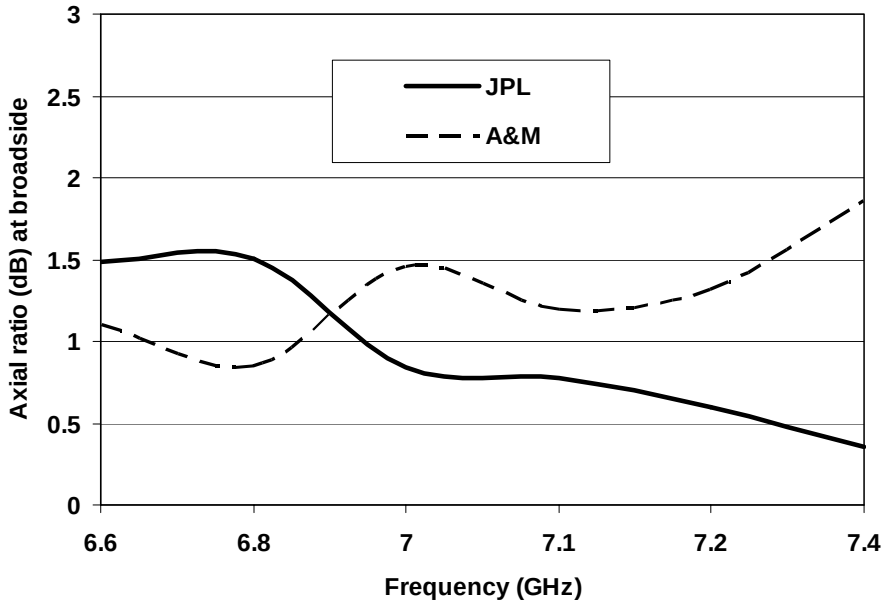

Fig. 17. Axial ratios at broadside versus frequency for a dual layer.

The theoretical efficiency estimated is 78 % by taking the overall gain into account, which assumes the element gain of 4 dB and the array factor of 26.4 dB. This efficiency difference is caused by the blockage attributed to the feed antenna and its supporting metal bars, the spillover effect due to the feed illuminating areas outside of the reflectarray, the feed's non-uniform illumination across the reflectarray's aperture, scattered fields from the edges, as well as some energy that is reflected by the array as left-handed CP.

Figure 17 shows the axial ratios at broadside versus frequency. It shows an axial ratio less than 3 dB for all frequency ranges tested. This superior CP performance at broadside is because the scattered and cross-polarized fields combine deconstructively due to the element rotations. This result also shows that the given ring structure operates as a CP antenna element by separating the co-polarized fields from the cross-polarized fields. Figure 18 shows the reflectarray's axial ratios versus incident angle over a frequency range

from 6.6 GHz to 7.4 GHz. It is observed that a plane wave can be incident upon the reflectarray between ± 3° for all frequencies and still have the axial ratio less than 3 dB.

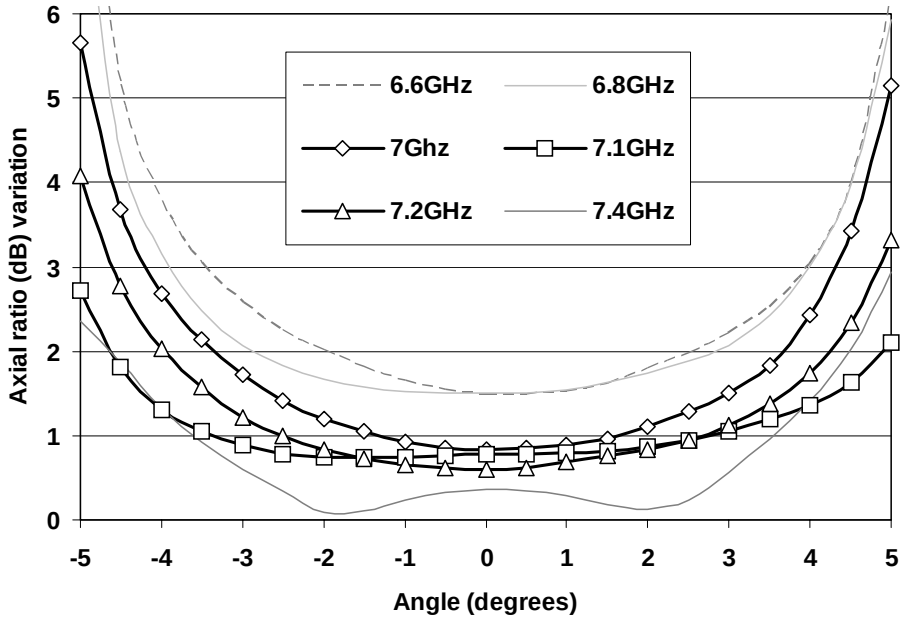

Fig. 18. Axial ratio variations versus incident angle for a dual layer.

B. Ka-band measurements for single and dual layer reflectarrays

Measurements at Ka band are conducted at JPL using circularly polarized corrugated horns for both the feed and transmit antennas. Approximately 9200 ring elements with variable rotations are constructed in the bottom layer. Again, the feed horn is placed at 350 mm above the center of the reflectarray aperture, which is 506 mm in diameter. The element spacing is 0.5 free space wavelengths at 32 GHz, or 4.7 mm, in both orthogonal directions. To assure good aperture efficiency, effort is made during measurements to maintain the flatness of the reflectarray's surface lest it should become delaminated.

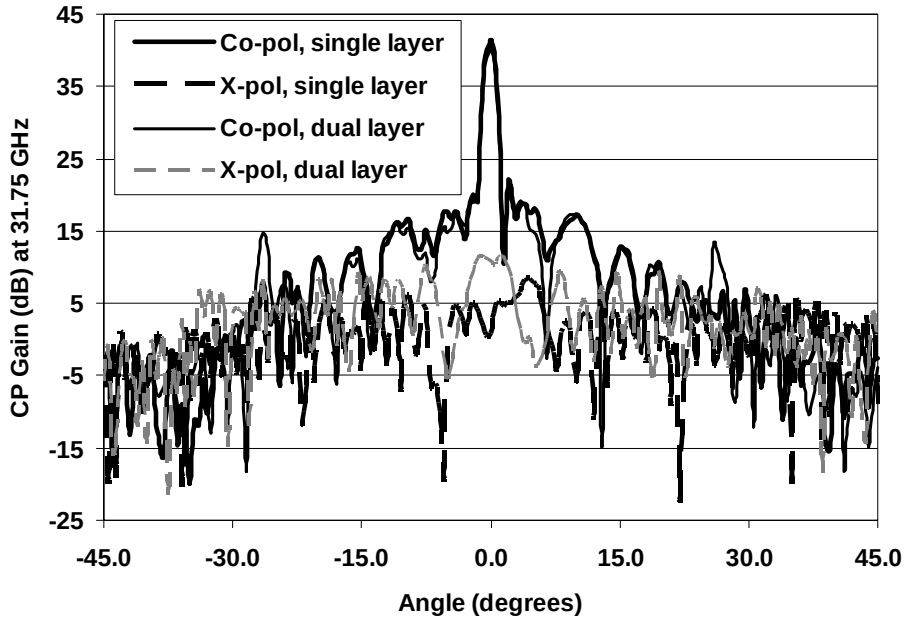

Fig. 19. CP radiation patterns at 31.75 GHz.

Typical radiation patterns at 31.75 GHz are shown in Figure 19. The main beam has a width of 1.3° for both the single (I) and dual layer case (II). The cross-polarization level is 40.7 dB (I) and 29.2 dB (II) down from the peak at broadside. The sidelobe suppression is greater than 19.5 dB (I) and 18.7 dB (II) occurring at 2°. This improved sidelobe suppression compared to that of C band is due to the large electrical aperture size, but it is still relatively high because of the feed blockage, edge scattering, scattering from the top layer elements and the illumination taper of the feed horn. The peak gain varies from 41.5 dB (I) to 40.3 dB (II) causing the aperture efficiency to drop from 50 % (I) to 38 % (II).

The CP gain variations versus frequency are shown in Figure 20. The co-polarized gain has a similar radiation pattern for both the single and dual layer cases. A large variation in the cross-polarized gain is observed over the frequency ranges for the dual

layer case, but the corresponding axial ratio is still less than 3 dB.

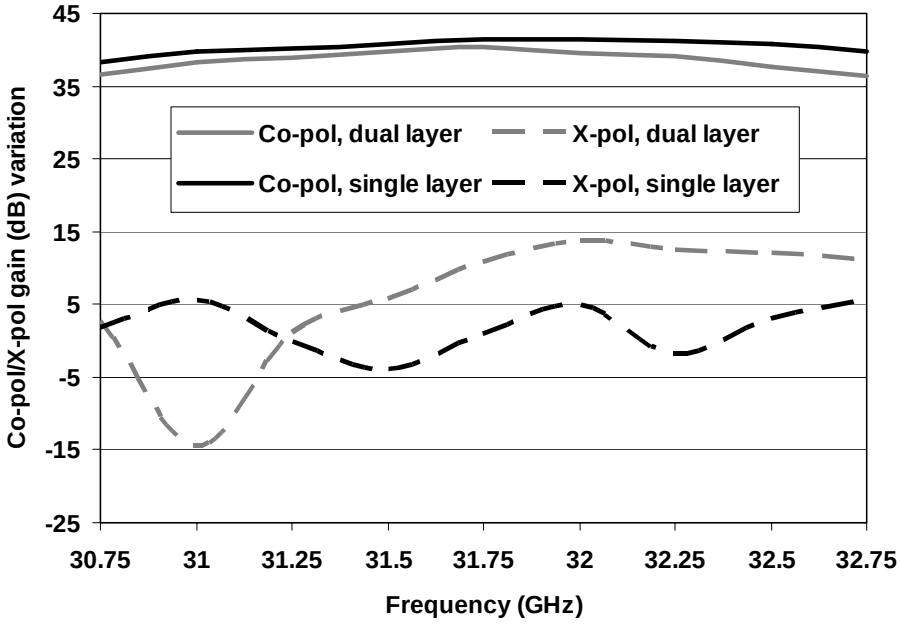

Fig. 20. CP gain variations versus frequency.

The measured aperture efficiencies versus frequency are shown in Figure 21. The highest efficiency achieved is 50 % (I) and 38 % (II) at 31.75 GHz. The efficiency drop is casued by the interference of the C-band layer. The spillover loss of -1.17 dB and aperture nonuniform illumination loss of -0.24 dB are calculated using the definition of the subtended angle [10] and the power pattern of the feed horn used in the measurement. A small amount of reflectarray element loss is not measured but predicted to be -0.4 dB by considering the equivalent dielectric and copper loss of 20 mil Duroid material [10]. The theoretical efficiency estimated is 80 % by considering the implicit element gain of 4 dB and the array factor of 39.6 dB. The bandwidth over 35 % efficiency is 1.5 GHz (I) and

250 MHz (II).

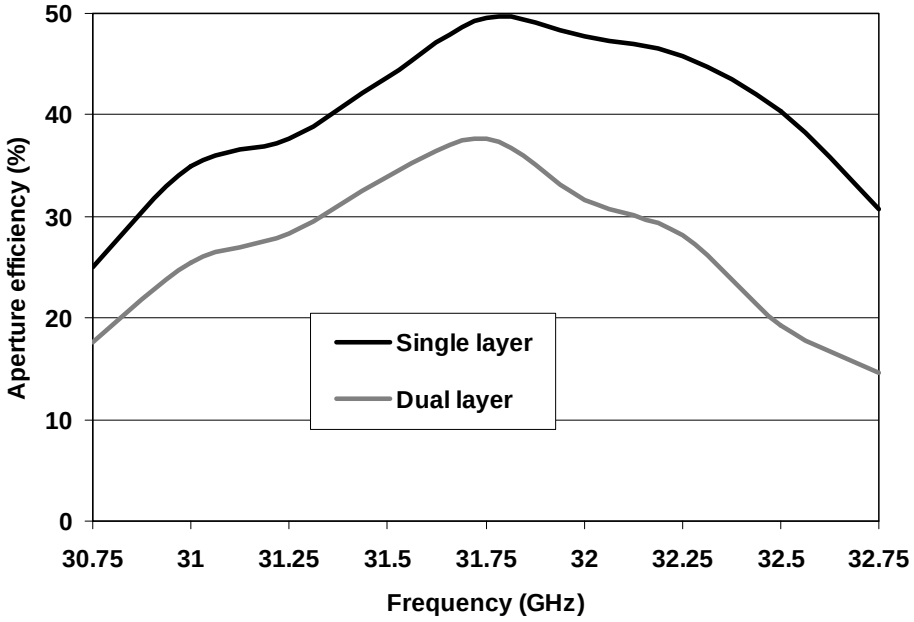

Fig. 21. Aperture efficiencies versus frequency.

Figure 22 shows the measured axial ratios versus frequency. Excellent axial ratio less than 0.5 dB is observed over all frequencies tested. Figure 23 shows the axial ratio variations versus incident angle. If the plane wave at 31.75 GHz is incident upon the reflectarray between ± 1°, the axial ratio will be better than 1.2dB.

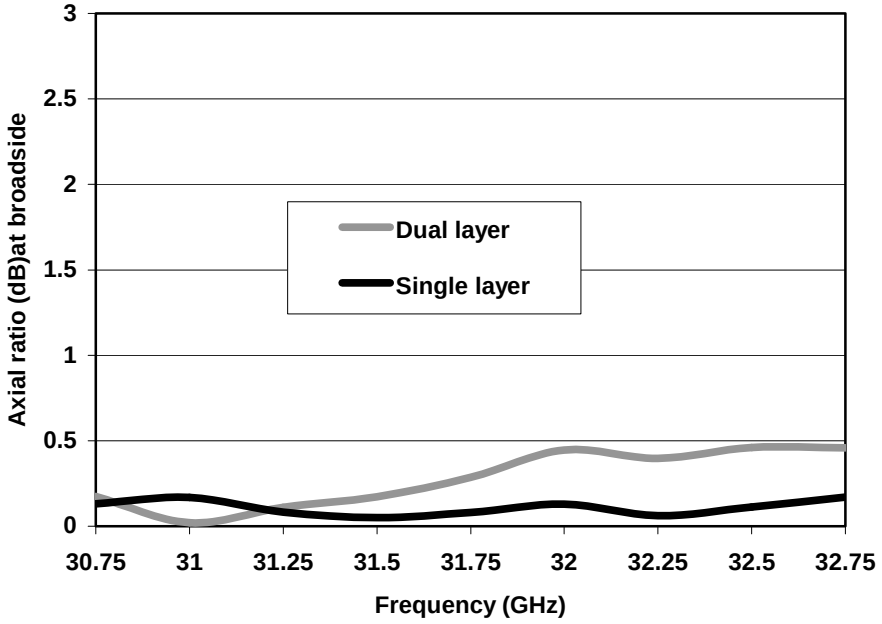

Fig. 22. Axial ratios at broadside versus frequency.

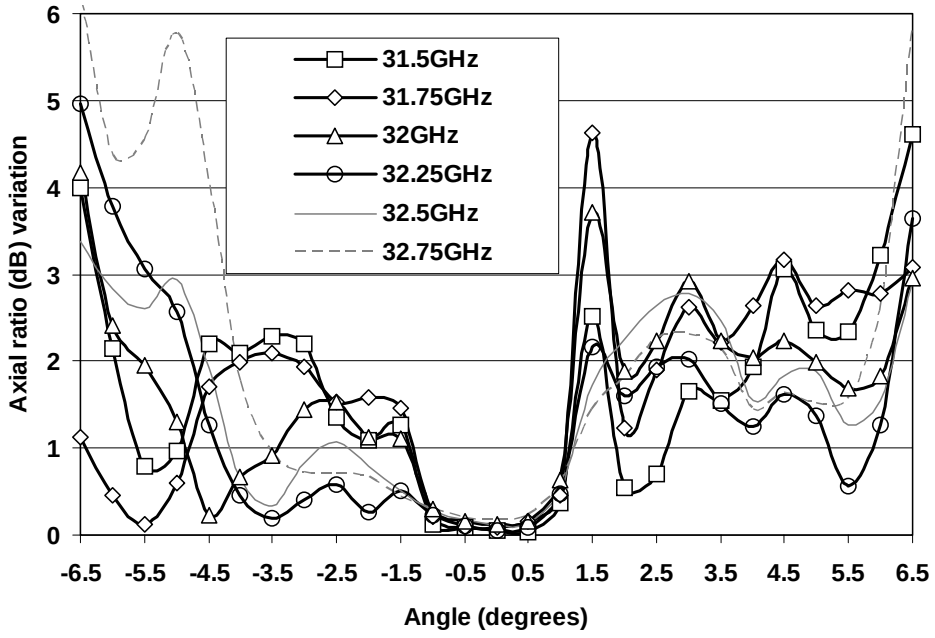

Fig. 23. Axial ratio variations versus frequency for a dual layer.

5. Conclusions

A dual layer dual frequency reflectarray is presented in this chapter. The reflectarray designed is right hand circularly polarized and uses the simple ring structures with variable rotations. The relatively good efficiency obtained at both frequencies shows that the proposed scheme should be useful in dual-band applications. Most of all, superior axial ratio is observed over broad frequency ranges. The performance summary is shown in Table 1.

Table 1. Performance summary for a center-fed reflectarray.

Performance parameters	C-band (a)	C-band (b)	Ka-band (c)	Ka-band (d)
Frequency	7.3 GHz	7.4 GHz	31.75 GHz	31.75 GHz
Aperture size	502 mm	502 mm	506 mm	506 mm
CP bandwidth (Axial ratio)	~ 1.1 GHz (3dB)	~ 1.2 GHz (2dB)	> 1 GHz (0.5dB)	> 1 GHz (0.5dB)
Gain	28.24 dBic	27.8 dBic	41.5 dBic	40.3 dBic
Efficiency	46 %	40 %	50 %	38 %
Cross-pol. level	- 21 dB	- 27.8 dB	- 40.7	- 29.2
Peak-sidelobe level	- 17.3 dB	- 13.1 dB	- 19.5	- 18.7
Beamwidth	5.0-deg	5.0-deg	1.3-deg	1.3-deg

Note: C-band (a): C-band measured with Ka-band layer at A&M.
C-band (b): C-band measured with Ka-band layer at JPL.
Ka-band (c): Ka-band measured without C-band layer at JPL.
Ka-band (d): Ka-band measured with C-band layer at JPL.
dBic: Circular polarized isotropic antenna gain in dB which is 3 dB higher than the linear polarized gain.

CHAPTER III

OFFSET-FED X/KA-BAND DUAL-BAND REFLECTARRAY ANTENNA USING THIN MEMBRANES*

1. Introduction

In recent years, there has been a growing demand for reduced mass, small launch volume, and at the same time, high-gain large-aperture antenna systems in space missions. To enable deployment of large-aperture antennas, the concept of an inflatable parabolic reflector has been proposed and experimented in the past [33-34]. However, the realization of this concept has found difficulty in achieving and maintaining the required large, thin curved-parabolic surface in the space environment. As an alternative to alleviate the burden associated with curved surfaces, a new concept of using an inflatable microstrip reflectarray antenna has been introduced by JPL in 1996 [35]. Because of the flat reflecting surface it uses, it is believed to be more reliable in maintaining the surface tolerance compared to its counterpart, the inflatable parabolic reflector. Although there are still many challenges to overcome, this chapter presents an antenna component with thin membranes to meet the demand in future inflatable antenna systems.

The reflectarray presented in this study is made of thin membranes with their thickness equal to 0.0508 mm at both layers. It is found that if a substrate consists of only a thin membrane, the CP bandwidth of the ring element would be significantly reduced to

an unacceptable value for either X or Ka-band. In addition, there would be some increase in substrate loss resulting in poor antenna efficiency, in particular at the Ka-band frequency. To improve the overall performance, a new configuration is proposed by inserting empty spaces of the proper thickness below both the X and Ka-band membranes. For this technology demonstration, low-dielectric constant foam layers are substituted for the empty spaces to act as support structures for the membrane layers. In an actual space flight unit, an inflatable structure will provide proper tensioning force and support to eliminate the use of foam layers. This study shows that, by using the new configuration, the degrading effects of thin substrates are eliminated resulting in excellence performance for both frequency bands. In particular, the CP bandwidth performance is significantly enhanced. The broader CP bandwidth of the ring element plays an important role in achieving high efficiency reflectarray performance. In addition, an offset feed scheme [36-40] is used to reduce the blockage of the center-fed feed horn and to improve the overall efficiency. With an offset configuration, the reaction of the reflectarray upon the primary feed horn can be reduced to a very low order, which implies the interaction of the primary feed horn with the reflectarray can be negligible. Also, the offset configuration can be accommodated more easily than an axis-symmetric design in the design of spacecraft antennas. In the design, the incidence angle of the feed horn should be carefully chosen close to the main beam scan angle to minimize the beam-squinting properties of the circularly polarized offset reflectarray [40]. The tested results show more than 50 % efficiencies at both frequency ranges, which is believed to be highest efficiency ever achieved using deployable thin membranes capable of dual-band operation.

A 0.5 m diameter dual-band printed reflectarray antenna designed consists of two very thin surfaces made up of many individual rings of variable rotations and an illuminating offset-feed as shown in Figure 24. The configuration of the dual layer reflectarray antenna with element dimensions is also shown in Figure 25. Compared to the Figure 10, the microstrip bar in the middle of the ring at C-band is removed since further simulations of the ring structure found it superfluous in achieving circular polarization. The reflectarray is fabricated on commercial Rogers R/flex 3000 liquid crystalline polymer (LCP) material with ε_r = 2.9 and 0.0508 mm (2 mil) thickness for both layers. Because it is found during simulations that the distance from the circuit layer to the ground plane should be within 5 %-20 % of free space operating wavelengths for the given ring structure to operate as an efficient CP, 1.6 mm foam is introduced between the Ka-band layer and the ground plane. Also, 3.2 mm foam is placed above the Ka-band layer to separate the X-band layer. With these foam widths, the effective substrate thickness from the circuit layer to the ground plane becomes 0.17 free space wavelengths at 32 GHz and 0.13 free space wavelengths at 8.4 GHz. Counter-clockwise rotations are applied to the array elements to achieve the right-hand circular polarization for both layers. The dielectric constant of the foam material is 1.03 (3.2 mm foam below X-band) and 1.06 (1.6 mm foam below Ka-band) respectively, which is very close to that of air. The foam layers also have a very low loss tangent of 0.0001.

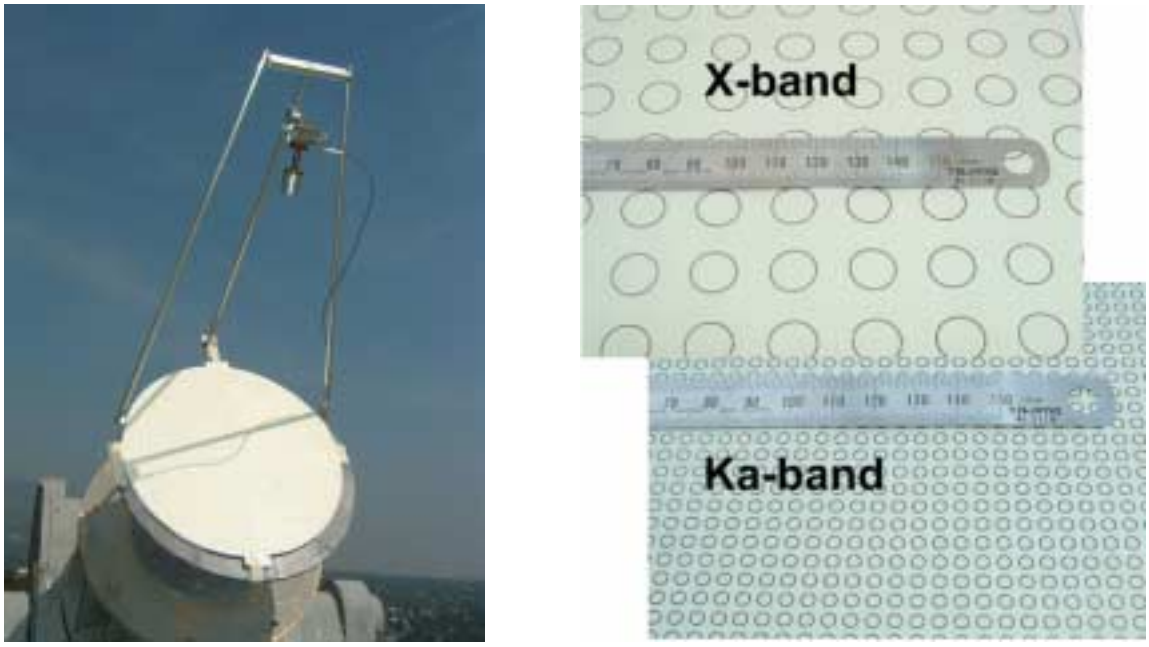

(a) (b)

Fig. 24. (a) A photo of the half-meter offset-fed reflectarray with microstrip rings of variable rotations (b) close-up view of the reflectarray element.

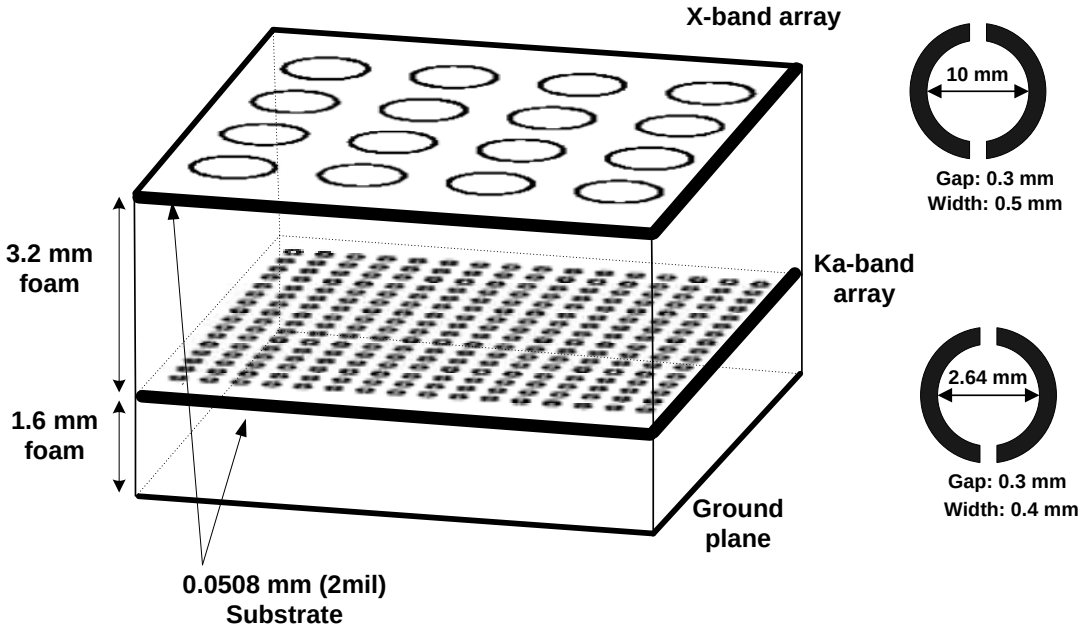

Fig. 25. Two-layer reflectarray topology with element dimensions.

2. Offset reflecting antenna analysis

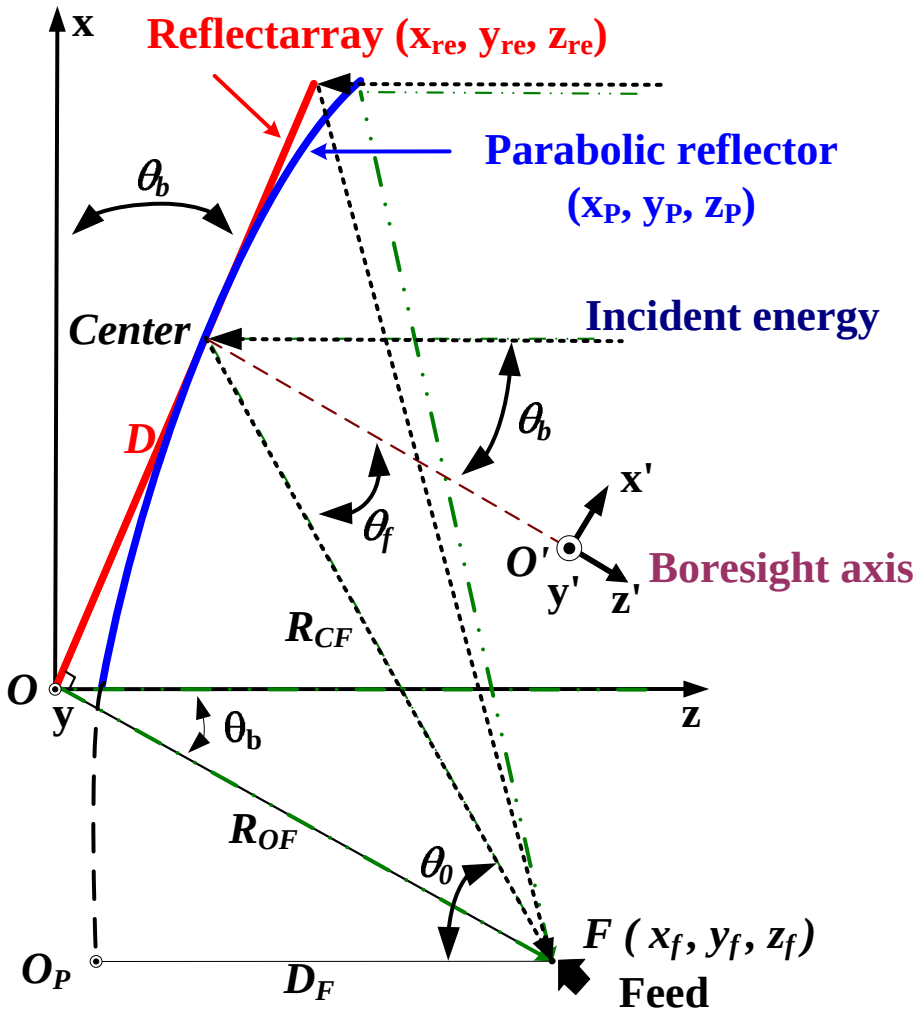

Fig. 26. Offset-fed reflectarray block diagram.

The analysis to calculate the needed phase delay is derived based on the comparison of the geometrical configurations between an offset parabolic reflector and a flat microstrip reflectarray.

The block diagram of the reflectarray with its virtual parabolic surface is shown in Figure 26. The microstrip reflectarray elements are placed at (x_{re}, y_{re}, z_{re}) in the

(x, y, z) coordinate system.

Referring to Figure 26 and specifying the reflectarray's dimension D, the vertical distance from the reflectarray's lower edge to the feed R_{OF}, and the desired scan angle θ_b, the phase center of the feed is

$$x_f = -R_{OF}\sin(\theta_b);\ y_f = 0;\ z_f = R_{OF}\cos(\theta_b) \tag{15}$$

From the phase center of the feed, the center of the microstrip arrays on the reflectarray's surface is obtained such that the incident angle of the feed horn θ_f relative to the normal of the reflectarray's surface is very close to the main beam scan angle θ_b. By choosing the value of θ_f very close to θ_b, the effect of beam squint with frequency can be minimized to a great extent for an offset feed system [40].

Since the center of the microstrip arrays on the reflectarray's surface lies on the surface formed by the parabolic reflector, the subtended angle θ_0 can be determined with its corresponding focal length defined as [28]

$$D_F = \frac{R_{CF}(1+\cos(\theta_0))}{2} \tag{16}$$

Now the origin in the (x, y, z) coordinate system is redefined such that the phase center (x_f, y_f, z_f) of the feed is placed at $(0, 0, D_F)$ and the (x_{re}, y_{re}, z_{re}) coordinates of the microstrip reflectarray elements are also transformed accordingly. Within the new

coordinate system, the surface of a parabolic reflector is described by the points (x_p, y_p, z_p) and it is formed simply by expressing the value of z_p coordinate in terms of x_{re} and y_{re}. That is,

$$z_p = \frac{x_{re}^{\ 2} + y_{re}^{\ 2}}{4D_F} \tag{17}$$

Finally, the path difference is given by

$$\Delta l = \sqrt{x_{re}^{\ 2} + y_{re}^{\ 2} + (z_{re} - D_F)^2} - \sqrt{x_{re}^{\ 2} + y_{re}^{\ 2} + (z_p - D_F)^2} + z_p - z_{re} \tag{18}$$

To compensate for the additional Δl path lengths, The CP antenna arrays are rotated. The center of the microstrip arrays has zero rotation since Δl is zero. As the elements are placed moving away from the center of arrays, the variable rotation increases. The variable rotation ψ in radians for a circularly polarized radiator that is necessary to compensate for Δl is

$$\psi = \frac{\Delta l}{2} \times \frac{2\pi}{\lambda_o} \tag{19}$$

In this work, the following values are used to design a 0.5 m diameter reflectarray.

A. X-band

Number of ring antenna elements= 593

Vertical distance from the reflectarray's lower edge to the feed, R_{OF} = 450 mm

Focal length of the virtual parabolic reflector, D_F = 407.8 mm

Physical origin of the reflectarray, $(x_{re}, y_{re}, z_{re}) = (252, 0, 117.5)$ mm in the (x, y, z) coordinate system

Electrical origin of the reflectarray, $(x_{re}, y_{re}, z_{re}) = (216, 0, 100.7)$ mm in the (x, y, z) coordinate system

Main beam scan angle, $\theta_b = 25^o$

Incidence angle of the feed horn, $\theta_f = 23.7^o$

B. Ka-band

Number of ring antenna elements= 8993

Vertical distance from the reflectarray's lower edge to the feed, R_{OF} = 540 mm

Focal length of the virtual parabolic reflector, D_F = 489.4 mm

Physical origin of the reflectarray, (x_{re}, y_{re}, z_{re}) = $(253.8, 0, 118.3)$ mm in the (x, y, z) coordinate system

Electrical origin of the reflectarray, (x_{re}, y_{re}, z_{re}) = $(258.5, 0, 120.5)$ mm in the (x, y, z) coordinate system

Main beam scan angle, $\theta_b = 25^o$

Incidence angle of the feed horn, $\theta_f = 25.2^o$

Figure 27 shows the required rotation angles calculated in MATLAB with element index starting from the bottom edge of the reflectarray's surface.

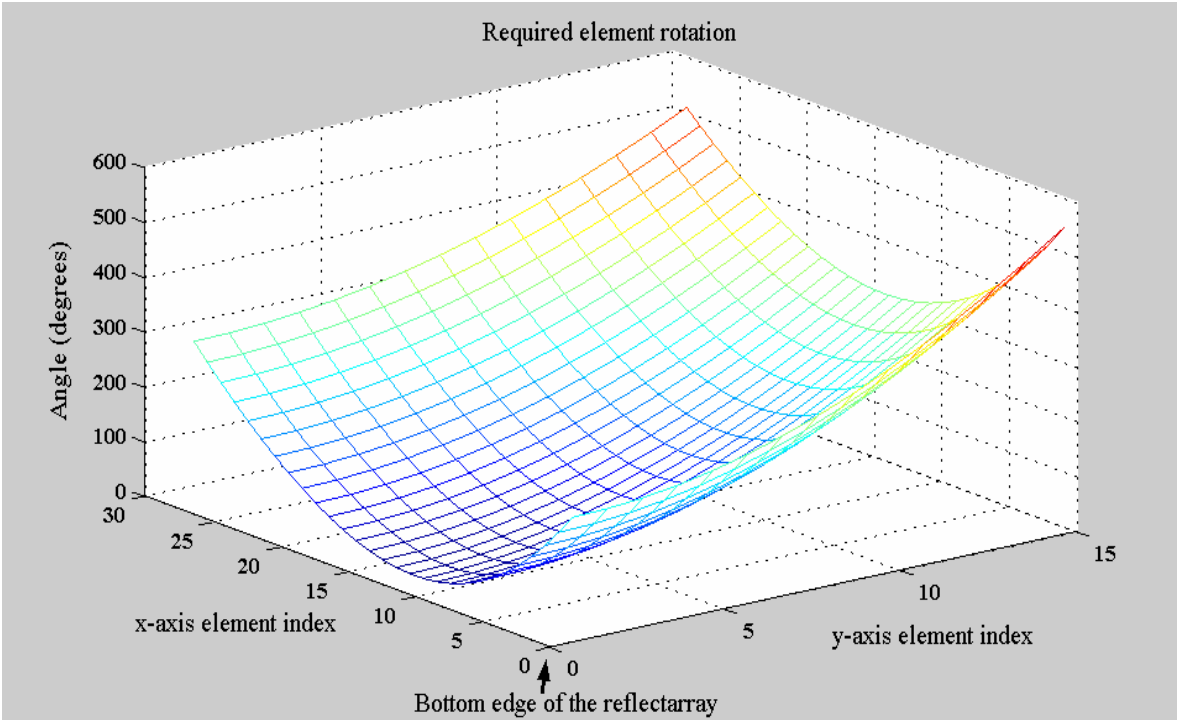

(a)

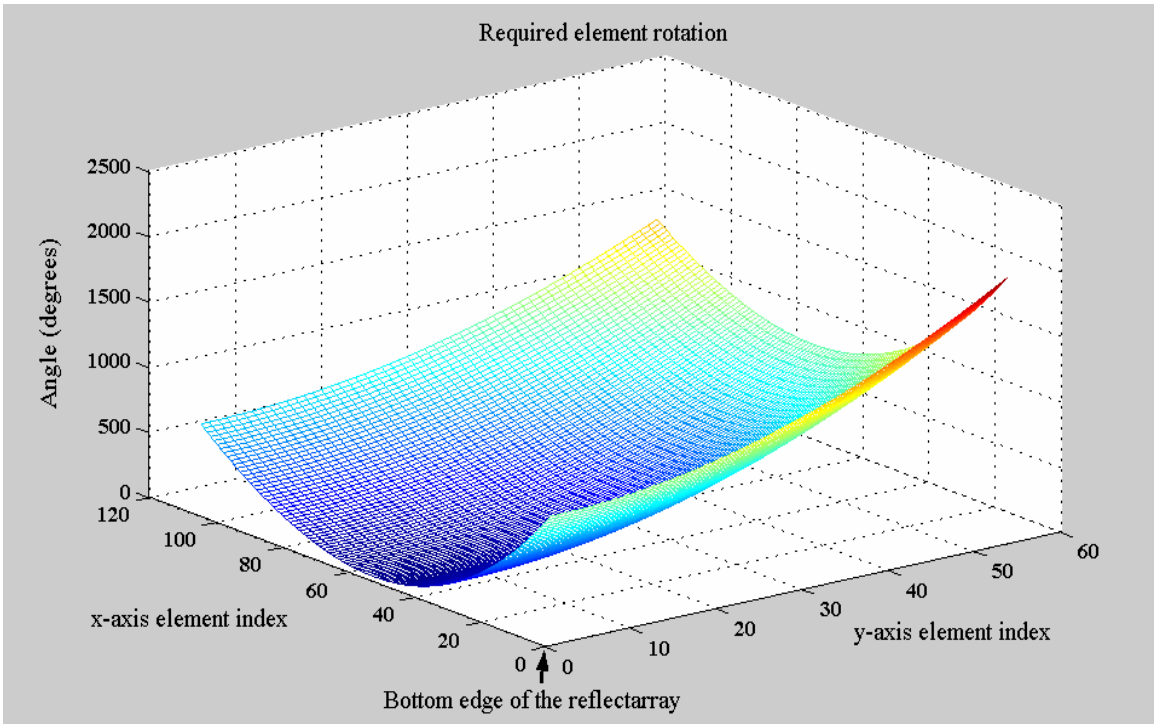

(b)

Fig. 27. Required rotation angles simulated in Matlab: (a) X-band; (b) Ka-band.

Another consideration in the design of the offset feed reflectarray is the effect of the feed horn pattern on the far-field pattern of the reflectarray. In a typical reflector design, the field at the edge is approximately 10 dB below that of the center for maximum gain and about 20 dB down for good sidelobe performance [41]. In this study, the edge taper characteristic of 10-15 dB is aimed to compromise between the gain and the first sidelobe level. The feed power pattern for the corrugated CP horn is characterized by commonly used cosine-q model with q equal to 12 and the path loss is calculated based on the geometry of the reflectarray. As a result of summing the feed taper with the path loss, the X-band reflectarray results in an edge taper characteristic of 15.6 dB and 10.3 dB for the upper and lower edge respectively. For the Ka-band reflectarray, 9.8 dB and 9.9 dB edge taper are obtained for the upper and lower edge of the reflectarray.

3. Element design

The ring antenna is simulated with Ansoft's HFSS simulator using the H-wall waveguide approach [30] as shown in Figure 28. In the actual simulation, more attention is given to the ring element at Ka-band because the effect of the thin substrate is most severe at Ka-band. Figure 29 shows the simulated cross-polarization level of the ring element at 32 GHz with different thicknesses of substrate. It is observed that the CP bandwidth is reduced significantly by using 8-mil thick substrate.

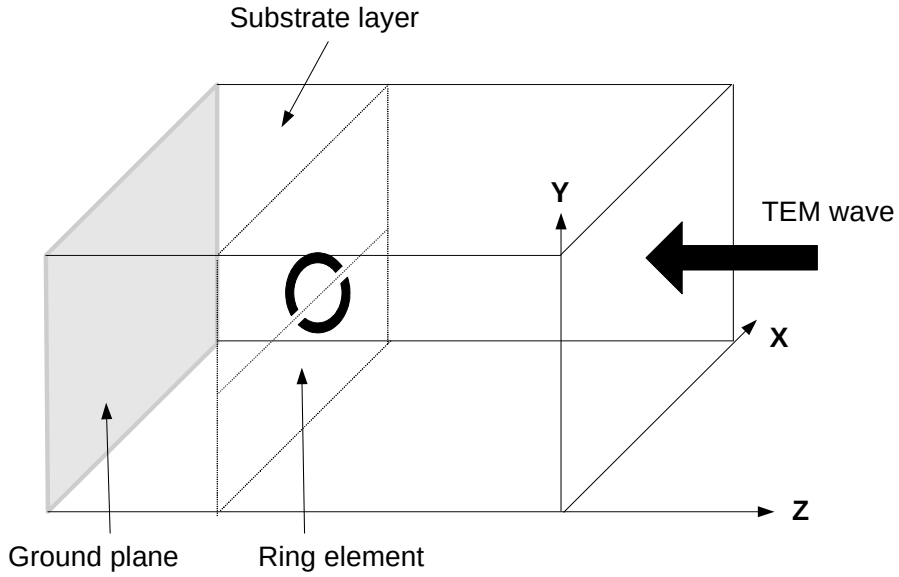

(a)

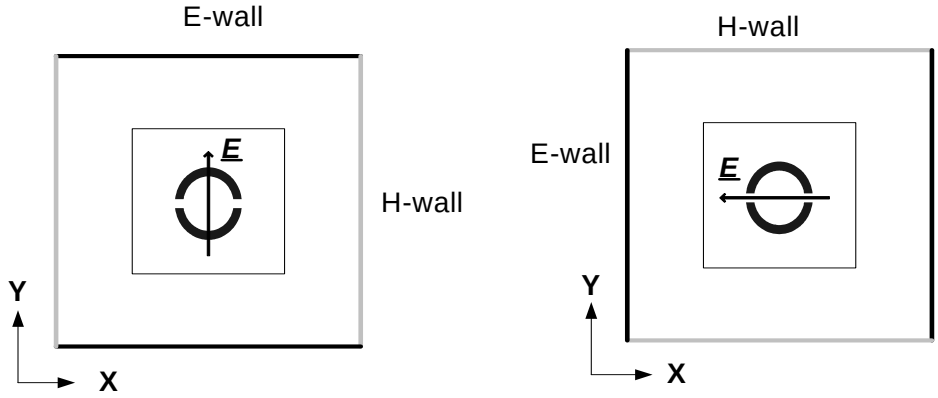

(b)

Fig. 28. H-wall waveguide approach: (a) Isometric view; (b) Boundary of four side walls and direction of electric field.

Obviously this reduced bandwidth will degrade the overall reflectarray's performance since the random phase errors introduced by surface tolerances and imprecise focal length in the measurement cannot be compensated at different frequencies in the

vicinity of the desired frequency if the CP bandwidth of the radiating elements is too narrow. The narrow bandwidth also imposes a very tight fabrication tolerance on the resonant frequency of the CP element.

Besides the narrow bandwidth, it is observed that using too thin a substrate makes it difficult to achieve circular polarization for a given ring structure with gaps because of the weak coupling through the gaps. This phenomenon can be easily explained by a simple simulation setup with two orthogonal excitations for the rings as shown in Figure 30. Because little coupling occurs across each gap, it is observed that the ring element sets up a resonance around half circumference with horizontal excitation while it resonates around full circumference with vertical excitation [29]. So it is quite difficult to achieve circular polarization at the desired frequency. During simulations, it is found that the effective substrate thickness from the layer to the ground plane should be within 5 %-20 % of the free space operating wavelength for the corresponding ring structure to operate as an efficient CP radiator.

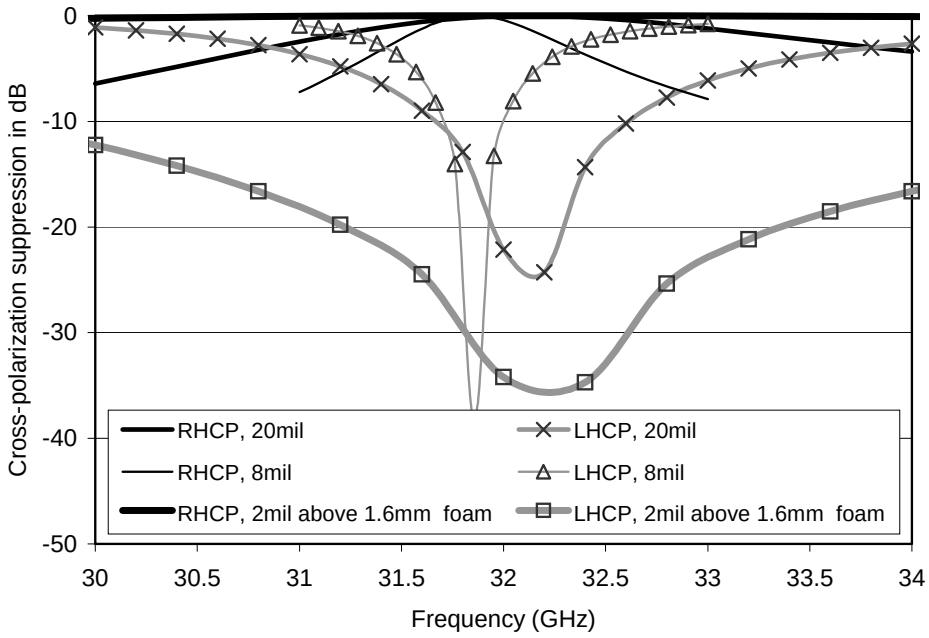

Fig. 29. Comparison of cross-polarization suppression level in dB at 32 GHz.

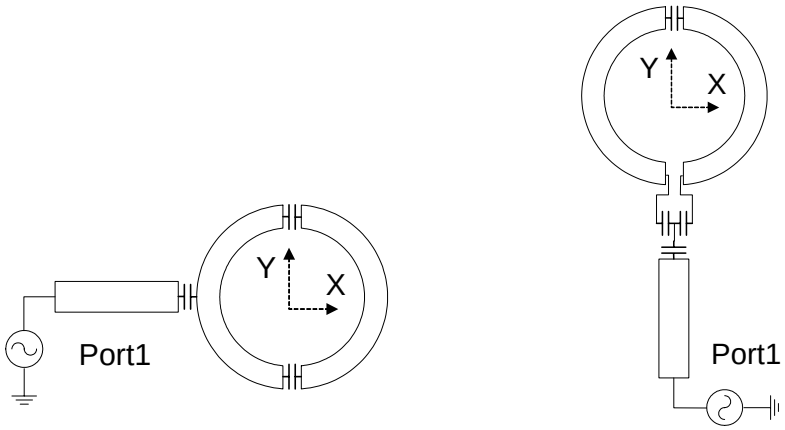

(a) (b)

Fig. 30. Simulation setup with different excitation scheme: (a) horizontal excitation; (b) vertical excitation.

To overcome above problems, a new configuration is proposed as shown in Figure

25. By inserting 1.6 mm foam below the Ka-band layer, the effective substrate thickness from the Ka-band layer to the ground plane becomes 17 % of the free space wavelength at 32 GHz. For the X-band reflectarray, 3.2 mm foam is used to separate the layers and its effective thickness from the X-band layer to the ground plane corresponds to 13 % of the free space wavelength at 8.4 GHz. With 0.0508 mm thick substrate in both layers and an inserted foam below the Ka-band, the right-hand CP (RHCP) bandwidth with the left-hand CP (LHCP) suppression is much broader at Ka-band as shown in Figure 29.

In addition to the CP bandwidth performance, using the thin substrate also increases the loss of the reflectarray [10]. The effect of substrate loss is examined by fabricating two 0.2 m diameter Ka-band reflectarrays on different thicknesses of substrate. The first reflectarray is etched on Rogers R/flex LCP material with ε_r = 2.9 and 0.2032 mm thickness, and the second reflectarray is etched on Rogers Duroid 5870 material with ε_r = 2.33 and 0.508 mm thickness. The specified loss tangents given by manufacturer for the Rogers R/flex LCP material and the Rogers Duroid 5870 material are 0.002 and 0.0012 at 10 GHz, respectively. With the ring dimensions adjusted to resonate near 32 GHz, the reflectarrays are constructed for the same scan angle, array spacing, and focal point. The measurement results show that the first reflectarray has the peak gain at 32 GHz, and the second reflectarray has the peak gain at 31.5 GHz, with a peak gain difference of 3.8 dB. Although the dielectric constant and loss tangent are different, and the highest peak gain occurs at different frequency, this experiment shows that the thin substrate causes a significant loss resulting in poor efficiency. Therefore, to avoid the dielectric loss of the thin substrate, a thicker substrate is preferable, and inserting foam below the Ka-band layer can avoid this problem.

4. Experiments

A. Ka-band measurements

Measurements at Ka band are conducted at Jet Propulsion Laboratory using circularly polarized corrugated horns for both the feed and transmit antennas. 8993 ring elements with variable rotations are constructed on the bottom layer. The ring elements are spaced by 0.5 free space wavelengths at 32 GHz, or 4.7 mm in both orthogonal directions. The Ka-band feed horn is placed 540 mm above the origin. The scan angle designed is 25^o in the plane of symmetry ($x'z'$ plane in Figure 26, offset plane) and 0^o in the plane of asymmetry ($y'z'$ plane in Figure 26).

In the Ka-band measurements, effort to obtain the true focus is made by way of finding the peak gain. During the measurements, the microstrip antenna array elements glued on the foam material are beginning to delaminate noticeably and a great deal of attention should be paid in the future design. The highest frequency tested is 32.8 GHz due to the operating ranges of test equipments including the corrugated CP horns.

Typical normalized radiation patterns in the plane perpendicular to the offset plane at 32.2 GHz are shown in Figure 31. The main beam is at broadside and the 3 dB beam width is 1.16^o. The peak sidelobe levels relative to the main beam are –21.0 dB /-19.3 dB (left/right side) for the single layer (Ka-band only without X-band layer) and –22.8 dB /-19.9 dB (left/right side) for the dual layer (Ka-band with X-band layer). Except the peak sidelobe occurring near the main beam, other sidelobe levels are less than –30 dB down from the main beam. The left-hand cross-polarization level is 34 dB for the single layer and 31.5 dB for the dual layer below the peak right-hand CP gain. Outside the main beam region, most cross-polarization levels are suppressed fluctuating around –40 dB.

Figure 32 shows the peak sidelobe level variations measured in the plane perpendicular to the offset plane at Ka-band. The higher sidelobe levels are observed at the lower frequency ranges. Figure 33 shows the axial ratio variations in the plane perpendicular to the offset plane at broadside. It shows an axial ratio less than 1 dB for all frequency ranges tested. In the plane perpendiculat to the offset plane, the measured results show that both the peak sidelobe level and the cross-polarization suppression level for the dual layer case are not influenced significantly compared to the single layer case.

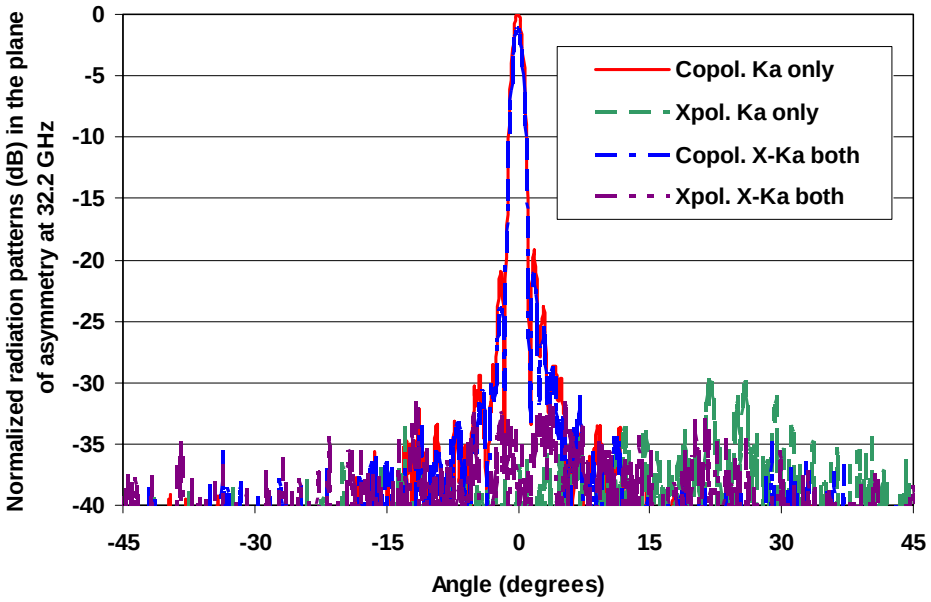

Fig. 31. Normalized radiation patterns in the plane perpendicular to the offset plane at 32.2 GHz.

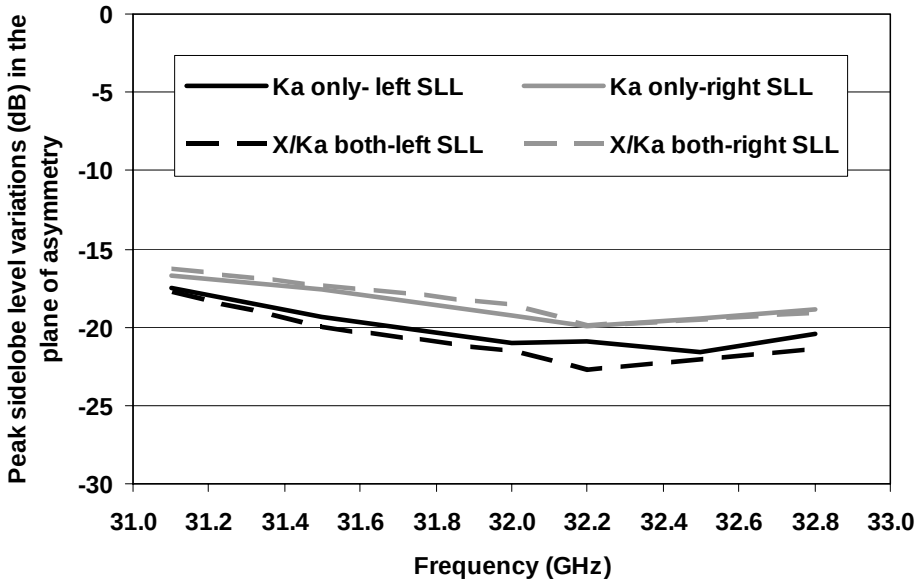

Fig. 32. Peak sidelobe level variations in the plane perpendicular to the offset plane at Ka-band.

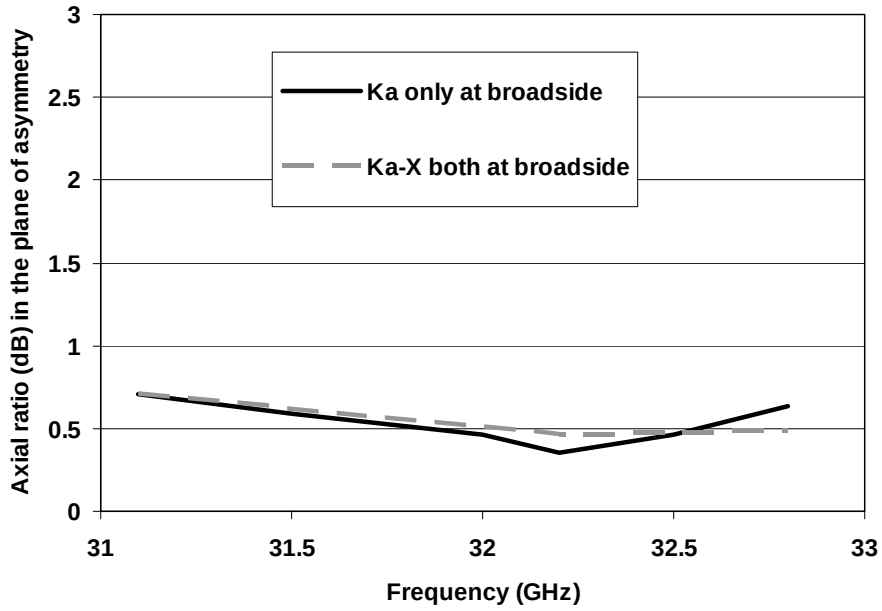

Fig. 33. Axial ratios versus frequency in the plane perpendicular to the offset plane at Ka-band.

Normalized radiation patterns in the offset plane at 32.2 GHz are shown in Figure 34. The main beam is scanned 25.6^{o} for the single layer and 25.4^{o} for the dual layer off the broadside direction. The 3 dB beam width is 1.29^{o} and 1.25^{o} respectively. The peak sidelobe levels are –17 dB/-18.8 dB (left/right side) for the single layer and –21 dB/-17.8 dB (left/right side) for the dual layer down from the main beam.

The left-hand cross-polarization level is 34 dB for the single layer and 31.8 dB for the dual layer below the peak right-hand CP gain. Figure 35 shows the peak sidelobe level variations measured in the offset plane at Ka-band. The sidelobe levels measured in the offset plane are degraded compared to those measured in the plane perpendicular to the offset plane with worst sidelobe level of –14 dB at 31.1 GHz. This degradation is due to the manual alignment procedure in finding the true focal point. More specifically, given the geometric structure of offset reflector, phase errors made by misalignment of the feed horn give more effects in the offset plane than in the plane perpendicular to the offset plane. The degradations include the sidelobe levels, peak gain, and the cross-polarization levels. Figure 36 shows the axial ratio variations in the offset plane at 25^{o}. The axial ratio is still less than 1 dB for all frequency ranges tested.

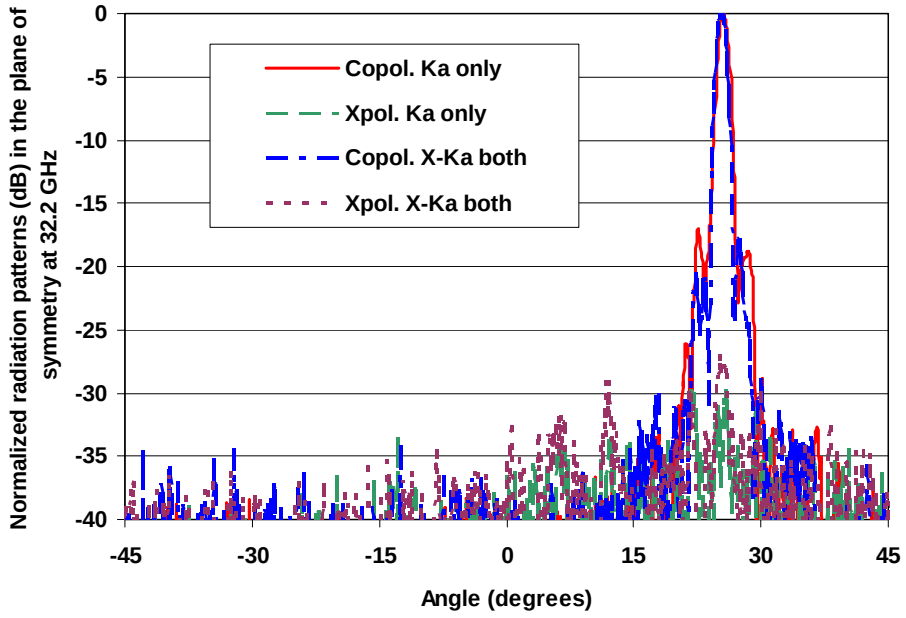

Fig. 34. Normalized radiation patterns in the offset plane at 32.2 GHz.

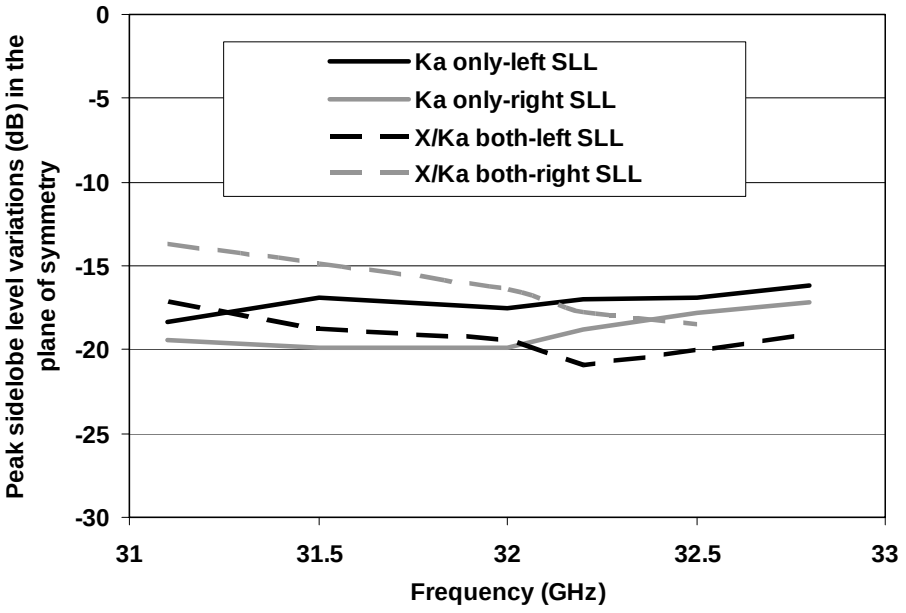

Fig. 35. Peak sidelobe level variations in the offset plane at Ka-band.

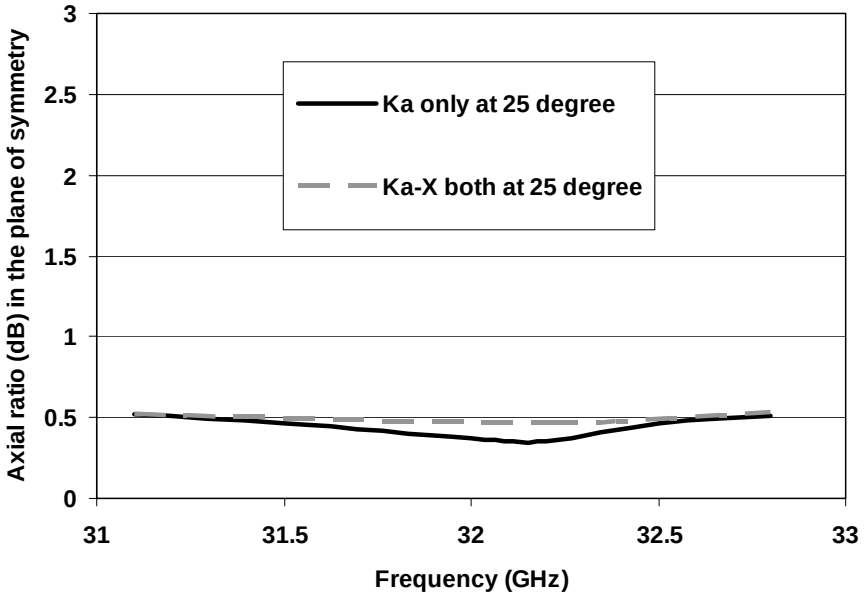

Fig. 36. Axial ratios versus frequency in the offset plane at Ka-band.

The measured aperture efficiencies versus frequency at Ka-band are shown in Figure 37. The aperture efficiency is calculated by comparing the co-polarized peak gain with the directivity, which is derived based on the physical aperture area. The efficiency at 32.2 GHz is 60.6 % for the single layer and 47.7 % for the dual layer. For the dual layer, the gain is reduced by 0.85 dB~1 dB compared to the single layer gain. It is expected that the dual layer gain due to the effect of the X-band layer will be influenced more severely at Ka-band than at X-band. At 31.5 GHz, 32.5 GHz, and 32.8 GHz, more than 62 % efficiency is achieved for the single layer with highest efficiency of 63.9 % at 32.8 GHz. Over 45 % efficiency is achieved over all frequencies for the dual layer case, which corresponds to 5.3 % bandwidth of the operating frequency. Some of radiation patterns are attached in Appendix B1.

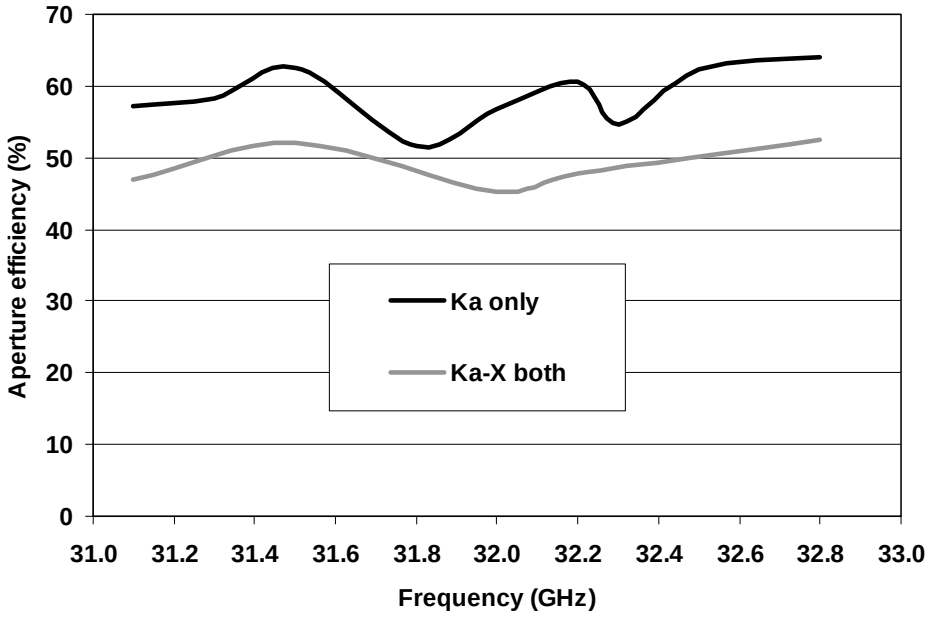

Fig. 37. Measured aperture efficiencies versus frequency at Ka-band.

B. X-band measurements

A 0.5 m diameter X-band right-hand CP planar reflectarray has been fabricated on the top layer using 593 ring elements. The ring elements are separated by 0.5 free space wavelength at 8.4 GHz or 18 mm in both orthogonal directions. The X-band feed horn is placed 450 mm above the origin (near the first element) of the X-band array elements. The scan angle designed is 25^{o} in the plane of symmetry ($x'z'$ plane in Figure 26, offset plane) and 0^{o} in the plane of asymmetry ($y'z'$ plane in Figure 26).

Typical normalized radiation patterns in the plane perpendicular to the offset plane at 8.7 GHz are shown in Figure 38. The 3 dB beam width of the main beam at broadside is 4.4^{o}. The peak sidelobe levels at 8.7 GHz are –23 dB/-20.5 dB (left/right side) for the single layer (X-band only without Ka-band layer) and –24.5 dB/-20.1 dB (left/right side) for the dual layer (X-band with Ka-band layer). The cross-polarization suppression level at

8.7 GHz is 21.04 dB for the single layer and 20.33 dB for the dual layer below the peak right-hand CP gain. Other than the peak sidelobes, all the sidelobes are less than –25 dB down from the main beam. Outside the main beam region, most cross-polarization levels are suppressed in the ranges between –30 dB and –40 dB. The peak sidelobe level variations in the plane perpendicular to the offset plane at X-band are shown in Figure 39. At lower frequency ranges, a slight higher peak sidelobe level is observed for both the single and dual layer, but the peak sidelobe level for the dual layer is not degraded compared to the single layer case. Figure 40 shows the axial ratio variations in the plane perpendicular to the offset plane at broadside. It shows an axial ratio less than 3 dB for all frequency ranges tested. Best axial ratio obtained is 1.24 dB for the single layer and 1.04 dB for the dual layer at 8.5 GHz. No significant degradation is observed in the axial ratio due to the bottom Ka-band layer.

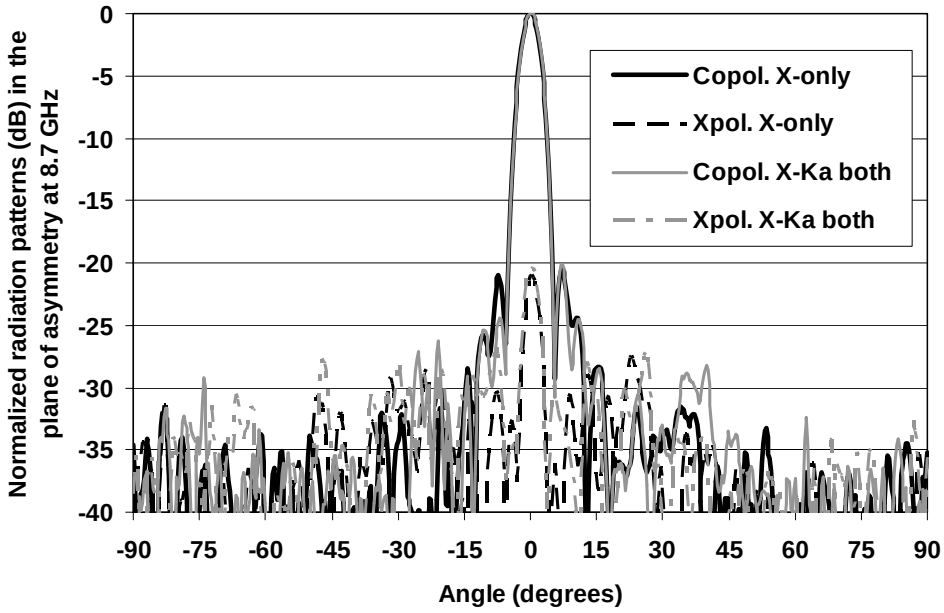

Fig. 38. Normalized radiation patterns in the plane perpendicular to the offset plane at 8.7 GHz.

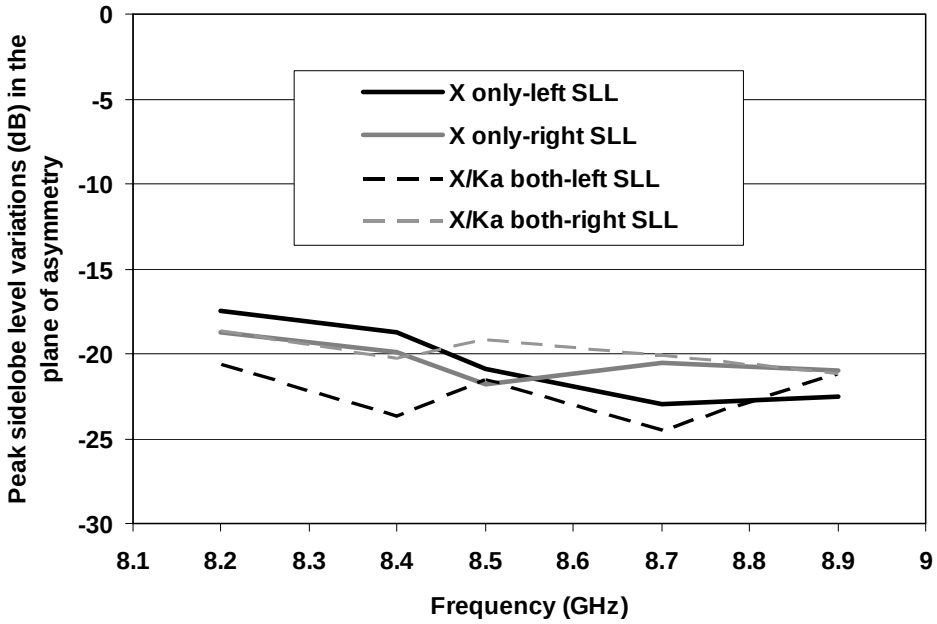

Fig. 39. Peak sidelobe level variations in the plane perpendicular to the offset plane at X-band.

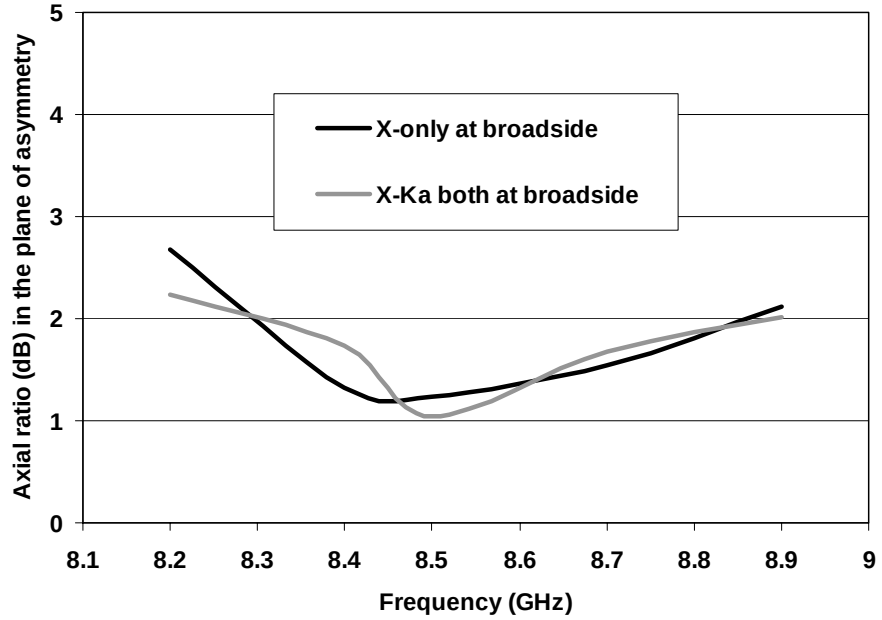

Fig. 40. Axial ratios versus frequency in the plane perpendicular to the offset plane at X-band.

Normalized radiation patterns in the offset plane at 8.7 GHz are shown in Figure 41. In the plane of symmetry, only the dual layer case is tested and no major effort is made to find the right focal point. The main beam is scanned 23.13^{o} off the broadside direction and the 3 dB beam width is 4.55^{o}. The measured scan angle is quite off from the designed scan angle showing misalignment of the feed horn to the true focal point. The peak sidelobe levels are –20.46 dB and –19.83 dB (left/right side) down from the main beam. The left cross-polarization level is 17.6 dB below the peak right-hand CP gain, which corresponds to the axial ratio of 2.31 dB. The peak sidelobe level variations are shown in Figure 42. The worst peak sidelobe level measured is –15.1 dB at 8.9 GHz. The measured axial ratio at 24^{o} in the offset plane is shown in Figure 43. It is observed that the axial ratio is degraded fluctuating around 3 dB showing the effect of misalignment on the axial ratio. Less than 3 dB axial ratio is observed only from 8.5 GHz to 8.7 GHz.

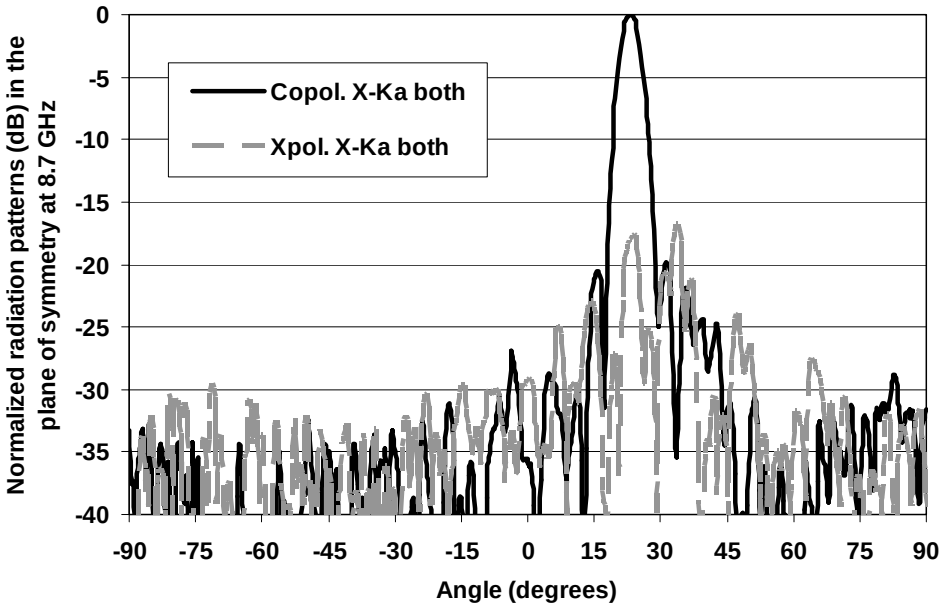

Fig. 41. Normalized radiation patterns in the offset plane at 8.7 GHz.

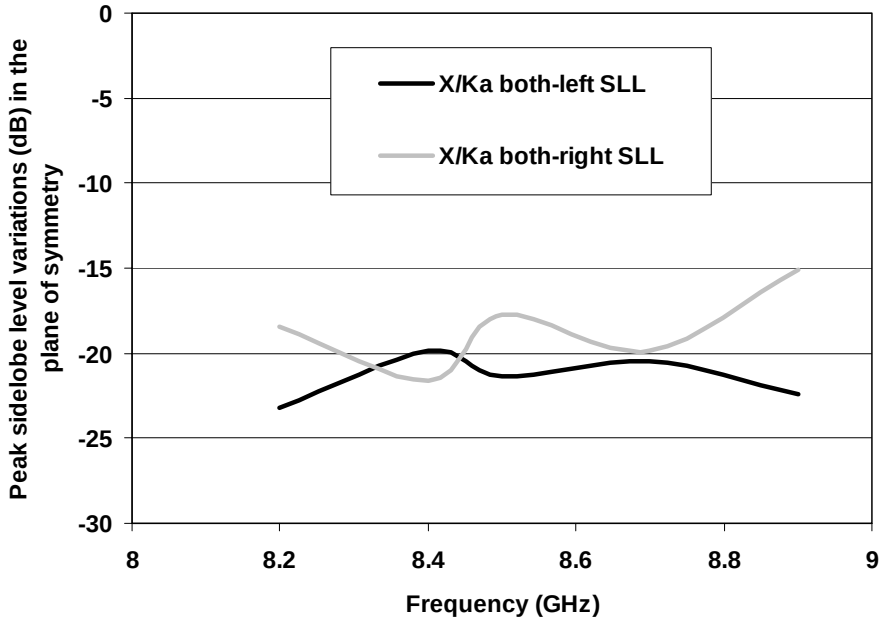

Fig. 42. Peak sidelobe level variations in the offset plane at X-band.

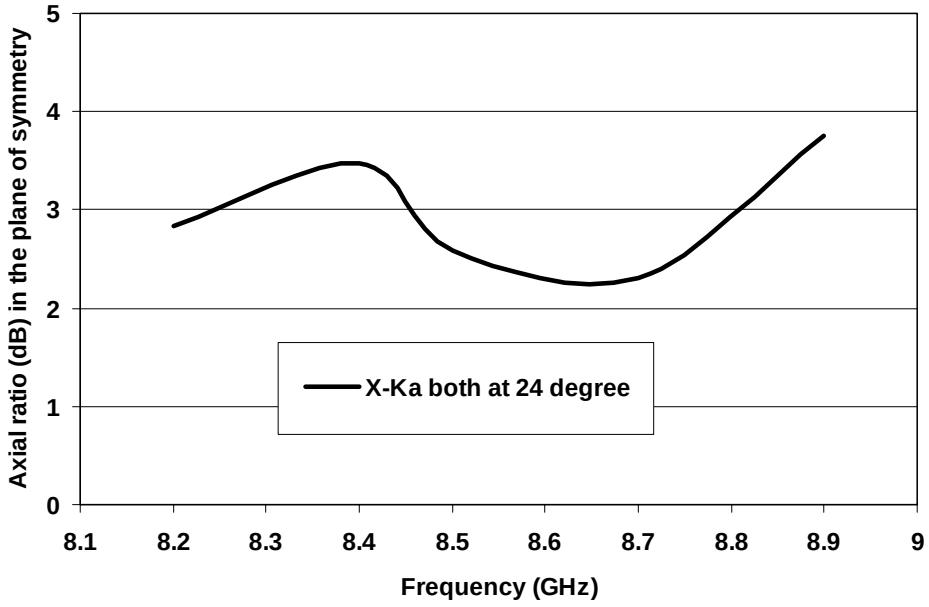

Fig. 43. Axial ratio versus frequency in the offset plane at X-band.

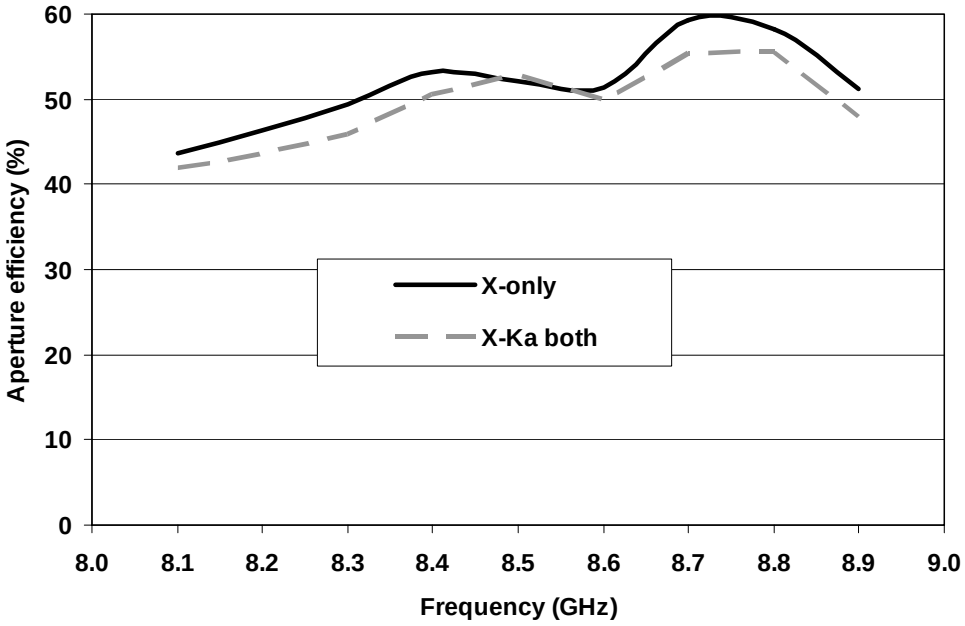

Fig. 44. Measured aperture efficiencies versus frequency at X-band.

The measured aperture efficiencies versus frequency at X-band are shown in Figure 44. The highest efficiency is 59.2 % for the single layer and 55.4 % for the dual layer at 8.7 GHz. The peak gain for the dual layer is reduced by 0.15 dB~0.3 dB compared to the single layer gain. Greater than 50 % efficiency is observed between 8.4 GHz and 8.8 GHz for the dual layer. Some of radiation patterns are attached in Appendix B2.

5. Conclusions

An offset-fed X/Ka-dual-band reflectarray is presented using inflatable thin membranes. With new topology adopted to incorporate the thin membrane structure for dual-band operation, it achieved more than 50 % efficiencies at both frequency bands. The measured 3 dB-gain bandwidths are 800 MHz at X-band and 1.7 GHz at Ka-band. The CP bandwidths are also extremely wide. It achieved more than 9.5 % at X-band and much wider than 5.3 % at Ka-band. This relatively wide CP bandwidth is partially due to the large f/D ratios of 0.9 at X-band and 1.08 at Ka-band. In addition, the relatively thick foam materials at both bands help improve the CP bandwidth performance. In final space applications, these foam spacers will be replaced by empty spaces. In general, the reflectarray shows better performance (efficiency, sidelobe and cross-pol. levels) at Ka-band than at X-band. This is because the Ka-band reflectarray is electrically larger in size than the X-band reflectarray. The results of the overall performance for both bands are summarized in Table II. The proposed scheme is expected to be a good candidate for even larger high-gain aperture antennas in future space inflatable applications.

Table II. Performance summary for an offset-fed reflectarrays using thin membranes.

Performance Parameters	X-band only	X-band with Ka-band layer		Ka-band only		Ka-band with X-band layer	
Scan plane	0^o	0^o	25^o	0^o	25^o	0^o	25^o
Frequency (GHz)	8.7	8.7		32.2		32.2	
CP gain (dBic)	30.89	30.6		42.36		41.32	
Efficiency (%)	59.2	55.4		60.6		47.0	
Cross-pol. (dB)	-21	-20.3	-17.6	-34	-34	-31.5	-31.8
Peak sidelobe. (dB)	-20.5	-20.1	-19.8	-19.3	-17	-19.9	-17.8
Beamwidth	4.39^o	4.39^o	4.55^o	1.16^o	1.29^o	1.16^o	1.25^o
CP bandwidth (MHz)	> 800	> 800	> 500	> 1700		> 1700	

CHAPTER IV

CASSEGRAIN OFFSET SUB-REFLECTOR-FED X/KA DUAL-BAND REFLECTARRAY WITH THIN MEMBRANES*

1. Introduction

In recent years, there has been a growing demand for large aperture antennas in modern communication and deep-space satellites and ground antenna systems. However, current technology precludes the deployment of very large aperture antennas because of weight and volume constraints. To provide cost-effective solutions featuring very low weight and low conformable packaged volume, the concept of an inflatable reflector has been proposed and experimented in the past [33-34]. Yet, the greatest concern to achieve and to maintain surface shape accuracies in real implementation has prompted the reflectarray antenna architecture which allows the use of a flat surface instead of a parabolic antenna surface. It is believed that the flat reflecting surface is comparatively easier to fabricate, package, and maintain in structure than a curved surface.

The objective of this study is to develop a 0.75 meter Cassegrain offset sub-reflector-fed X/Ka dual-band reflectarray antenna using thin membranes. The use of thin membranes has been reported in [24]. In [24], low-dielectric constant foam layers are inserted below both the X and Ka-band membranes to act as support structures and to avoid the risks of thin substrates. In the current work, the reflectarray is made of the same thin

* © 2006 IEEE. Parts of this chapter are reprinted, with permission, from C. Han, J. Huang and K. Chang, "Cassegrain offset sub-reflector-fed X/Ka dual-band reflectarray with thin membranes," accepted by *IEEE Trans. Antennas Propagat.*

materials with their thickness equal to 0.0508 mm for both layers. The reflectarray utilizes the annular ring elments to achieve circular polarization since the preceding work reported in [21-24] showed good electrical performance. To mock-up most likely future spacecraft launch configuration, Cassegrain offset dual-reflector system [42-53] consisting of a main reflectarray surface and a small metallic sub-reflector feed is considered here.

One of advantages of the Cassegrain offset dual-reflector antenna [42] is the ability to place the feed in a convenient position, while utilizing main reflector (MR) as the focusing element. Compared with single reflector, it obtains an equivalent focal length much greater than the physical length. In addition, dual-reflector configurations present lower noise due to the limited noise introduced by the feed spillover beyond the sub-reflector. This is because it is directed to cold sky rather than noisy ground as in the single reflector case. With the addition of the sub-reflector, more degrees of freedom can be introduced to enhance the electrical performance such as by cancelling cross-polarizations in offset systems, or by prescribing the main aperture amplitude and phase distributions in dual shaped reflectors.

The sub-reflector profile, which is a convex hyperboloid, has been determined following the general design procedure presented in [52-53]. In addition to the fabrication of the sub-reflector, two microstrip feed arrays are designed to illuminate the sub-reflector's surface at each frequency band. The designed microstrip patch antenna arrays are left-hand circularly polarized so that incident wave to the main reflectarray becomes right-handed upon reflection from the sub-reflector. As presented in [24] for dual-band operation, same layer topology is adopted with Ka-band ring element arrays located at the bottom layer due to the large number of elements occupied at Ka-band.

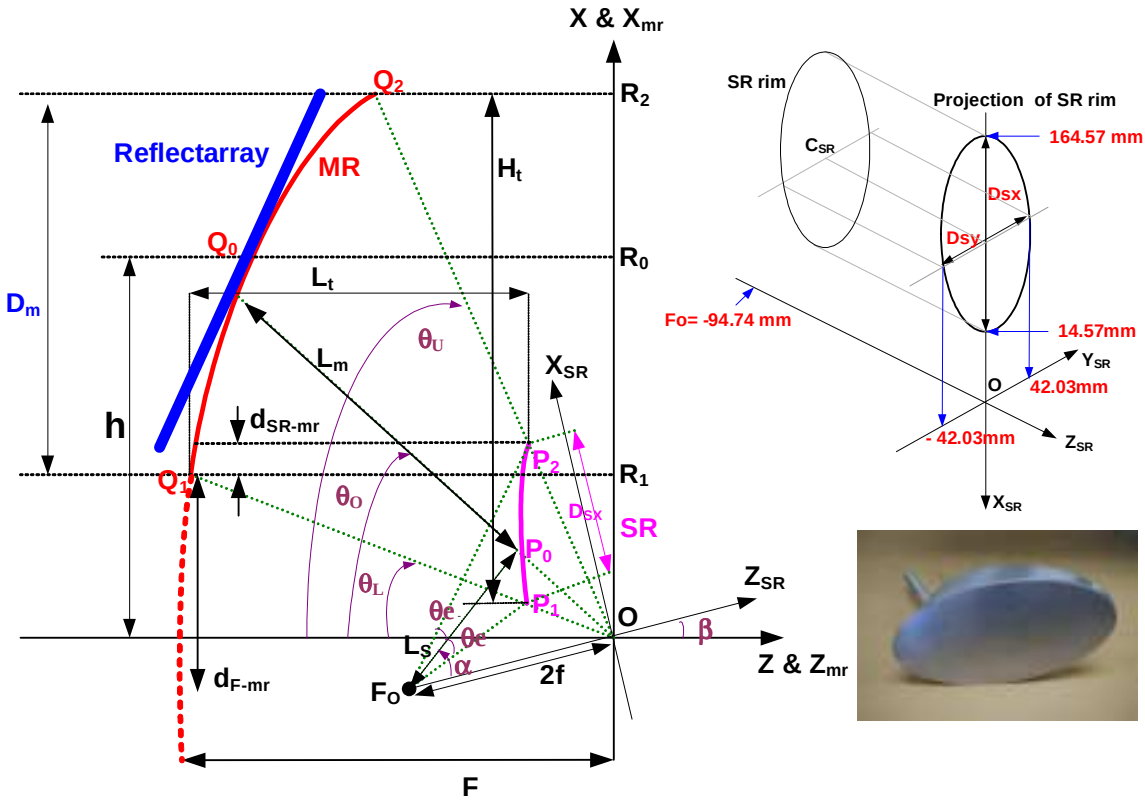

Fig. 45. The offset Cassegrain geometry and the projected sub-reflector rim shape with photo of fabricated sub-reflector.

2. Cassegrain sub-reflector design

The geometries of the offset Cassegrain antenna and the projected sub-reflector (SR) rim shape in the SR coordinate system are shown in Figure 45 with a photo of the fabricated sub-reflector. The parabolic main reflector is described by the diameter D_m of its *xy* plane projected circular aperture, focal length F, and offset distance h. The sub-reflector has a projected aperture in the *xy* plane with a major axis D_{SX} and minor axis

D_{Sy} , axis tilt angle β, interfocal distance *2f*, and eccentricity *e*. The feed parameters are the sub-reflector edge angle θ_e, as observed from the reflector system focus, and the feed pointing angle α. Two additional parameters are the clearance d_{SR-mr} between the top of the sub-reflector and the bottom of the main reflector, and the total length L_t of the antenna system. All the design parameters are described in Table 3.

Following the general design rule described in [52-53], all the parameters were determined as shown in Table 4 with five initial parameters of D_m, F, h, β , and D_{SX}. To minimize the height of the overall antenna system, the sub-reflector was moved in beyond the bottom edge of the main reflector resulting in negative d_{SR-mr} value . One thing to note that is, originally the scan angle designed was 30^o in the plane of symmetry (offset-plane, XZ-plane in Figure 45) and 0^o in the plane of asymmetry and it was initiated with respect to the boresight of the plane of the reflectarray's surface. When viewed with respect to the boresight of the equivalent virtual parabolic reflector's surface, it was re-evaluated to be 28^o.

Table 3. Design parameters of a Cassegrain dual-reflector system [16].

Parameter	Description
D_m	Diameter of the MR aperture when projected on the *xy* plane
F	Focal length of the MR
h	Offset of the MR (the distance between the point Q_0 on the MR coordinate system z_{mr} axis)
θ_0	Offset angle of MR
θ_U	Offset angle of the top of the MR
θ_L	Offset angle of the bottom of the MR
θ_e	Angle between the z_f axis and the edge of the SR
β	Tilt angle between the SR coordinate system z_{SR} axis and the MR coordinate system z_{mr} axis
e	SR eccentricity
a	SR surface parameter
f	SR surface parameter (half the interfocal distance, $f=ae$)
D_{SX}	Major axis of the SR elliptical aperture taken parallel to the x_{SR} axis
D_{SY}	Major axis of the SR elliptical aperture taken parallel to the y_{SR} axis
α	Tilt angle between the SR coordinate system z_{SR} axis and the feed coordinate system z_f axis
L_S	Distance between the focal point F_O and the point P_0 on the SR
L_m	Distance between the SR point P_O and the point Q_0 on the MR
$d_{SR\text{-}mr}$	Minimum vertical distance (along the *x* axis) between the SR edges and the MR edges
$d_{F\text{-}mr}$	Minimum vertical distance (along the *x* axis) between the feed F_O and the MR edge
L_t	Maximum length (along the *z* axis) of the two reflector combination
H_t	Maximum vertical length (along the *x* axis) of the two reflector combination
C_{SR}	Point expressed in the SR coordinate system defining the center of the SR elliptical aperture

Table 4. Calculated design values of a Cassegrain dual-reflector system.

Step	Parameter		Ka-band (32 GHz)	X-band (8.4 GHz)
	D_m	750 mm	80 λ_o	21 λ_o
	F	480 mm	51.2 λ_o	13.44 λ_o
	h	480 mm	51.2 λ_o	13.44 λ_o
	β	15 ^{o}	15^o	15^o
6	θ_e		20.9^o	20.9^o
1	θ_O		-53.13^o	-53.13^o
2	θ_U		-83.38^o	-83.38^o
3	θ_L		-12.48^o	-12.48^o
4	e		2.579	2.579
7	a	18.365 mm	1.959 λ_o	0.514 λ_o
8	f	47.37 mm	5.053 λ_o	1.326 λ_o
	D_{SX}	150 mm	16 λ_o	4.2 λ_o
15	D_{SY}	84.06 mm	8.96 λ_o	2.354 λ_o
5	α		33.22^o	33.22^o
9	L_s	89.68 mm	9.566 λ_o	2.511 λ_o
10	L_m	547.05 mm	58.35 λ_o	15.317 λ_o
12	$d_{SR\text{-}mr}$	- 0.237 mm	- 6.425 λ_o	- 1.687 λ_o
11	$d_{F\text{-}mr}$	129.52 mm	13.81 λ_o	3.626 λ_o
13	L_t	455.07 mm	48.54 λ_o	12.74 λ_o
14	H_t	848.17 mm	90.47 λ_o	23.75 λ_o
16	C_{SR}	Xc_{SR}	9.55 λ_o	2.508 λ_o
		Zc_{SR}	-0.583 λ_o	-0.153 λ_o

3. Feed array design

Microstrip patch antenna arrays are designed to illuminate the surface of the sub-reflector. The truncated corners square patch element is chosen to generate a left-hand circular polarization [54]. The substrate material used is Duroid 5870 with a dielectric constant of 2.33 with 0.7874 mm (31 mils) thickness for X-band and Duroid 5880 with a dielectric constant of 2.2 with 0.254 mm (10 mils) thickness for Ka-band. The substrate material is chosen considering the input VSWR and the axial ratio. When the thickness of the substrate material is reduced, the input VSWR improves while the axial ratio degrades [54].

In designing the microstrip patch arrays, the size of array should be carefully selected. Table 5 shows the sub-reflector parameters to be considered in the feed array design. D_{SX} and D_{SY} are the major axes of the sub-reflector's elliptical aperture taken parallel to the X_{SR}, Y_{SR} axis respectively. The parameter θ_e is the angle between the feed axis and the edge of the sub-reflector. L_S is the distance between the feed focal point and the center of the sub-reflector.

Table 5. Sub-reflector parameters to be considered in the feed design.

	D_{sx}	D_{sy}	θ_e	L_S at 32 GHz	L_S at 8.4 GHz
Sub-reflector parameters	150 mm	84.06 mm	20.91^o	9.56 λ_o (far field)	2.51 λ_o (near field)

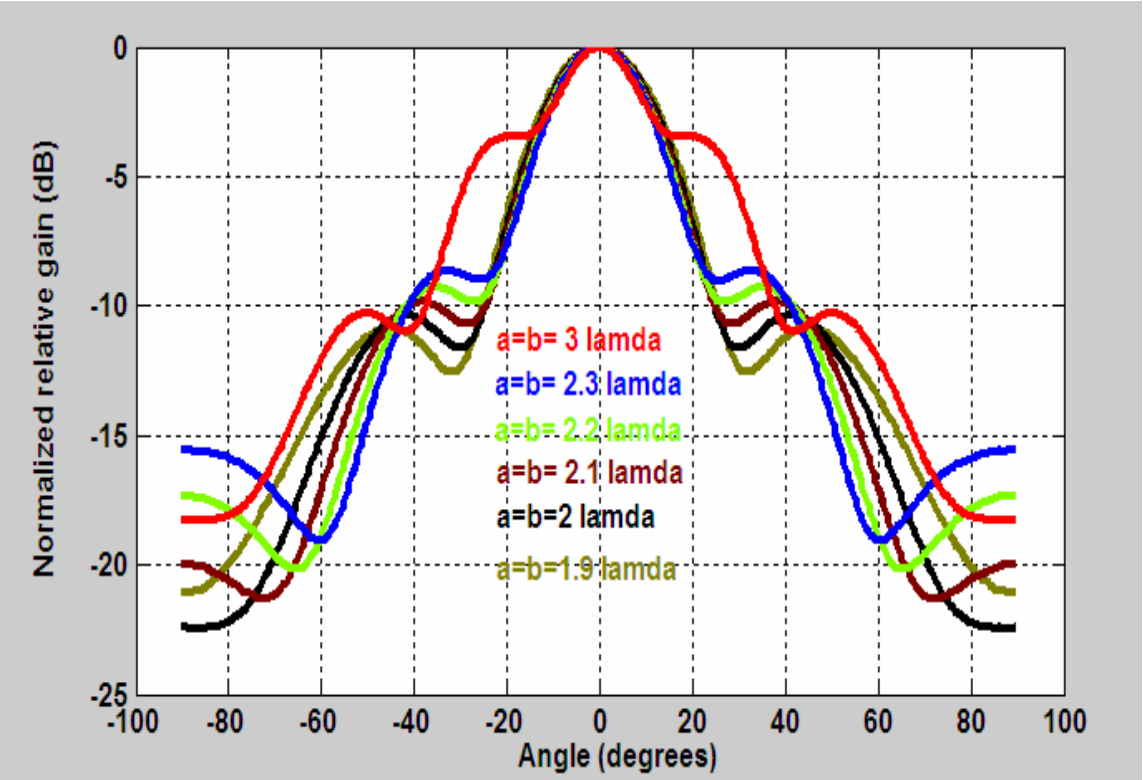

Fig. 46. Normalized radiation patterns at a distance of r=2.5 λ_o versus aperture size.

Assuming 2 λ_o rectangular aperture size, the minimum distance to the far field region is 8 λ_o. In Table 5, by looking at the distance L_S, it can be seen that the sub-reflector lies in the far field region at Ka-band and in the near field region at X-band. Figure 46 shows a normalized near field radiation pattern [55] for a rectangular aperture size of a by b at a distance of 2.5 λ_o at 8.4 GHz. The field over the opening is assumed to be uniform. Initially it is expected that using a large array will take care of the possible beam broadening effects of near field operation at X-band. However, the near field pattern shows that although the main beam is narrower, the sidelobe level goes up

quickly for an aperture size greater than 2.3 λ_o because the physical range L_S looks even shorter (even more near field region) in terms of wavelength for a large aperture. For an aperture size of 2.1 λ_o, approximately -8 dB feed taper is seen at an angle of 21^o.

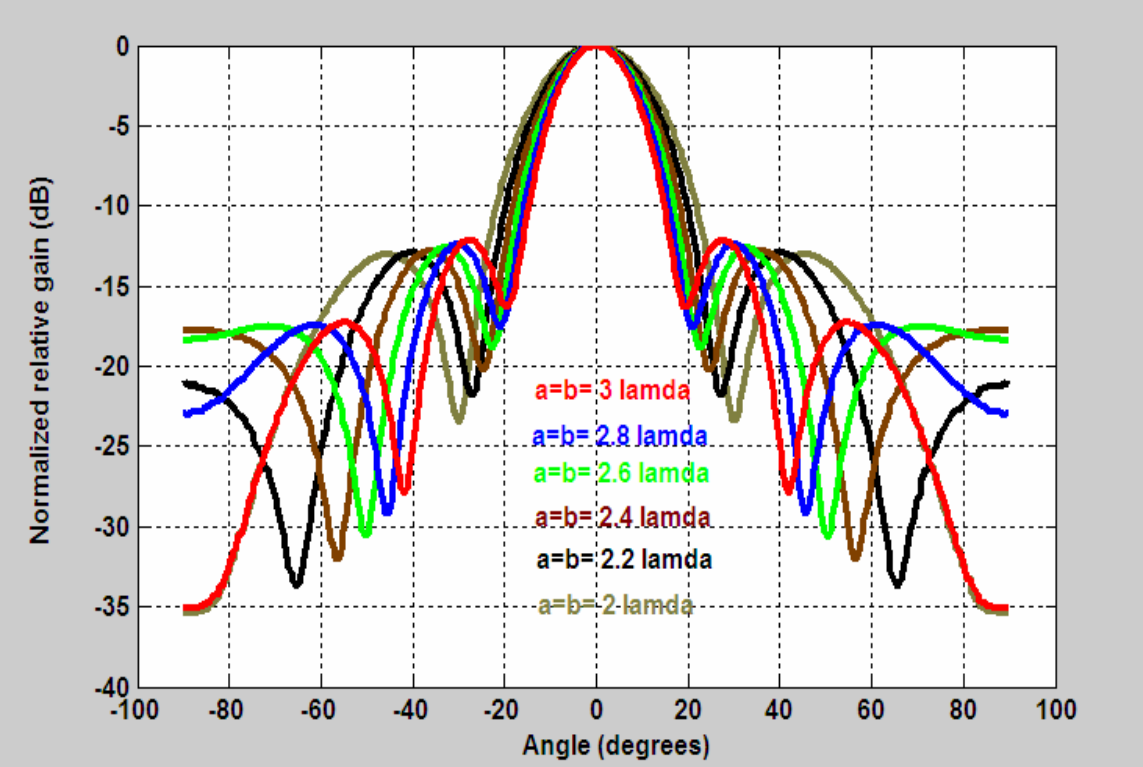

Fig. 47. Normalized radiation patterns at a distance of r=9.5 λ_o versus aperture size.

Figure 47 shows a normalized radiation pattern at a distance of 9.5 λ_o at 32 GHz. The feed taper between –10 dB and –15 dB is observed for an aperture size of 2.2 λ_o, 2.4 λ_o and 2.6 λ_o at an angle of 21^o.

4 by 4 feed arrays, assuming aperture size close to 2 λ_o, are designed at both bands as shown in Figure 48. With the aid of Zeland's IE3D, first 2 by 2 subarrays are constructed with sequential rotations to achieve a left-hand circular polarization. Then the subarrays are one more time rotated sequentially in 0 degrees, -90 degrees, -180 degrees, and –270 degrees to improve CP bandwidth performance [56-58]. In combining each subarray, the 360^o delay lines are added in the top and bottom part of the microstrip feed lines. The minimum line width used is 0.15 mm because of fabrication tolerance in the etching process. The element spacing chosen is 0.588 free-space wavelengths at X-band and 0.64 free-space wavelengths at Ka-band. The probe feed is used to excite the microstrip antenna arrays.

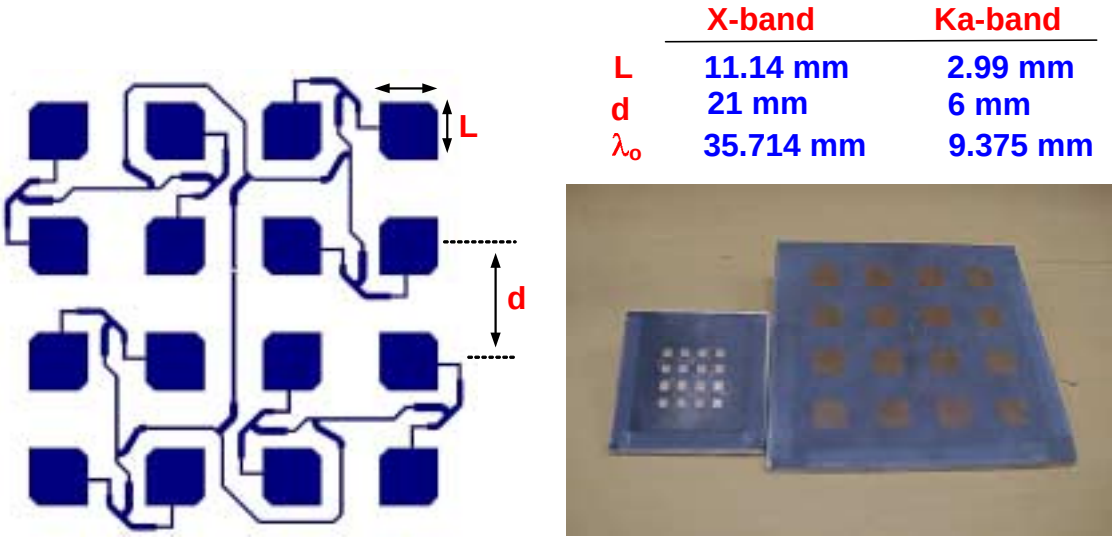

(a) (b)

Fig. 48. Feed arrays at both X and Ka-bands: (a) schematic of feed arrays; (b) photo of fabricated feed arrays.

A. Measured results of X-band feed array

The measured return loss characteristic at X-band is shown in Figure 49. The return loss at 8.4 GHz is –14.12 dB and less than –10 dB return loss is observed from 8.2 GHz to 8.7 GHz. The typical measured CP radiation patterns for X-band feed arrays and the corresponding axial ratios are shown in Figures 50 and 51. The best axial ratio of 0.4 dB occurs at 8.5 GHz. Less than 2 dB axial ratio is observed below 8.55 GHz and the worst axial ratio is 3.1 dB at 8.6 GHz.

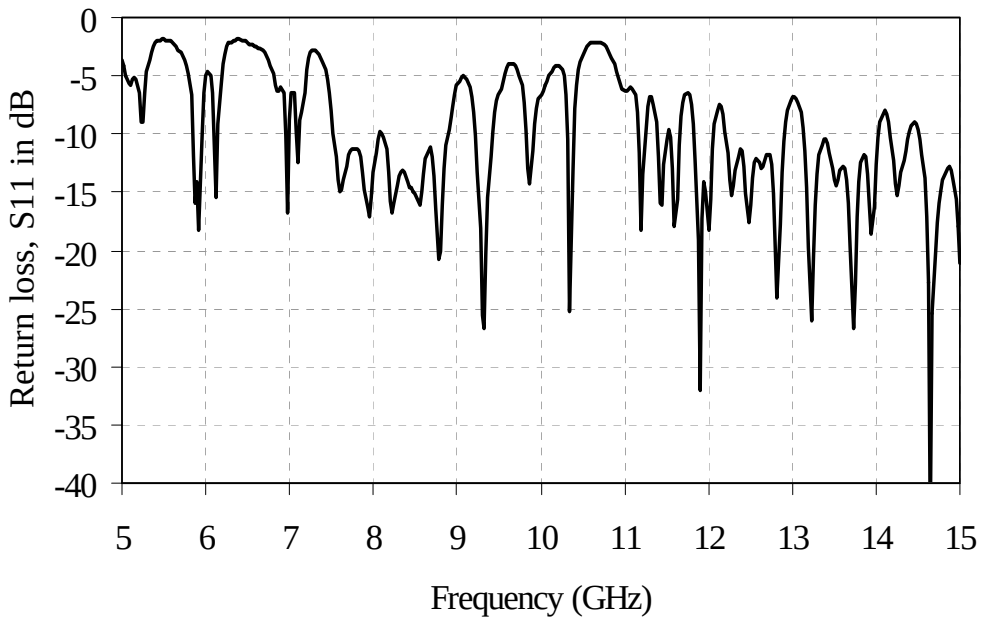

Fig. 49. Measured return loss at X-band.

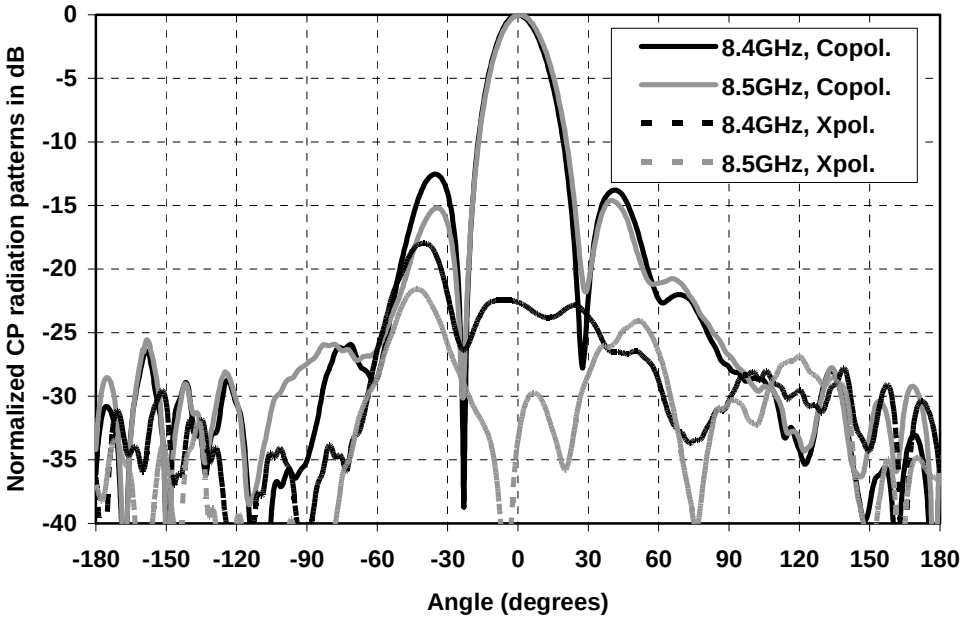

Fig. 50. Normalized CP radiation patterns for X-band feed arrays.

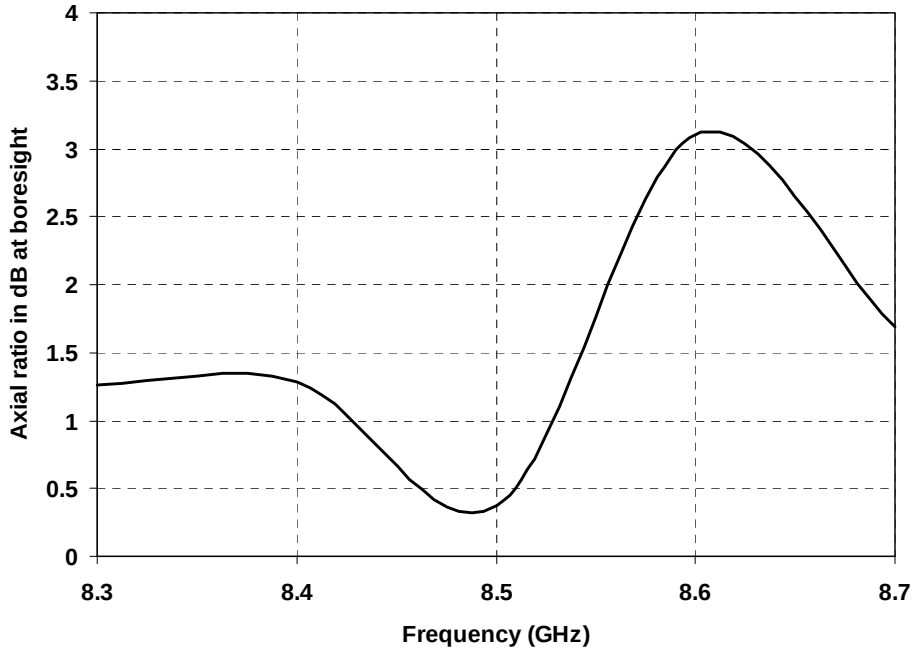

Fig. 51. Axial ratio in dB at boresight for X-band feed arrays.

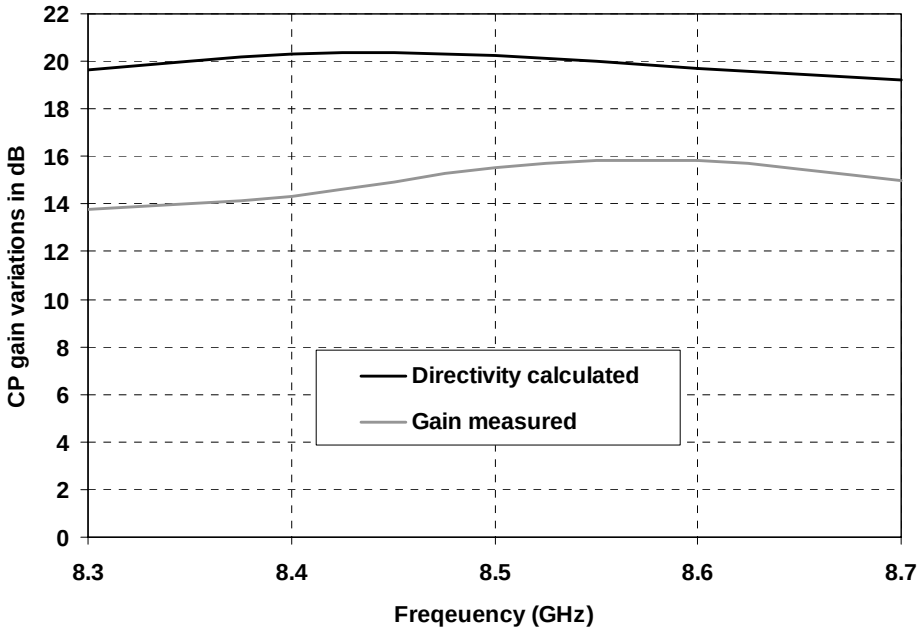

Fig. 52. Gain and directivity variations versus frequency for X-band feed arrays.

Initially, the subreflector edge angle, which is observed from the reflector system focus, was designed to be 21^{o}. But because the actual phase center on the surface of the sub-reflector at X-band was moved upward in the real implementation of the reflectarray, the sub-reflector edge angle has been changed to be 15^{o} at the upper edge and 18^{o} at the lower edge. In Figure 50, the far field feed taper at these angles are -7.3 dB and -8.5 dB for both the upper and lower edge tip of the sub-reflector respectively. The gain and directivity variations are shown in Figure 52. The directivity shown in Figure 52 is calculated based on the measured co-polarized (left-handed) pattern. Since the CP antenna has two orthogonal polarization components, the partial directivities, D_{θ} and

D_ϕ of an antenna for the θ and ϕ components are needed and the total maximum directivity D_o is simply sum of D_θ and D_ϕ. The partial directivities, D_θ and D_ϕ are written as [28]

$$D_\theta = \frac{4\pi U_\theta}{(\mathrm{P}_{rad})_\theta + (\mathrm{P}_{rad})_\phi} \tag{20}$$

$$D_\phi = \frac{4\pi U_\phi}{(\mathrm{P}_{rad})_\theta + (\mathrm{P}_{rad})_\phi} \tag{21}$$

Where U_θ, U_ϕ are radiation intensities in a given direction and $(\mathrm{P}_{rad})_\theta, (\mathrm{P}_{rad})_\phi$ are total radiated powers obtained by integrating the measured radiation power pattern in a given direction. One thing to note is that the X-band feed arrays are located at the near-field region. In other words, the feed power pattern becomes less directive on the sub-reflector's edge resulting in lower spillover efficiency.

B. Measured results of Ka-band feed array

For Ka-band, good input matching is obtained at 32 GHz with the return loss of –32 dB. The measured return loss characteristic is shown in Figure 53. The typical measured CP radiation patterns for Ka-band feed arrays and the corresponding axial ratios are shown in Figures 54 and 55. The best axial ratio of 0.3 dB occurs at 32.3 GHz and less than 3 dB axial ratio is observed from 31.8 GHz to 32.6 GHz. Like the X-band,

the phase center on the surface of the sub-reflector at Ka-band reflectarray was moved upward in the actual implementation of the Ka-band reflectarray. This movement occurs because the physical center of the microstrip reflectarrays on the reflectarray's surface has moved upward to reduce the interaction due to the sub-reflector, which is located beyond the bottom edge of the main reflector as shown in Figure 45. Consequently the sub-reflector edge angle has been changed to be 14^{o} at the upper edge and 21^{o} at the lower edge. In Figure 54, the far field feed taper at these angles are -6.0 dB and -15.5 dB for both the upper and lower edge tip of the sub-reflector, respectively. The gain and directivity variations are shown in Figure 56.

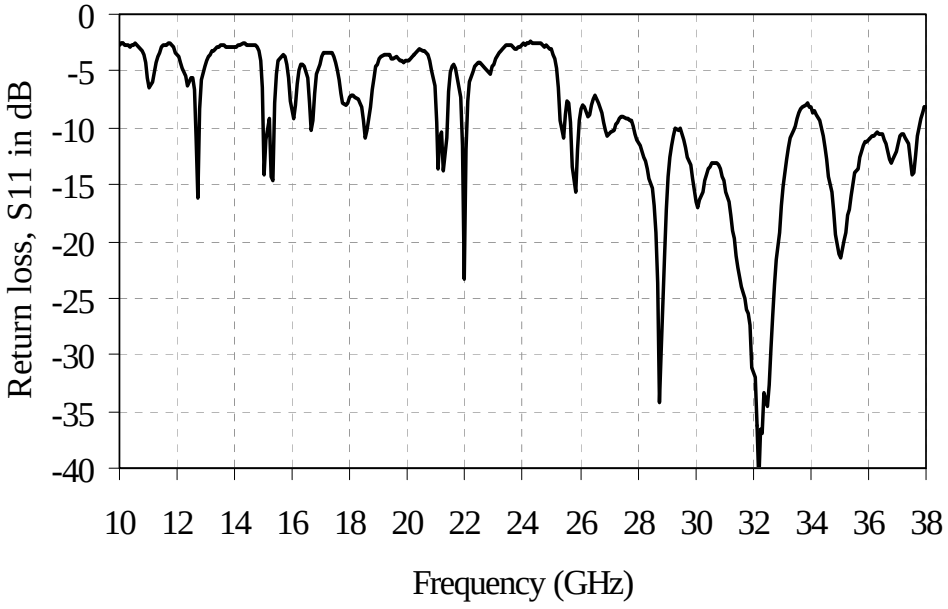

Fig. 53. Measured return loss at Ka-band.

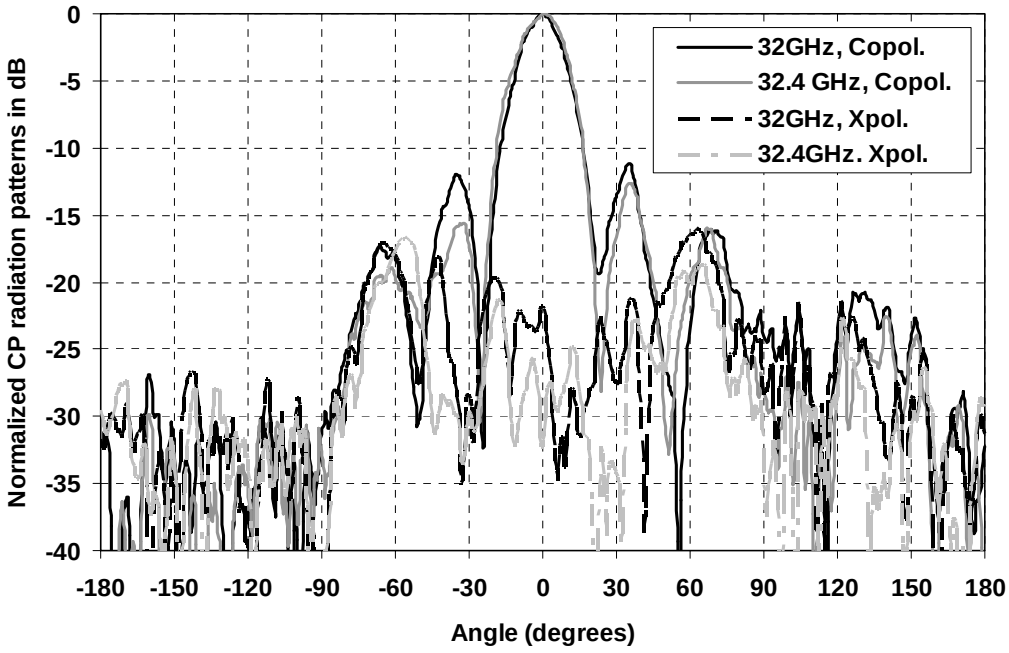

Fig. 54. Normalized CP radiation patterns for Ka-band feed arrays.

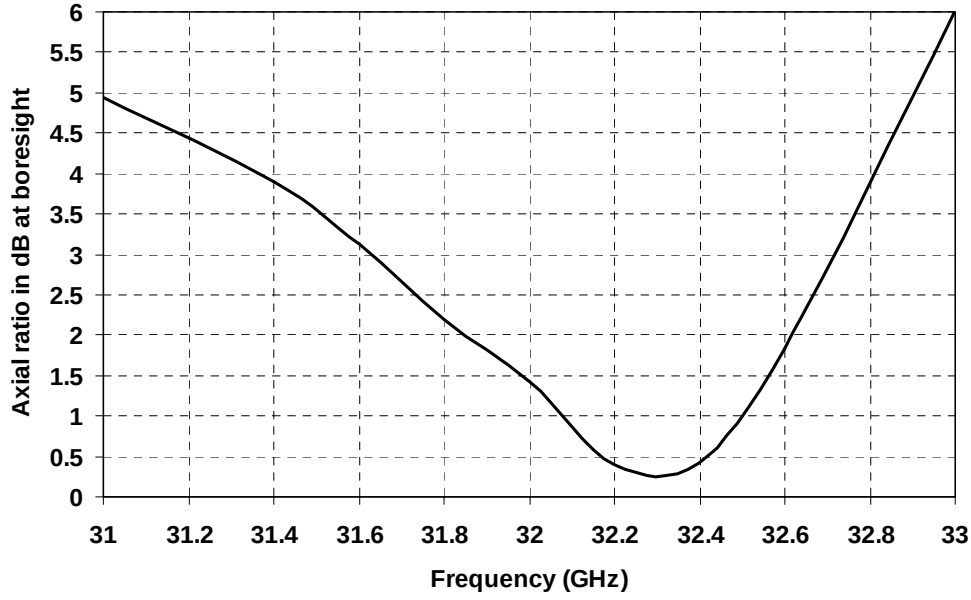

Fig. 55. Axial ratio in dB at boresight for Ka-band feed arrays.

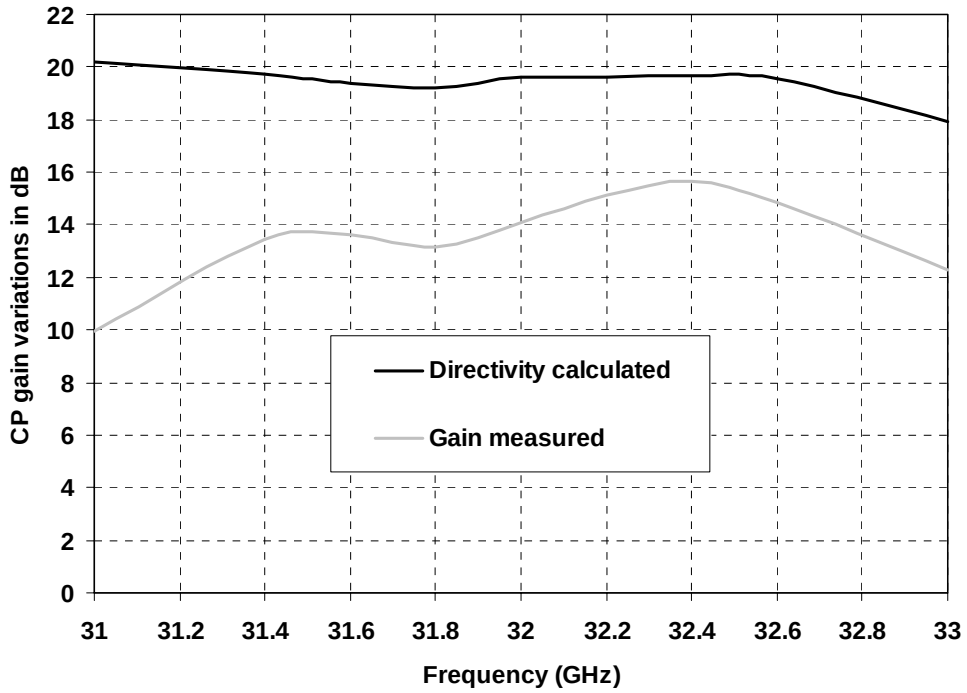

Fig. 56. Gain and directivity variations versus frequency for Ka-band feed arrays.

4. Offset reflecting antenna analysis

The analysis to calculate the needed phase delay is derived based on the comparison of the geometrical configurations between the dual reflector system and the flat microstrip reflectarray. The modified side view of the dual reflector system is shown in Figure 57. The real focal point of the system is located at F_o and the virtual focal point is located at F_e [48]. Since for a Cassegrain system, all parts of a wave originating at the real focal point, and then reflected from both reflector surfaces, travel equal distances as same as a wave originating at the virtual focal point, and then reflected from

the main reflector itself, the dual reflector system can be simply treated as the single-reflector case in phase calculations with its focal point located at F_e. The microstrip reflectarray elements are placed at (x_{re}, y_{re}, z_{re}) in the (x, y, z) coordinate system.

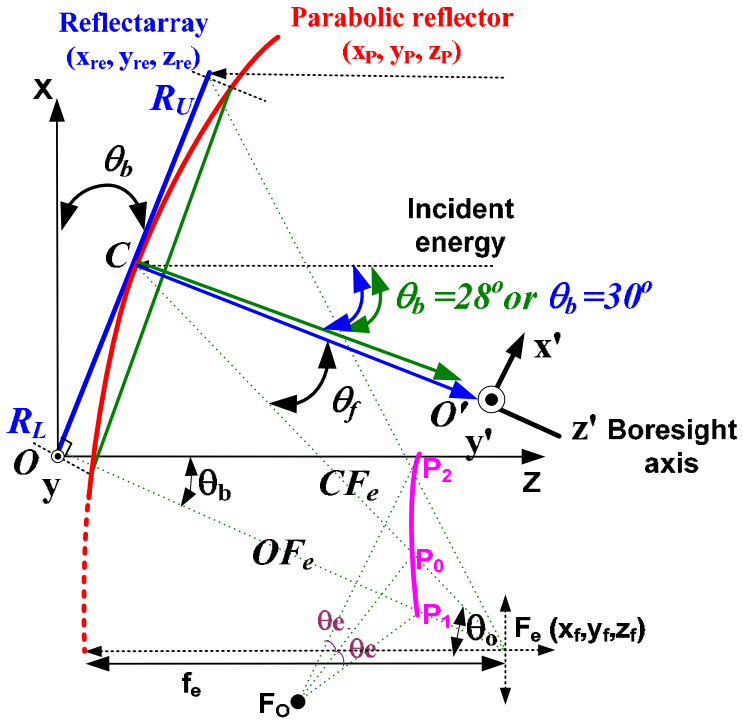

Fig. 57. Modified side view of the dual-reflector system.

Referring to Figure 57, and specifying the reflectarray's dimension, the vertical distance OF_e from the reflectarray's lower edge to the virtual feed, and the desired scan angle θ_b, the virtual phase center of the feed is

$$x_f = -OF_e \sin(\theta_b);\ y_f = 0;\ z_f = OF_e \cos(\theta_b) \tag{22}$$

From the virtual phase center of the feed, the subtended angle θ_0 can be determined with its corresponding equivalent focal length defined as

$$f_e = \frac{CF_e(1+\cos(\theta_0))}{2} \tag{23}$$

Since the center of the microstrip arrays on the reflectarray's surface lies on the surface formed by the parabolic reflector and the scan angle θ_b is already known.

Now the origin in the (x, y, z) coordinate system is redefined such that the virtual phase center (x_f, y_f, z_f) of the feed is placed at $(0, 0, f_e)$ and the (x_{re}, y_{re}, z_{re}) coordinates of the microstrip reflectarray elements are also transformed accordingly. The surface of a parabolic reflector is formed simply by expressing the value of z_p coordinate in terms of x_{re} and y_{re}. That is,

$$z_p = \frac{{x_{re}}^2 + {y_{re}}^2}{4 f_e} \tag{24}$$

Finally, the path difference is given by

$$\Delta l = \sqrt{{x_{re}}^2 + {y_{re}}^2 + (z_{re} - f_e)^2} - \sqrt{{x_{re}}^2 + {y_{re}}^2 + (z_p - f_e)^2} + z_p - z_{re} \tag{25}$$

One thing to note that is, originally the scan angle designed is 30^o in the plane of syemmetry (offset-plane) and 0^o in the plane of asymmetry. But as indicated in Figure 57, this scan angle is with repect to the boresight of the plane of the reflectarray's surface. The recalculated scan angle becomes 28^o when the angle is viewed with respect to the boresight of the virtual parabolic reflector's surface. In this study, the following locations in the MR coordinate system in Figure 45 are used to design the flat reflectarray as shown in Table 6.

Table 6. Locations of the reflectarray surface (units in mm).

Locations, (x_{re}, z_{re}) with $y_{re} = 0$	Lower tip	center	Upper tip
Initial location at both bands	(155.2,-547.5)	(480,-360)	(804.7,-172.5)
Modifed location at X-band	(257.8, -491)	(554, -320)	(881.3, -131)
Modifed location at Ka-band	(212.1,-517.4)	(554, -320)	(855.2, -146.1)

5. Experiments

A 0.75 meter reflectarray was fabricated on commercial Rogers R/flex 3000 liquid crystalline polymer (LCP) material with ε_r=2.9 and 0.0508 mm (2 mils) thickness for both layers. The ring elements are separated by 0.5 free-space wavelengths at 8.4 GHz and 32 GHz in both orthogonal directions. The scan angle designed is 28^o in the plane of symmetry (offset-plane, $x'z'$- plane in Figure 57) and 0^o in the plane of asymmetry ($y'z'$- plane in Figure 57), which is with respect to the boresight of the virtual parabolic

reflecctor's surface. Measurements were conducted at the Jet Propulsion Laboratory in the outdoor ranges using CP corrugated horn for the transmit antenna.

A. Test setup

The fixture was made to incorporate the sub-reflector and the feed array with the reflectarray antenna as shown in Figure 58. The detailed layout dimensions for the measurements at both bands are shown in Figures 59 and 60.

Fig. 58. A photo of the reflectarray incorporated with the sub-reflector and the feed array.

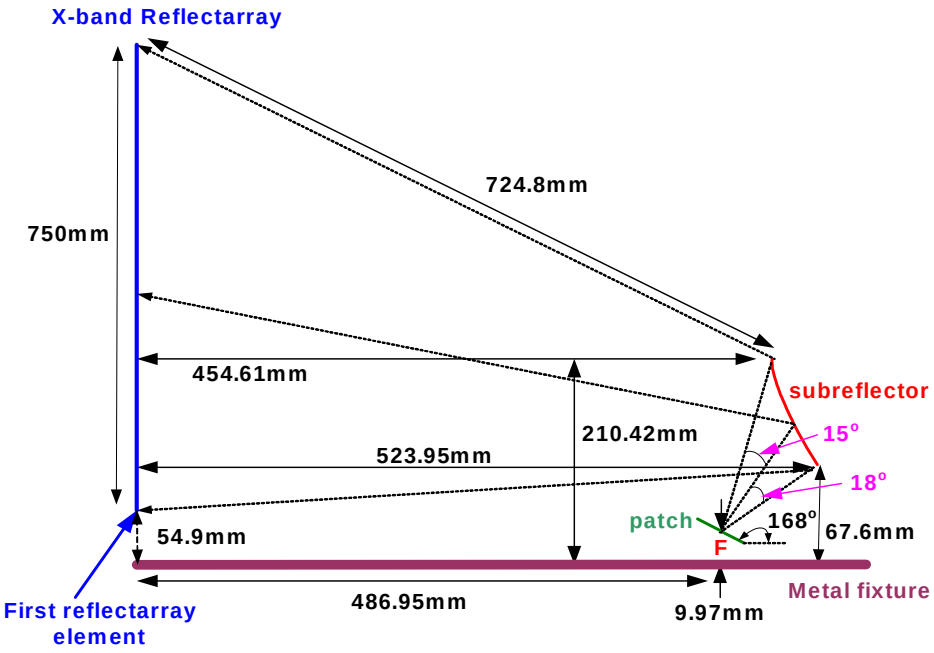

Fig. 59. Measurement layout dimensions for X-band reflectarray.

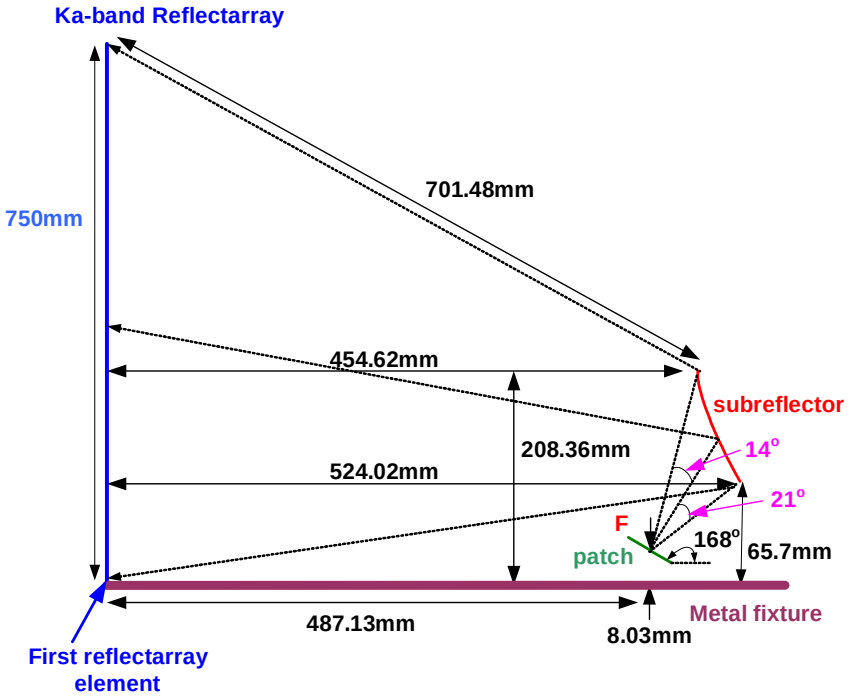

Fig. 60. Measurement layout dimensions for Ka-band reflectarray.

B. Measured results of X-band reflectarray

Typical normalized radiation patterns at 8.4 GHz for X-band reflectarray are shown in Figure 61. In Figure 61, the main beam (in (a)) is scanned 27^{o} off the broadside direction and the 3 dB beam width (in (a)) is 3.81^{o}. The measured scan angle is 1^{o} off from the designed scan angle, showing the misalignment of the measured antenna system.

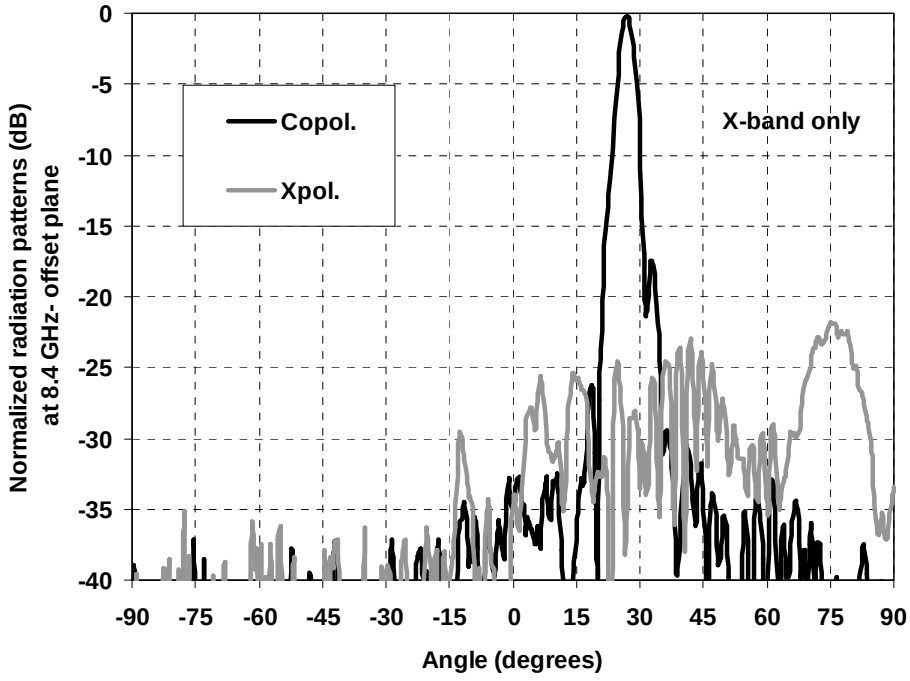

(a)

Fig. 61. Normalized CP radiation patterns at 8.4 GHz: (a) in the offset-plane for X-band only layer; (b) in the offset-plane for both X/Ka-band layer; (c) in the plane of asymmetry for X-band only layer; (d) in the plane of asymmetry for both X/Ka-band layer.

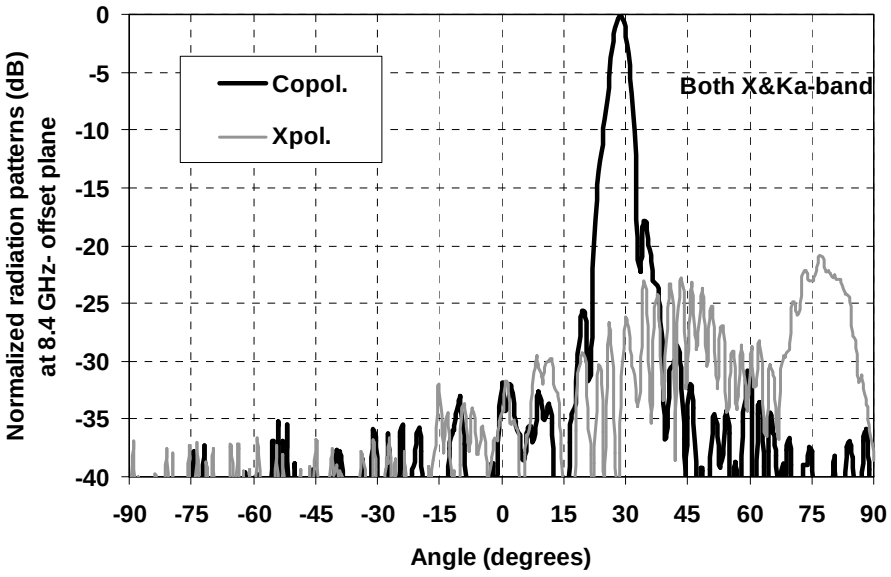

(b)

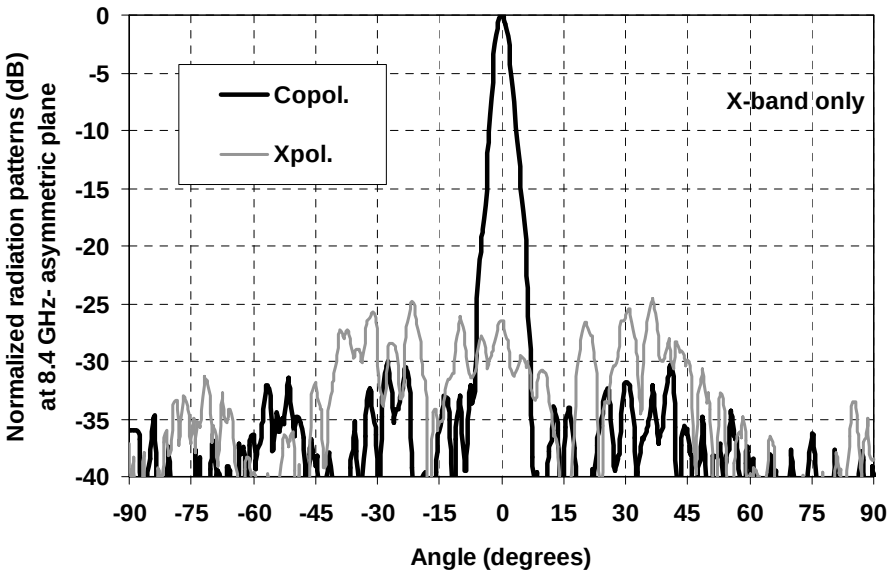

(c)

Fig. 61. Continued.

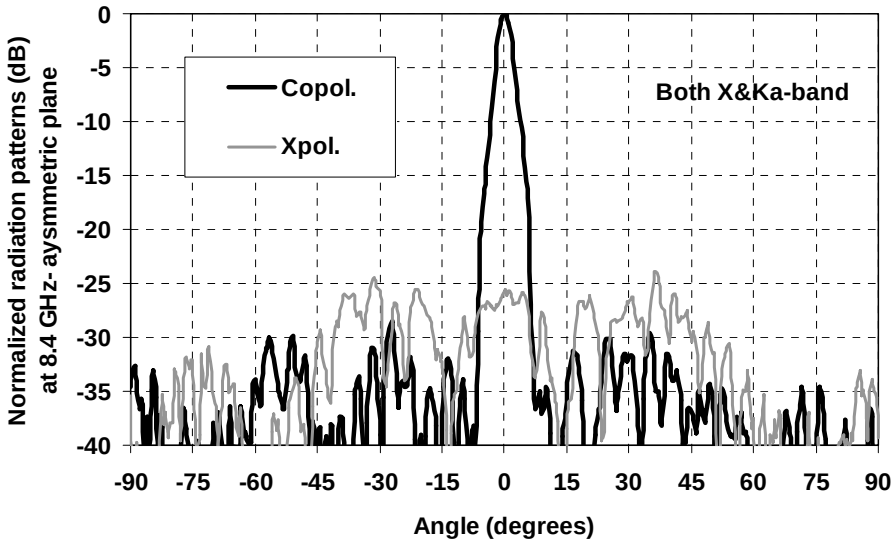

(d)

Fig. 61. Continued.

The peak sidelobe levels (in (a)) are 26.2 dB and 17.7 dB (left/right) down from the main beam. The cross-polarization level (in (a)) is 28 dB below the peak right-hand CP gain. As the frequency goes down to 8.0 GHz, the peak sidelobe level is degraded to -15.1 dB from the main beam. However, the cross-polarization level is still suppressed below -19 dB, which corresponds to the axial ratio of less than 2 dB. When the frequency goes up to 8.7 GHz, the peak sidelobe level is not much changed, but the cross-polarization level is degraded to -13.7 dB from the co-polarized beam peak.

The peak gains for the dual layer are reduced by 0.3-0.6 dB compared to the single layer gains except for 8.4 GHz. At 8.4 GHz, the peak gain for the dual layer is increased by 0.11 dB. This unusual increase in gain is probably due to the change of the

measurement setup under windy weather circumstance on the mountain. It is believed that the rigid mounting structure is needed to improve the overall alignment process. In the asymmetric planes of (c) and (d) in Figure 61, all the sidelobe levels are less than -30 dB and the most cross-polarization levels are suppressed below -25 dB from the co-polarized beam peak. The aperture efficiency is calculated from the measured data by comparing the measured co-polarized peak gain with the directivity, which is derived based on the physical aperture area. Also, the loss factor of feed arrays in Figure 52 is added to evaluate the pure aperture efficiency of the reflectarray itself. The measured aperture efficiencies versus frequency are shown in Figure 62. The highest efficiency is 48.5 % for the single layer and 49.8 % for the dual layer at 8.4 GHz. Greater than 40 % efficiency is observed between 8.2 GHz and 8.6 GHz for the dual layer case. Figure 63 shows the axial ratio variations versus frequency. It shows an axial ratio of less than 2 dB for all frequency ranges tested except for 8.7 GHz. At X-band, the size of feed arrays is found to be relatively large compared to the size of the sub-reflector. To reduce the possible spillover, the smaller feed arrays are advised. Some of radiation patterns are attached in Appendix C1.

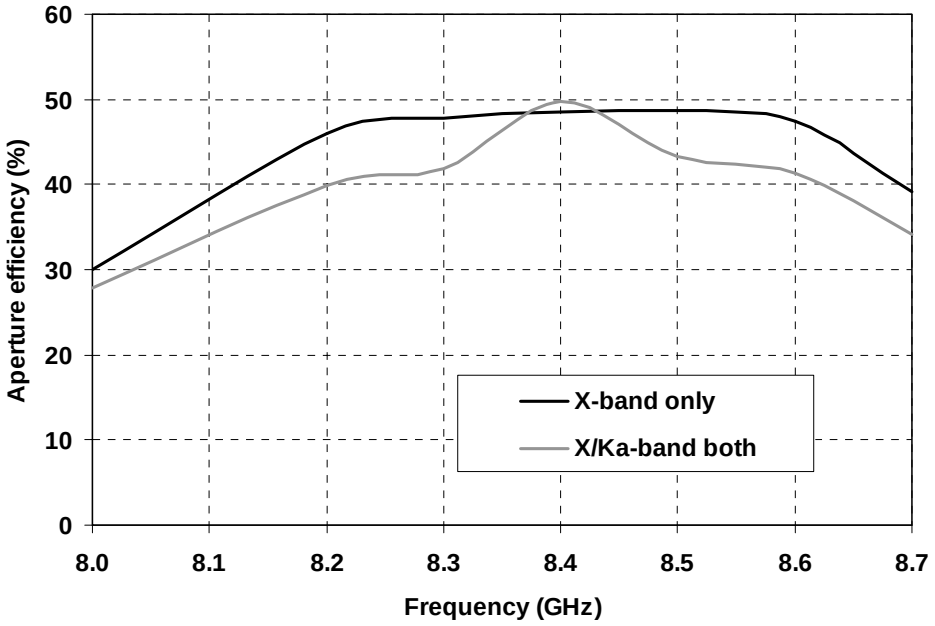

Fig. 62. Aperture efficiencies versus frequency at X-band.

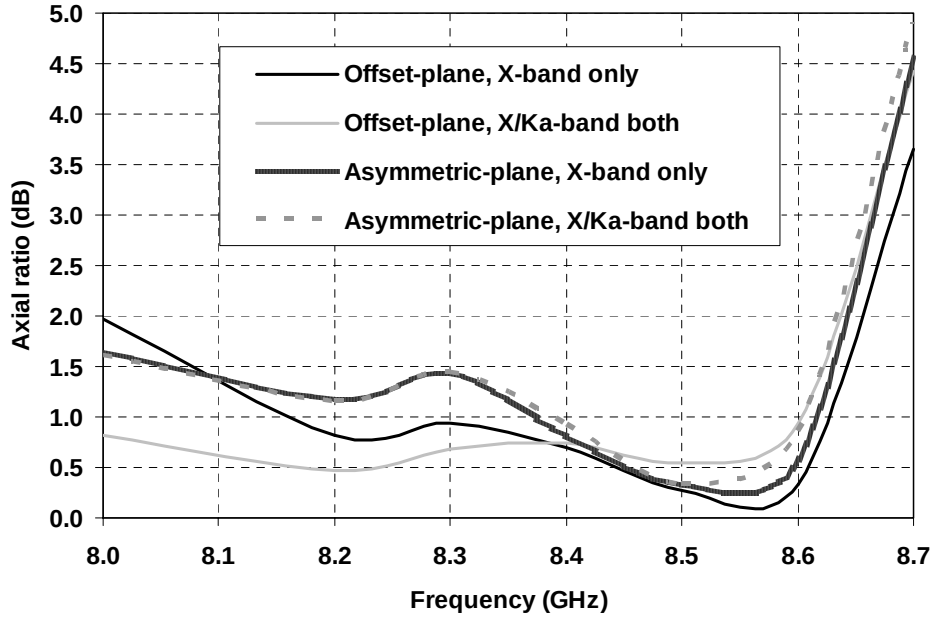

Fig. 63. Axial ratios versus frequency at X-band.

C. Measured results of Ka-band reflectarray

Typical normalized radiation patterns at 31.8 GHz for Ka-band reflectarray are shown in Figure 64. For the Ka-band only layer in the offset-plane, the main beam (in (a)) is scanned 28.2^{o} off the broadside direction and the 3 dB beam width is 1.08^{o}. The measured scan angle is very close to the desired scan angle.

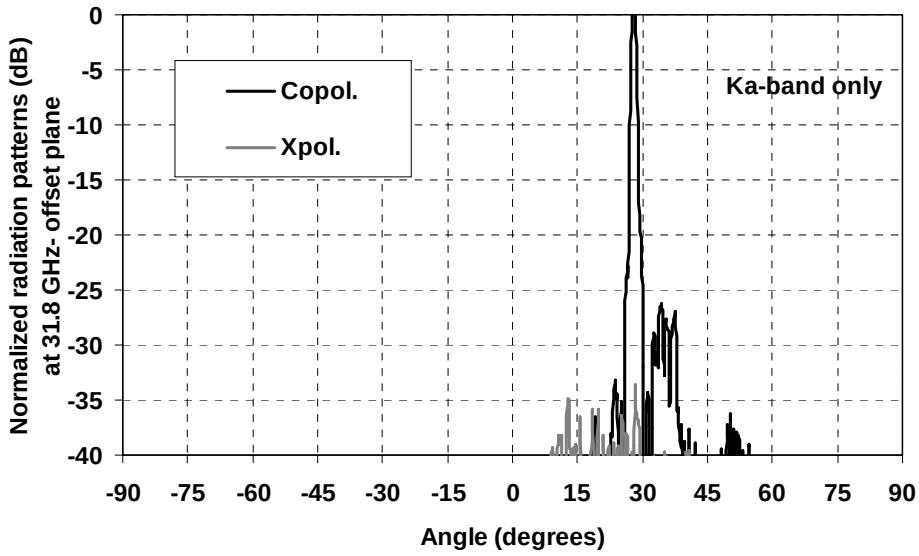

(a)

Fig. 64. Normalized CP radiation patterns at 31.8 GHz: (a) in the offset-plane for Ka-band only layer; (b) in the offset-plane for both X/Ka-band layer; (c) in the plane of asymmetry for Ka-band only layer; (d) in the plane of asymmetry for both X/Ka-band layer.

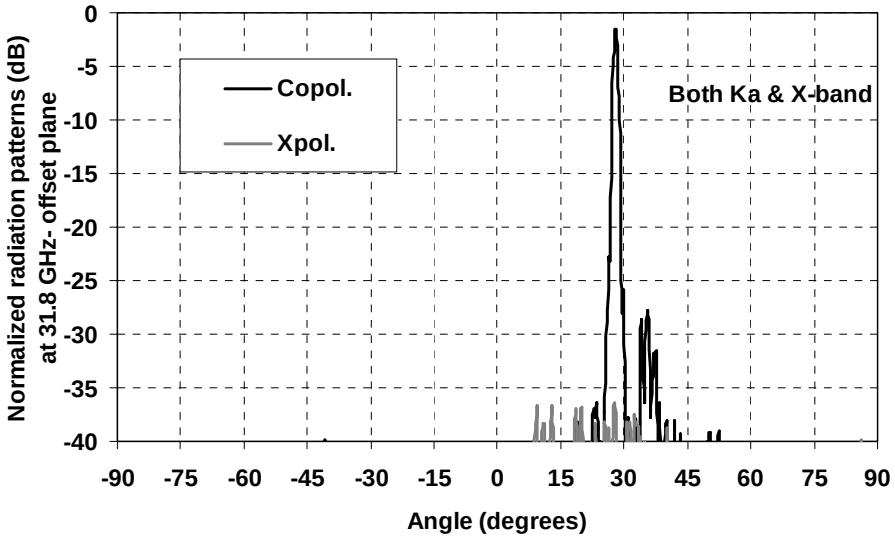

(b)

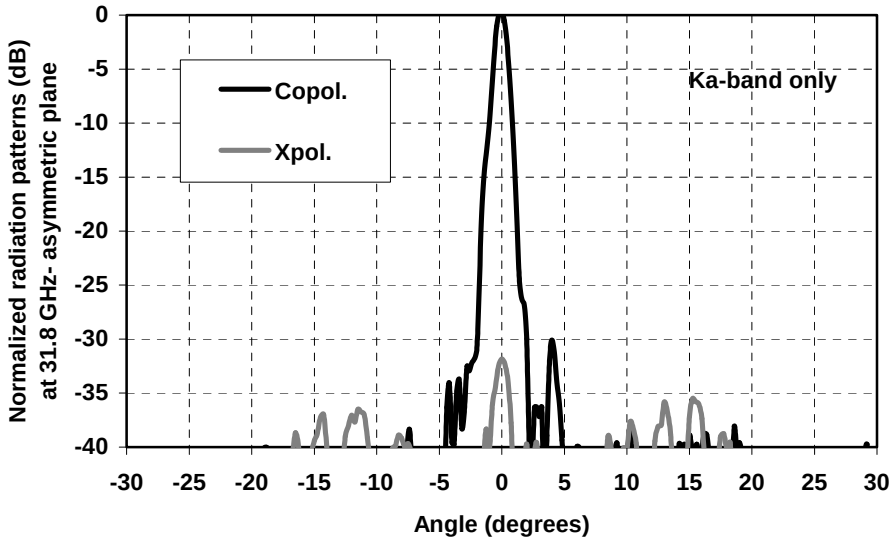

(c)

Fig. 64. Continued.

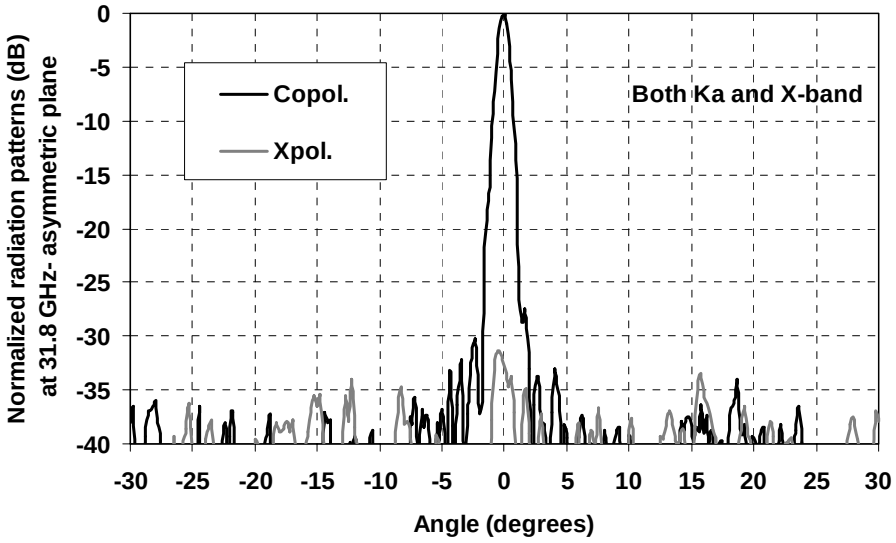

(d)

Fig. 64. Continued.

The peak sidelobe levels (in (a)) are 33.2 dB and 26.5 dB (left/right) down from the main beam. The cross-polarization level (in (a)) is 39.5 dB below the peak right-hand CP gain. As the frequency goes down to 31 GHz, the peak sidelobe level is degraded to -18.9 dB from the main beam while the peak sidelobe level at 33 GHz is degraded to -15 dB from the main beam. For the dual layer case (in (b)), the peak sidelobe levels are almost in the same levels. Good cross-polarization levels are observed for all cases in Figure 64 with values of below -32 dB from the co-polarized beam peak.

The peak gains for the dual layer are reduced by 1.0-1.3 dB compared to the single layer gains across the measured frequency ranges. In the asymmetric plane of (c) and (d), all the sidelobe levels are less than -28.5 dB, which is believed to be under-illuminated. Further considerations on the illumination taper are recommended to increase the overall aperture efficiency. The measured aperture efficiencies versus frequency are shown in Figure 65 after taking consideration of the loss factor in Figure 56. The highest efficiency is 64.4 % for the single layer and 48.2 % for the dual layer at 31.8 GHz. The corresponding gain variations are within ± 0.65 dB from the nominal value throughout the frequency ranges tested. This constant gain over frequencies is due to two factors. For example, at higher frequency, the aperture size of the feed arrays is electrically large producing the narrower beam pattern. Then, it is expected that on the surface of the main reflectarray, a sinc function-like surface current is generated and when Fourier transformed to form the far-field pattern, the resulting main beam lobe becomes broader. However, there exists less spillover due to a sine function-like surface current. As a result, these two factors compromise each other to establish the constant gain over frequencies. The phenomena at lower frequency can be explained vice versa. Figure 66 shows the axial ratio variations versus frequency. Excellent axial ratios of less than 0.7 dB are observed over all frequency ranges tested. Some of radiation patterns are attached in Appendix C2.

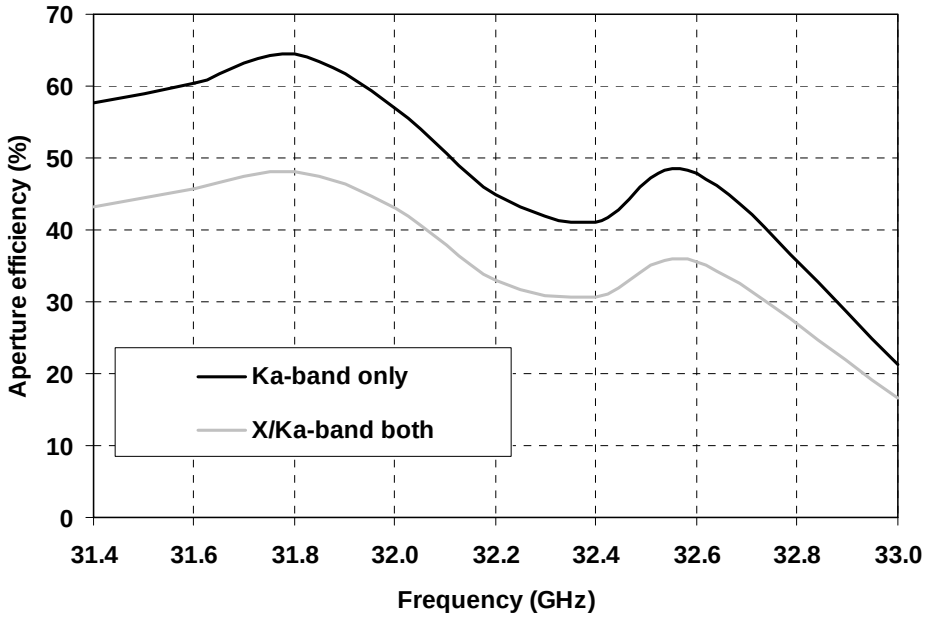

Fig. 65. Aperture efficiencies versus frequency at Ka-band.

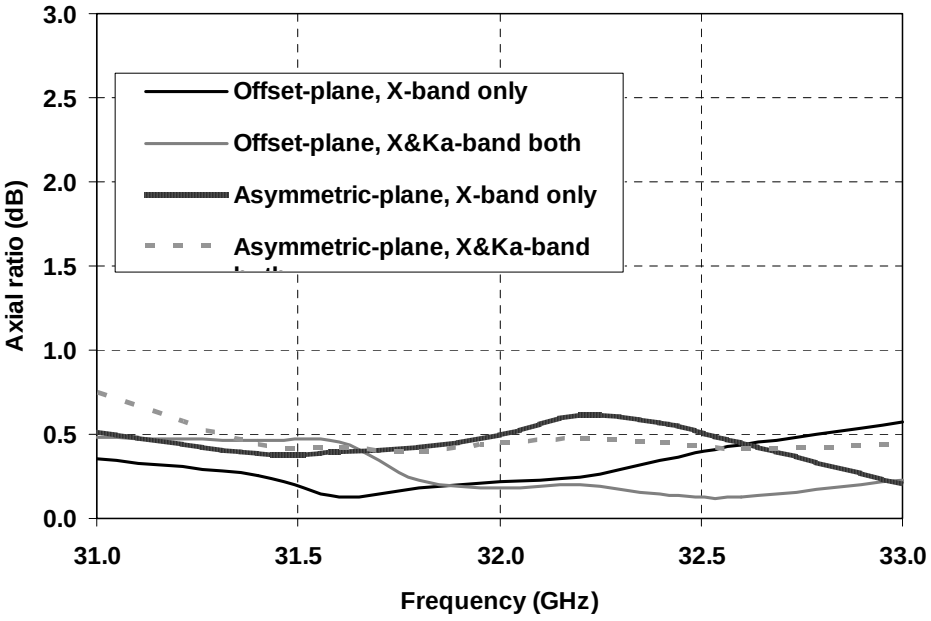

Fig. 66. Axial ratios versus frequency at Ka-band.

6. Conclusions

A 0.75 meter Cassegrain offset sub-reflector-fed X/Ka dual-band reflectarray using thin membranes is presented for the first time in this work. The sub-reflector is fabricated using combinations of prescribed geometric parameters and two separate microstrip feed arrays at each band are designed to illuminate the sub-reflector's surface. The measured peak efficiencies are 49.8 % at X-band and 48.2 % at Ka-band. The measured patterns are well behaved with relatively low cross-pol. and sidelobe levels, in particular for the Ka-band results. The CP bandwidths are more than 8 % at X-band and far more than 6 % at Ka-band, which is significantly wider than those of the fabricated feed arrays. In other words, the reflectarray lends itself to good CP performance even for the narrower CP bandwidth feed arrays because the cross-pol. radiations from all elements are diffused using the angular rotations. The reflectarray's peak gains are reduced by approximately 1.2 dB at Ka-band and 0.5 dB at X-band due to the existence of other layer. However, the gain variations are within ± 0.65 dB from the nominal value for both bands through the tested frequency ranges.

With further optimization, there is room for improvements and it is expected to be a good candidate that can be implemented in real system in no time. Several problems encountered in this study are: First, the mounting structure needs to be improved for the sub-reflector and feed arrays to survive in heavy wind environment. Second, the thin film spacing needs to be more uniformly distributed, especially for Ka-band reflectarray. Third, for the X-band reflectarray, the 4 by 4 feed array seems to be too large in size

relative to the size of the sub-reflector, which means high spillover on the surface of the sub-reflector. For this reason, 3 by 3 feed arrays or larger sub-reflector are desirable to improve the overall X-band aperture efficiency. The performance summary is shown in Table 7.

Table 7. Performance summary of a Cassegrain offset-fed reflectarray.

Parameters	X-band only (single-layer)		X-band (dual-layer)		Ka-band (single-layer)		Ka-band (dual-layer)	
Scan plane	0^o	28^o	0^o	28^o	0^o	28^o	0^o	28^o
Frequency (GHz)	8.4		8.4		31.8		31.8	
CP gain (dBic)	33.25		33.36		45.99		44.73	
Efficiency (%)	48.5		49.8		64.4		48.2	
X-pol. level (dB)	26.6	28	25.6	27.4	32.2	39.5	33.0	37.7
Peak sidelobe. (dB)	32.1	17.7	28.5	17.9	32.5	26.5	30.2	26.3
Beamwidth	3.48^o	3.81^o	3.58^o	3.89^o	0.95^o	1.08^o	0.94^o	1.10^o
CP Bandwidth (MHz)	> 600		> 600		> 2000		> 2000	

CHAPTER V

SUMMARY AND RECOMMENDATIONS

1. Summary

With the advancement of space exploration, there is an increasing demand for larger aperture antennas with very small masses and launch volumes. As one of the solutions, deployable antenna technology using inflatable structures and thin membranes has recently being investigated, particularly, the technology of inflatable flat reflectarray. The reflectarray, however, suffers from limited bandwidth typically less than 10 %.

In this dissertation, A series of developments have been carried out to demonstrate the dual-band capability of the reflectarray to meet the multi-band requirements. First, a 0.5 meter center-fed C/Ka dual-band reflectarray has been successfully developed. This reflectarray used annular ring elements with the angular rotation technique to achieve the required phase delays for circular polarization. A subsequent development for an offset –fed configuration was also successfully demonstrated using two-layer thin membranes. Finally, a Cassegrain offset-fed X/Ka dual-band reflectarray with a 0.75 meter diameter was successfully developed using two-layer thin membranes. For very large apertures, Cassegrain offset-fed configuration, in addition to minimizing the feed blockage, would allow the feed and its associated electronics to be located close to the spacecraft for easier thermal control, in particular, when minimizing of RF loss in the feed cable is in consideration. This Cassegrain dual-band technology presented in this dissertation is

currently being implemented onto a 3 meter reflectarray with inflatable structures and is planned for application to an 8 meter inflatable reflectarray in the near future.

2. Recommendations for future research

Further optimizations in the analysis of reflector antenna with various feed arrangements are suggested for performance improvements in the future. The gain loss of a Ka-band reflectarray due to the interference of the top X-band reflectarray needs more study to reduce the performance degradation at Ka-band. A Ka-band reflectarray which was in the bottom in this study can be positioned in the top layer to investigate the further improvements. A dual-band CP reflectarray may be constructed on the single layer using the proposed annular ring elements. Because there exist some restrictions in the element spacings in order to share the same layer, careful attention needs to be given when choosing the most favorable two frequency bands. A triple-band reflectarray can be done using the annular rings if there are applications. A study for a dual-band linearly polarized reflectarray made of thin membranes needs to be followed for the LP applications. Since the angular rotation technique is not applicable for the LP applications and the required phase curves are more vulnerable to the substrate's thickness, a new type of element needs to be developed in this case. For example, currently, a Ku/Ka dual-band reflectarray is being investigated for the NASA Titan Cloud Precipitation Radar and Altimeter (TCPRA) system. The reflectarray supports dual-linear polarizations with both vertical and horizontal polarizations, while the feed arrays are 0.5 meter long microstrip arrays with single linear polarization.

REFERENCES

[1] Marco A. B. Terada, “Reflector antennas,” *Encyclopedia of RF and Microwave Engineering*, edited by K. Chang, vol. 5, pp 4450-4474, John Wiley & Sons, New York, 2005.

[2] J. Huang, “Reflectarray antenna,” *Encyclopedia of RF and Microwave Engineering*, edited by K. Chang, vol. 5, pp 4428-4436, John Wiley & Sons, New York, 2005.

[3] R. E. Munson and H. Haddad, “Microstrip reflectarray for satellite communication and RCS enhancement and reduction,” *U.S. Patent 4 684 952*, Washington, DC, Aug. 1987.

[4] J. Huang, “Microstrip reflectarray antenna for the SCANSCAT radar application,” Jet Propulsion Lab., Pasadena, CA, No. 90-45, Nov. 1990.

[5] R. D. Javor, X. D. Wu, and K. Chang, “Offset-fed microstrip reflectarray antenna,” *Electron. Lett.*, vol. 30, pp. 1363-1365, Aug. 1994.

[6] R. D. Javor, X. Wu, and K. Chang, “Design and performance of a microstrip reflectarray antenna,” *IEEE Trans. Antennas Propagat.*, vol. 43, pp. 932-939, Sept. 1995

[7] D. M. Pozar and T. A. Metzler, “Analysis of a reflectarray antenna using microstrip patches of variable size,” *Electron. Lett.*, vol. 29, pp. 657-658, Apr. 1993.

[8] D. C. Chang and M. C. Huang, “Multiple polarization microstrip reflectarray antenna with high efficiency and low cross-polarization,” *IEEE Trans. Antennas*

Propagat., vol. 43, pp. 829-834, Aug. 1995.

[9] S. D. Targonski, D. M. Pozar, and H. D. Syrigos, "Analysis and design of millimeter wave microstrip reflectarrays," in *Proc. IEEE AP-S Symp.*, June 1995, vol. 1, pp. 578-581.

[10] D. M. Pozar, S. D. Targonski, and H. D. Syrigos, "Design of millimeter wave microstrip reflectarrays," *IEEE Trans. Antennas Propagat.*, vol. 45, pp. 287-296, Feb. 1997.

[11] D. M. Pozar, S. D. Targonski, and R. Pokuls, "A shaped-beam microstrip patch reflectarray," *IEEE Trans. Antennas Propagat.*, vol. 47, pp. 1167-1173, July 1997.

[12] J. A. Encinar, "Design of two-layer printed reflectarrays using patches of variable size," *IEEE Trans. Antennas Propagat.*, vol. 49, pp. 1403-1410, Oct. 2001.

[13] D. M. Pozar and S. D. Targonski, "A microstrip reflectarray using crossed dipoles," in *Proc. IEEE AP-S Symp.*, June 1998, vol. 2, pp. 1008-1011.

[14] J. Shaker and M. Cuhaci, "Planar reflector for LMCS application," *Electron. Lett.*, vol. 35, pp. 103-104, Jan. 1999.

[15] J. Huang and R. Pogorzelski, "A Ka-band microstrip reflectarray with elements having variable rotation angles," *IEEE Trans. Antennas Propagat.*, vol. 46, pp. 650-656, May 1998.

[16] J. Huang, "Capabilities of printed reflectarray antennas," in *Proc. IEEE Int. Symp.*

Phased Array Systems Technology, Oct. 1996, pp. 131-134.

[17] J. Huang, "Bandwidth study of microstrip reflectarray and a novel phased reflectarray concept," in *Proc. IEEE AP-S Symp.*, June 1995, vol. 1, pp. 582-585.

[18] D. M. Pozar, "Bandwidth of reflectarrays," *Electron. Lett.*, vol. 39, pp. 1490-1491, Oct. 2003.

[19] D. I. Wu, R. C. Hall, and J. Huang, "Dual-frequency microstrip reflectarray," in *Proc. IEEE AP-S Symp.*, June 1995, vol. 4, pp. 2128-2131.

[20] J. A. Encinar, "Design of a dual frequency reflectarray using microstrip stacked patches of variable size," *Electron. Lett.*, vol. 32, pp. 1049-1050, June 1996.

[21] C. Han and K. Chang, "Ka-band reflectarray using ring elements," *Electron. Lett.*, vol. 39, pp. 491-493, Mar. 2003.

[22] B. Strassner, C. Han, and K. Chang, "Circularly polarized reflectarray with microstrip ring elements having variable rotation angles," *IEEE Trans. Antennas Propagat.*, vol. 52, pp. 1122-1125, Apr. 2004.

[23] C. Han, C. Rodenbeck, J. Huang, and K. Chang, "A C/Ka dual frequency dual layer circularly polarized reflectarray antenna with microstrip ring elements," *IEEE Trans. Antennas Propagat.*, vol. 52, pp. 2871-2876, Nov. 2004.

[24] C. Han, J. Huang, and K. Chang, "A high efficiency offset-fed X/Ka-dual-band reflectarray using thin membranes," *IEEE Trans. Antennas Propagat.*, vol. 53, pp. 2792-2798, Sep. 2005.

[25] J. Huang, C. Han, and K. Chang, “A Cassegrain offset-fed dual-band reflectarray.” to be presented at *IEEE AP-S/URSI Symp.*, Albuquerque, July 2006.

[26] C. Han, J. Huang, and K. Chang, “Cassegrain offset sub-reflector-fed X/Ka dual-band reflectarray with thin membranes,” in preparation, June 2006.

[27] R. P. Jedlicka, M. T. Poe, and K. R. Carver, “Measured mutual coupling between microstrip elements,” *IEEE Trans. Antennas Propagat.*, vol. 29, pp. 147-149, Jan. 1981.

[28] C. Balanis, *Antenna Theory*, Wiley & Sons, New York, 1982, chap. 15.

[29] K. Chang, *Microwave Ring Circuits and Antennas*, Wiley & Sons, New York, 1996, chap. 2.

[30] M. E. Bialkowsk and F. E. Tsai, “A unit cell waveguide model of a reflectarray formed by microstrip patches and slots,” *Microwave and Optical Technology Letters*, vol 36, pp. 206-210, Feb. 2003.

[31] HFSS ver. 8.0, Ansoft Inc., Four Station Square- Suite 200, Pittsburgh, PA 15219-1119.

[32] B. Y. Toh, R. Cahill, and V. F. Fusco, “Understanding and measuring circular polarization,” *IEEE Trans. Antennas Propagat.*, vol. 46, pp. 313-318, Aug. 2003.

[33] M. Thomas and G. Veal, “Highly accurate inflatable reflectors,” Report AFRPL Tr. 84-023, May 1984.

[34] R. E. Freeland, G. D. Bilyeu, and G. R. Veal, “Large inflatable deployable antenna

flight experiment results,", in *48th Congress of the International Astronautical Federation*, Turin, Italy, Oct. 1997, IAF Paper 97-1.3.01.

[35] J. Huang and A. Feria, "A 1-m X-band inflatable reflectarray antenna," *Microwave and Optical Technology Letters*, vol. 20, pp. 97-99, Jan. 1999.

[36] A. W. Rudge and N. A. Adatia, "Offset-parabolic-reflector antennas," in *Proc. IEEE AP-S Symp.*, Dec. 1978, vol. 66, pp. 1592-1618.

[37] A. C. Ludwig, "The definition of cross polarization," *IEEE Trans. Antennas Propagat.*, vol. 21, pp. 116-119, Jan. 1973.

[38] W. Stutzman and M. Terada, "Design of offset-parabolic-reflector antennas for low cross-pol and low sidelobes," in *IEEE Antennas Propagat. Magazine*, vol. 35, pp. 46-49, Dec. 1993.

[39] Y. Rahmat-Samii, R. A. Hoferer, and H. Mosallaei, "Beam efficiency of reflector antennas: The simple formula," in *IEEE Antennas and Propagation Magazine*, Vol. 40, pp 82-87, Oct. 1988.

[40] S. D. Targonski and D. M. Pozar, "Minimization of beam squint in microstrip reflectarrays using an offset feed," in *Proc. IEEE AP-S Symp.*, July 1996, vol. 2, pp. 1326-1329.

[41] R. C. Johnson, *Antenna Engineering Handbook*, McGraw-Hill, New York, 1993, chap. 17.

[42] P. W. Hannan, "Microwave antennas derived from the Cassegrain telescope," *IRE*

Trans. Antennas Propagat., vol. 9, pp. 140-153, Mar. 1961.

[43] G. W. Collins "Shaping of subreflectors in Cassegrainian antennas for maximum aperture efficiency," *IEEE Trans. Antennas Propagat.*, vol. 21, pp. 309-313, May 1973.

[44] Y. Mizuguch, M. Akagawa, and H. Yokoi, "Offset dual reflector antenna," in *Proc. IEEE* A*P-S Int. Symp. Dig.*, Oct. 1976, vol. 14, pp. 2-5.

[45] V. Jamnejad-Dailami and Y. Rahmat-Samii, "Some important geometrical features of conic-section-generated offset reflector antennas," *IEEE Trans. Antennas Propagat.*, vol. 28, pp. 952-957, Nov. 1980.

[46] R. A. Shore, "A simple derivation of the basic design equation for offset dual reflector antennas with rotational symmetry and zero cross polarization," *IEEE Trans. Antennas Propagat.*, vol. 33, pp.114-116, Jan. 1985.

[47] Y. Rahmat-Samii, "Subreflector extension for improved efficiencies in Cassegrain antennas- GTD/PO analysis," *IEEE Trans. Antennas Propagat.*, vol. 34, pp. 1266-1269, Oct. 1986

[48] W. V. T. Rusch, A. Prata, Jr., Y. Rahmat-Samii, and R. A. Shore, "Derivation and application of the equivalent paraboloid for classical offset Cassegrain and Gregorian antennas," *IEEE Trans. Antennas Propagat.*, vol. 38, pp. 1141-1149, Aug. 1990.

[49] K. W. Brown and A. Prata, Jr., "A design procedure for classical offset dual reflector

antennas with circular apertures," *IEEE Trans. Antennas Propagat.*, vol. 42, pp. 1145-1153, Aug. 1994.

[50] C. Granet, "Designing axially symmetric Cassegrain or Gregorian dual-reflector antennas from combinations of prescribed geometric parameters," *IEEE Antennas and Propagation Magazine*, Vol. 40, pp 76-82, Apr. 1998.

[51] C. Granet, "A simple procedure for the design of Classical displaced-axis dual-reflector antennas using a set of geometric parameters," *IEEE Antennas and Propagation Magazine*, Vol. 41, pp 64-71, Dec. 1999.

[52] C. Granet, "Designing classical offset cassegrain or Gregorian dual-reflector antennas from combinations of prescribed geometric parameters," *IEEE Antennas and Propagation Magazine*, Vol. 44, pp 114-123, June 2002.

[53] C. Granet, "Designing classical offset cassegrain or Gregorian dual-reflector antennas from combinations of prescribed geometric parameters- Part 2: feed-horn blockage conditions," *IEEE Antennas and Propagation Magazine*, Vol. 45, pp 86-89, Dec. 2003.

[54] P. C. Sharma and K. C. Gupta, "Analysis and optimized design of single point feed circularly polarized microstrip antennas," *IEEE Trans. Antennas Propagat.*, vol. 31, pp. 949-955, Nov. 1983.

[55] Y. T. Lo, and S. W. Lee, *Antenna Handbook: theory, applications, and design*, New York: Van Nostrand Reinhold, New York, 1988, chap. 5.

[56] T. Teshirogi, M. Tanaka, and W. Chujo, “Wideband circularly polarized array antenna with sequential rotation and phase shifts of elements,” in *Proc. IEEE AP-S Int. Symp.*, Aug. 1985, vol. 1, pp 117-120.

[57] J. Huang, “A technique for an array to generate circular polarization with linearly polarized elements,” *IEEE Trans. Antennas Propagat.*, vol. 34, pp. 1113-1124, Sept. 1986.

[58] J. Huang, “A Ka-band circularly polarized high-gain microstrip array antenna,” *IEEE Trans. Antennas Propagat.*, vol. 43, pp.113-116, Jan. 1995.

APPENDIX A

A1. MATLAB code to create the required phase of the reflectarray element

```
clear;        % clears all variables from previous execution
clc;          % clears command terminal

% user input variables

at=input('Enter 1 for square and 2 for circle ');

if at~=1&at~=2
    sprintf('%d an invalid array type!!',at)
else
    frg=input('Enter the reflectarray operating frequency in GHz     ');
    f=input('Enter the focal length from the reflector in mm ');
    d=input('Enter the diameter of the parabolic reflector in mm     ');
    dx=input('Enter the element spacing in the x direction in mm     ');
    dy=input('Enter the element spacing in the y direction in mm     ');

    fr=frg*1e9;     % frequency in Hz
    c=3e8;          % speed of light in m per s
    tho_rad=atan(abs((1/2*(f/d))/((f/d)^2-1/16)));     % the largest angle in radian
    tho_deg=tho_rad*180/pi; % the largest angle in degree
    dr=2*f*tan(tho_rad);  % diameter of the reflectarray

    nx=round((dr/2)/dx);  % number of elements in the x direction minus the origin
    ny=round((dr/2)/dy);  % number of elements in the y direction minus the origin

    for m=1:nx+1       % +1 includes the patch at the origin (0,0)
```

```
for n=1:ny+1   % +1 includes the patch at the origin (0,0)

    if at==1
        thp_rad=atan(((((m-1)*dx)^2+((n-1)*dy)^2)^(1/2))/f);
        rp=2*f/(1+cos(thp_rad));
        rpplot(m,n)=rp;
        rmn=f/cos(thp_rad);
        rmnplot(m,n)=rmn;
        s=rmn-f; % the phase difference
        s_rad=2*pi*fr*(s/1000)/c;
        mx(m,n)=(m-1)*dx;
        my(m,n)=(n-1)*dy;
        mxmy(m,n)=(mx(m,n)^2+my(m,n)^2)^(1/2);
        psi_deg(m,n)=s_rad/2*180/pi;     % the required phase
        thp_deg(m,n)=thp_rad*180/pi;
    else
        if ((((m-1)*dx)^2+((n-1)*dy)^2)^(1/2))<(dr/2)
            thp_rad=atan(((((m-1)*dx)^2+((n-1)*dy)^2)^(1/2))/f);
            rp=2*f/(1+cos(thp_rad));
            rpplot(m,n)=rp;
            rmn=f/cos(thp_rad);
            rmnplot(m,n)=rmn;
            s=rmn-f;    % the phase difference
            s_rad=2*pi*fr*(s/1000)/c;
            mx(m,n)=(m-1)*dx;
            my(m,n)=(n-1)*dy;
            mxmy(m,n)=(mx(m,n)^2+my(m,n)^2)^(1/2);
            psi_deg(m,n)=s_rad/2*180/pi;     % the required phase
            thp_deg(m,n)=thp_rad*180/pi;
```

```
                else
                    rp=2*f/(1+cos(tho_rad));
                    rpplot(m,n)=rp;
                    rmn=f/cos(tho_rad);
                    rmnplot(m,n)=rmn;
                    s=rmn-f;
                    s_rad=2*pi*fr*(s/1000)/c;
                    mx(m,n)=(m-1)*dx;
                    my(m,n)=(n-1)*dy;
                    mxmy(m,n)=(mx(m,n)^2+my(m,n)^2)^(1/2);
                    psi_deg(m,n)=s_rad/2*180/pi;
                    thp_deg(m,n)=tho_rad*180/pi;
                end
            end
        end
    end

% element location
x_element_location=mx;
y_element_location=my;

% required element rotation
element_rotation=rem(psi_deg,360)

% plot
subplot(3,2,1),plot(mxmy,rpplot),grid on,
    title('rp vs distance from origin')
subplot(3,2,2),plot(mxmy,rmnplot),grid on,
```

```
    title('rmn vs distance from origin')
subplot(3,2,3),plot(mxmy,thp_deg),grid on,
    title('theta off focal axis')
subplot(3,2,4),plot(mxmy,psi_deg),grid on,
title('element rotation vs distance from origin')
subplot(3,2,5),contourf(mx,my,psi_deg,10) ,grid on,
xlabel('Distance from origin,mm');
ylabel('Distance from origin,mm');
title('element rotation')
subplot(3,2,6),plot3(mx,my,psi_deg,'bp-'),grid on,
title('element rotation vs distance from origin')
xlabel('Distance from origin,mm');
ylabel('Distance from origin,mm');
zlabel('Phase,degree')
end
```

APPENDIX B

B1. Ka-band measurement patterns

The right-hand co-polarized radiation patterns in the plane of asymmetry are provided at 31.1 GHz, 31.5 GHz, 32 GHz, and 32.8 GHz respectively. Because radiation patterns for the left-hand cross-polarizations are similar, only the patterns at 32.8 GHz are provided.

The right-hand co-polarized radiation patterns in the plane of symmetry are provided at 31.1 GHz, 31.5 GHz, 32 GHz, and 32.8 GHz respectively. Radiation patterns for the left-hand cross-polarizations are only provided at 32.8 GHz.

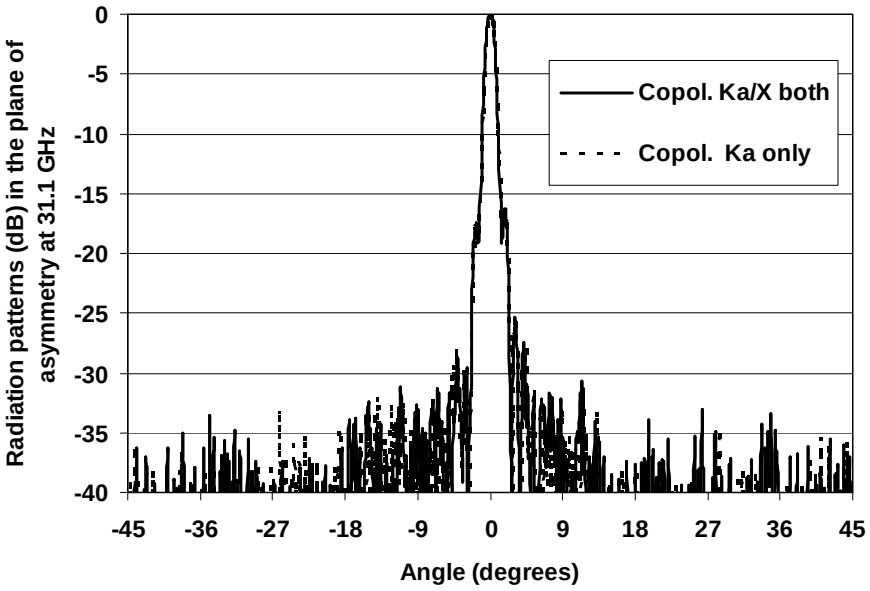

(a)

Fig. B1. Normalized radiation patterns (dB) in the plane of asymmetry at Ka-band: (a) 31.1 GHz; (b) 31.5 GHz; (c) 32 GHz; (d) 32.8 GHz (co-pol.); (e) 32.8 GHz (cross-pol.).

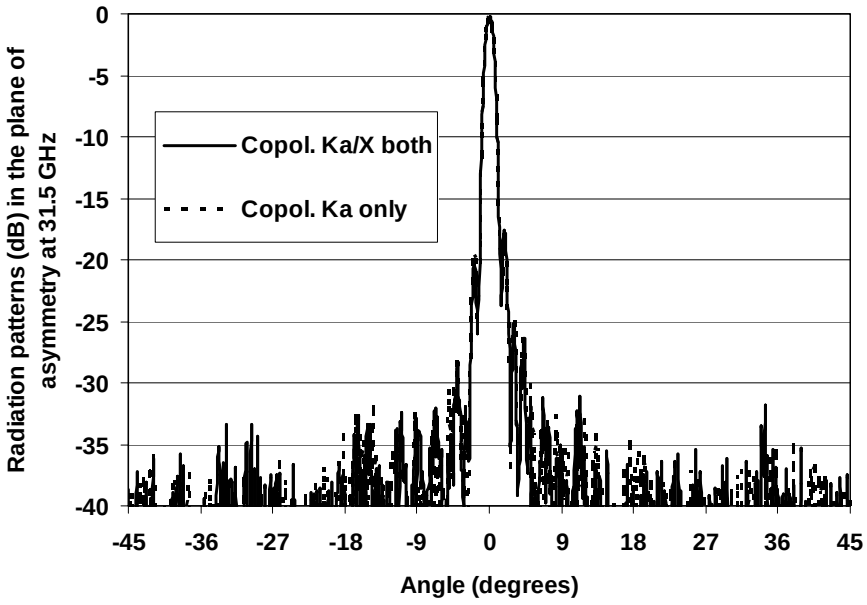

(b)

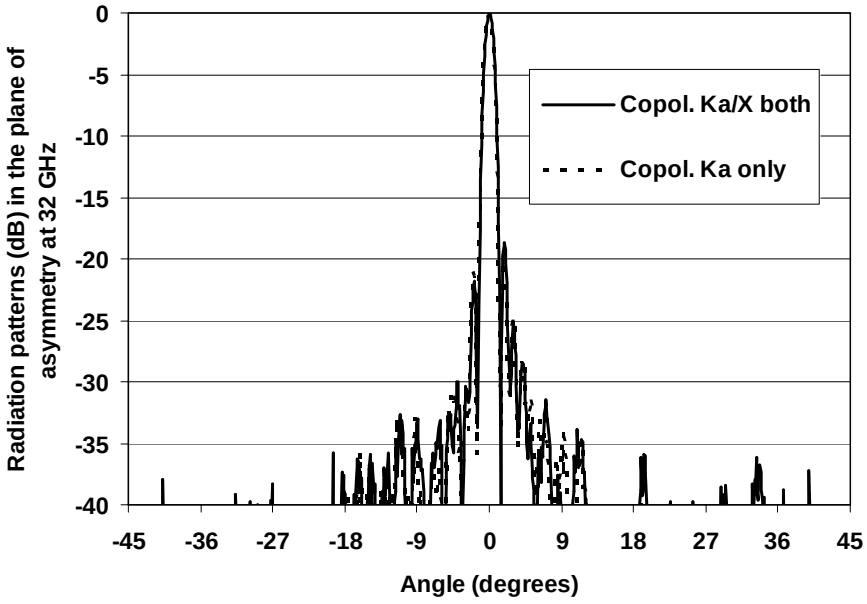

(c)

Fig. B1. Continued.

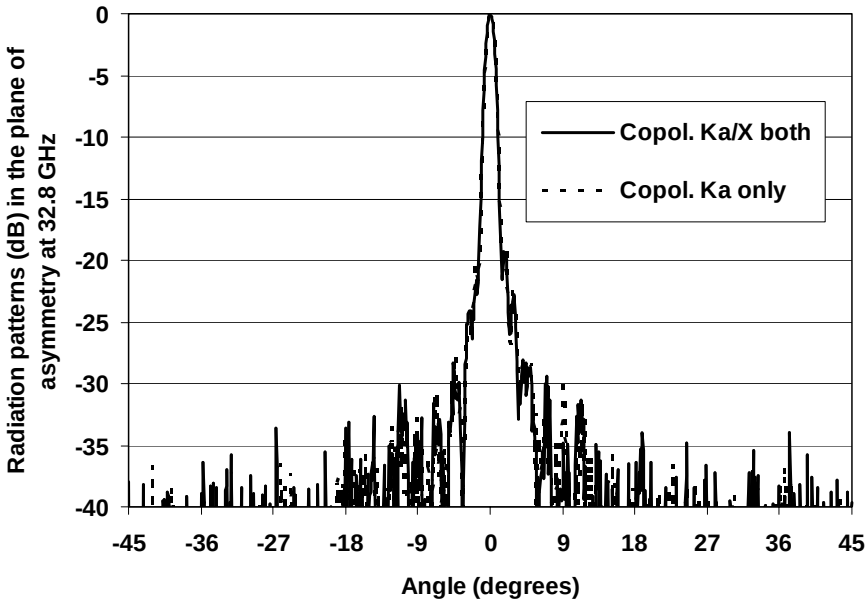

(d)

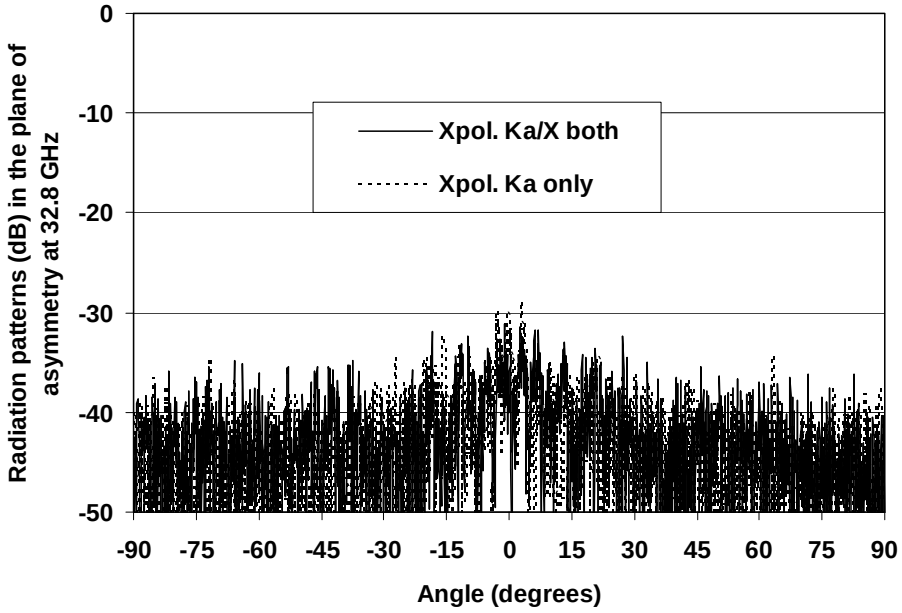

(e)

Fig. B1. Continued.

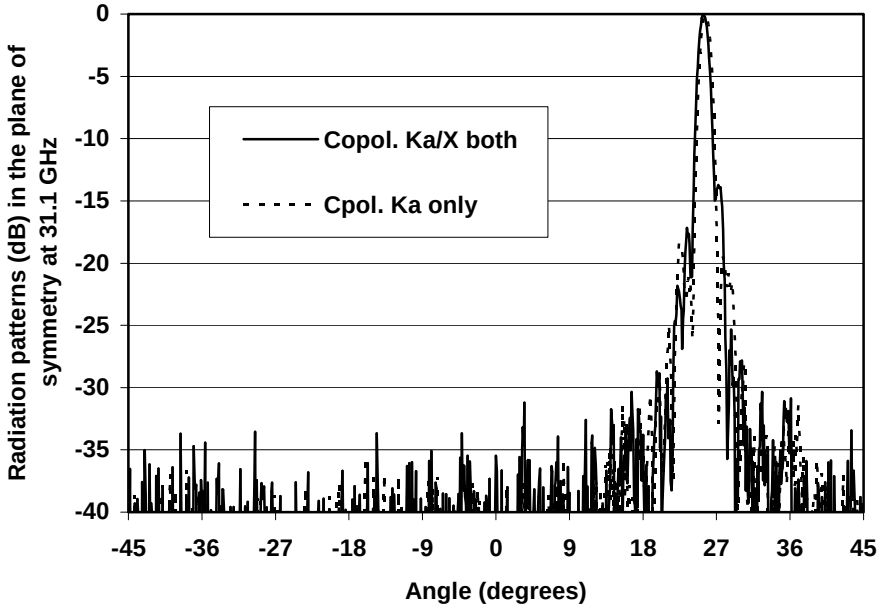

(a)

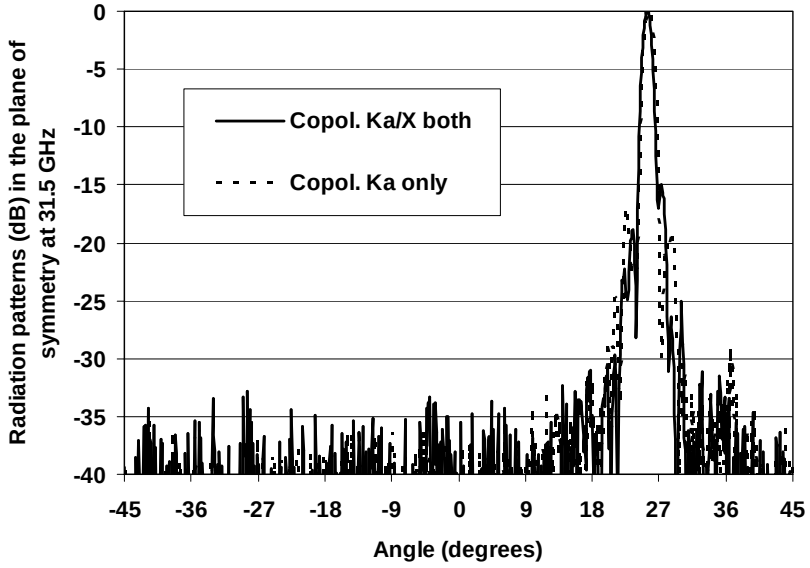

(b)

Fig. B2. Normalized radiation patterns (dB) in the plane of symmetry at Ka-band: (a) 31.1 GHz; (b) 31.5 GHz; (c) 32 GHz; (d) 32.8 GHz (co-pol.); (e) 32.8 GHz (cross-pol.).

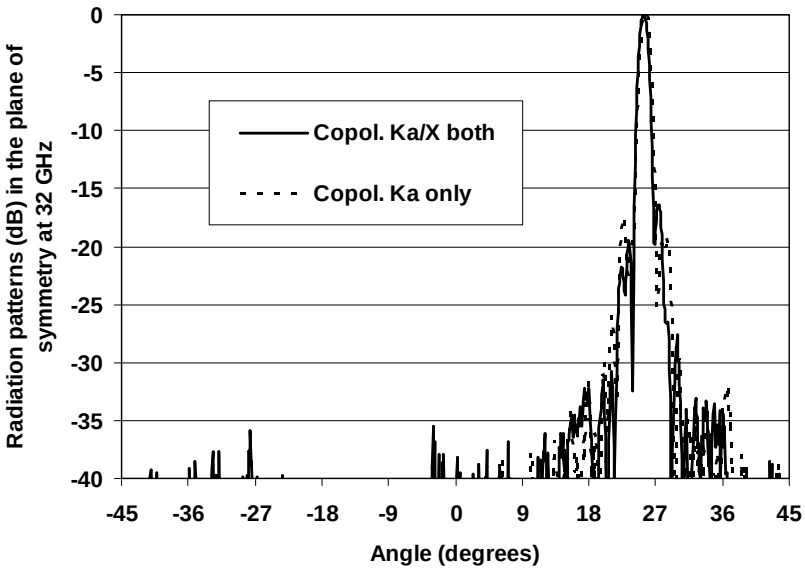

(c)

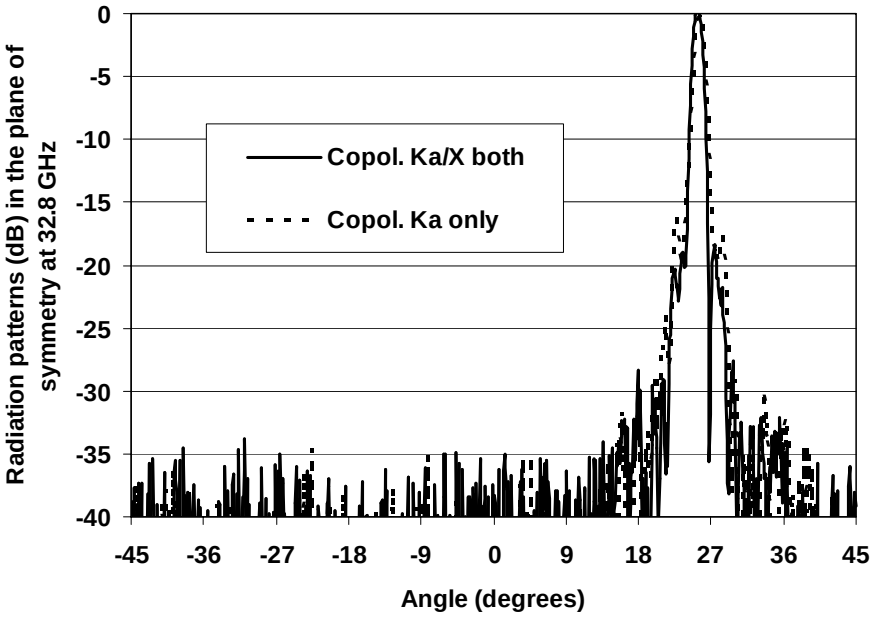

(d)

Fig. B2. Continued.

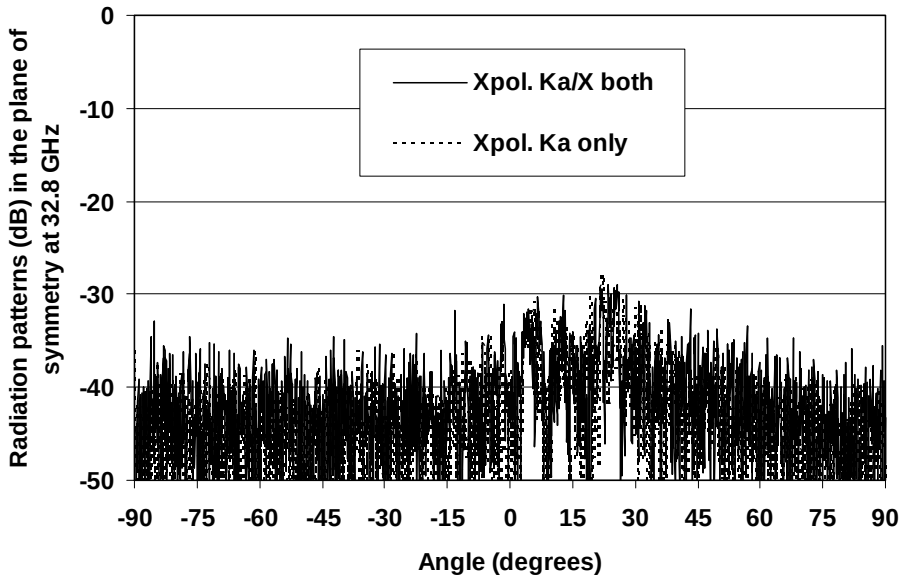

(e)

Fig. B2. Continued.

B2. X-band measurement patterns

The right-hand co-polarized radiation patterns in the plane of asymmetry are provided at 8.2 GHz, 8.4 GHz, 8.5 GHz, and 8.9 GHz respectively. Radiation patterns for the left-hand cross-polarization are given only at 8.5 GHz.

Radiation patterns in the plane of symmetry are provided at 8.2 GHz, 8.4 GHz, 8.5 GHz, and 8.9 GHz respectively. Only the radiation patterns for the dual layer case are measured in the plane of symmetry.

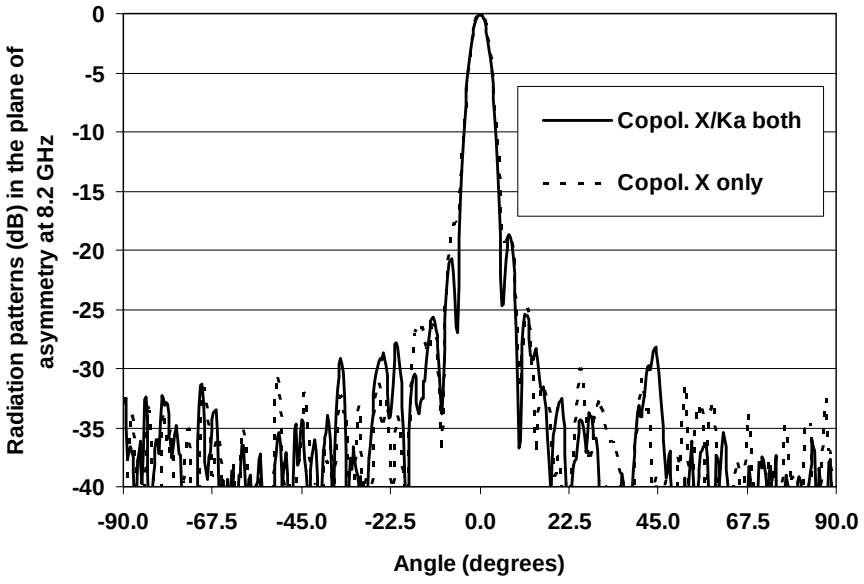

(a)

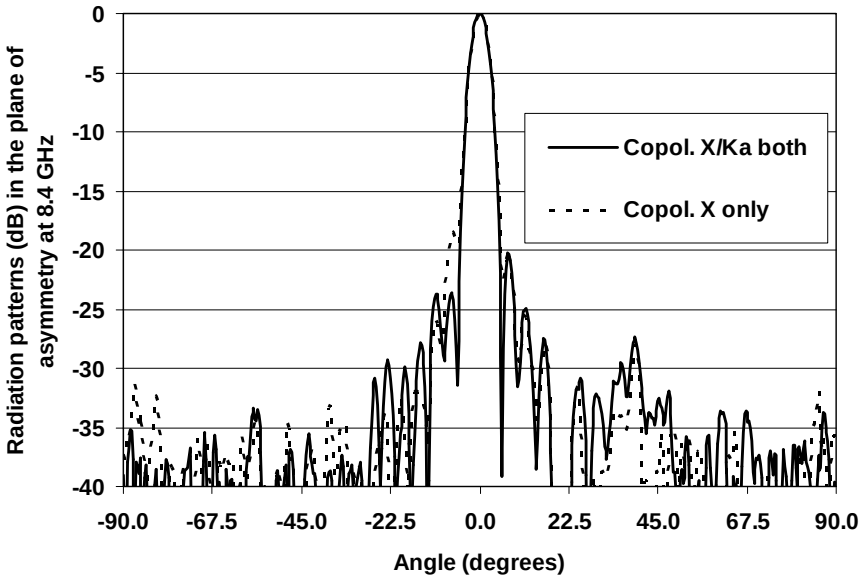

(b)

Fig. B3. Normalized radiation patterns (dB) in the plane of aymmetry at X-band: (a) 8.2 GHz; (b) 8.4 GHz; (c) 8.5 GHz (co-pol.);(d) 8.9 GHz; (d) 8.5 GHz (cross-pol.).

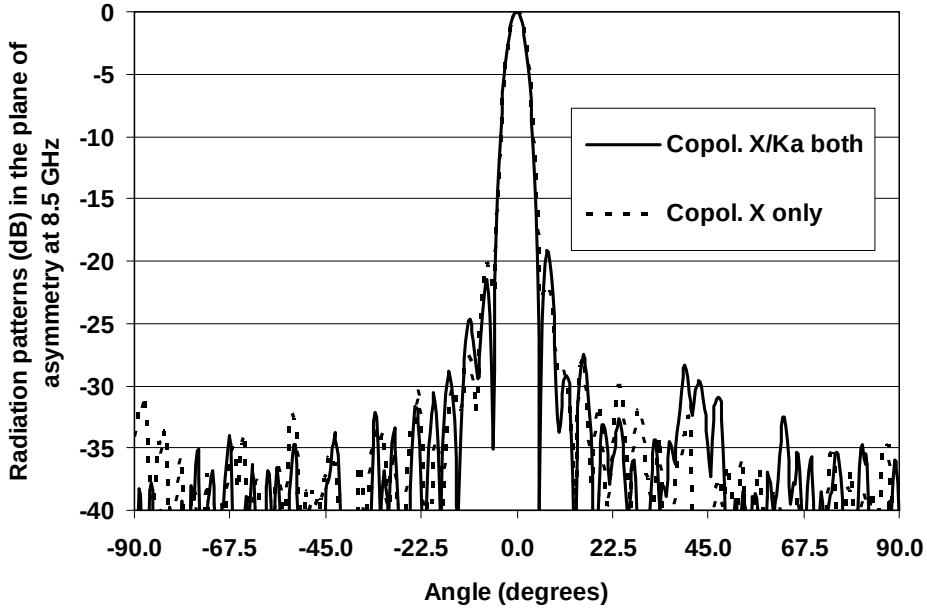

(c)

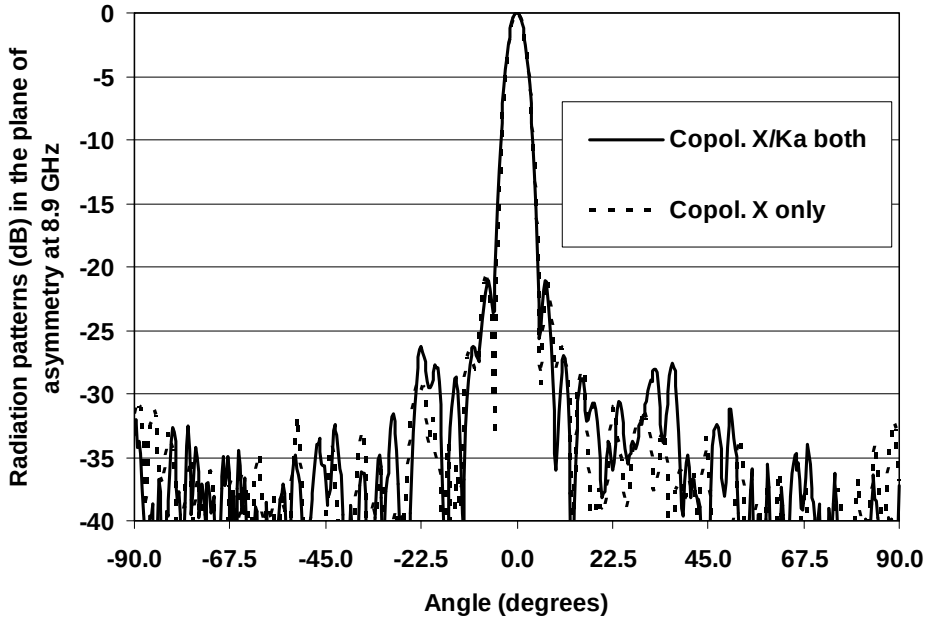

(d)

Fig. B3. Continued.

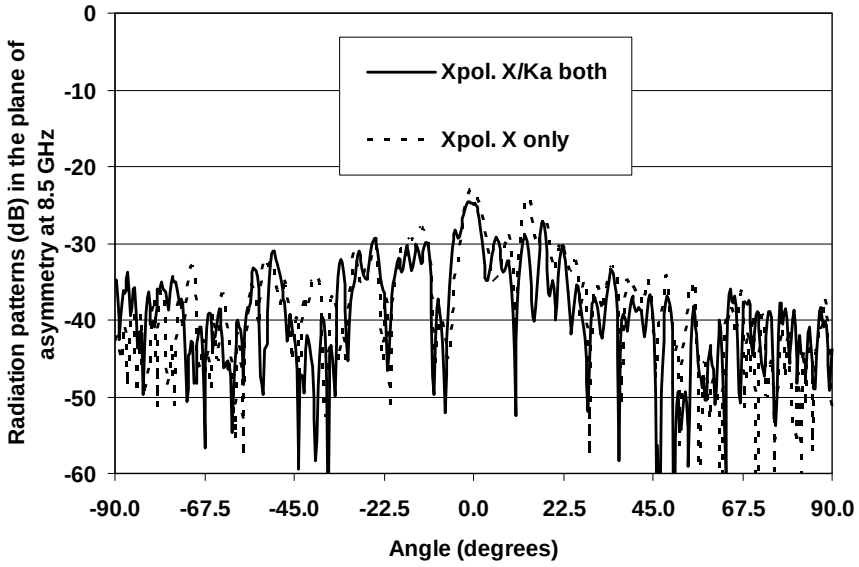

(e)

Fig. B3. Continued.

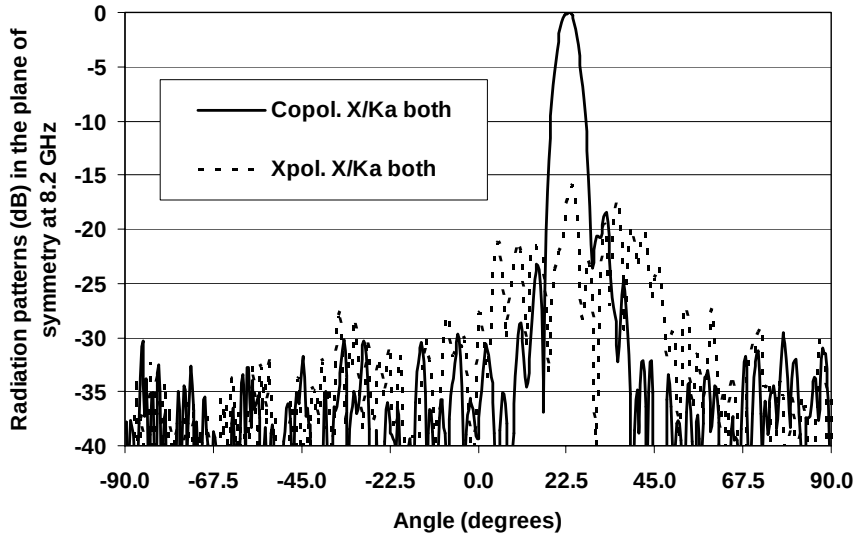

(a)

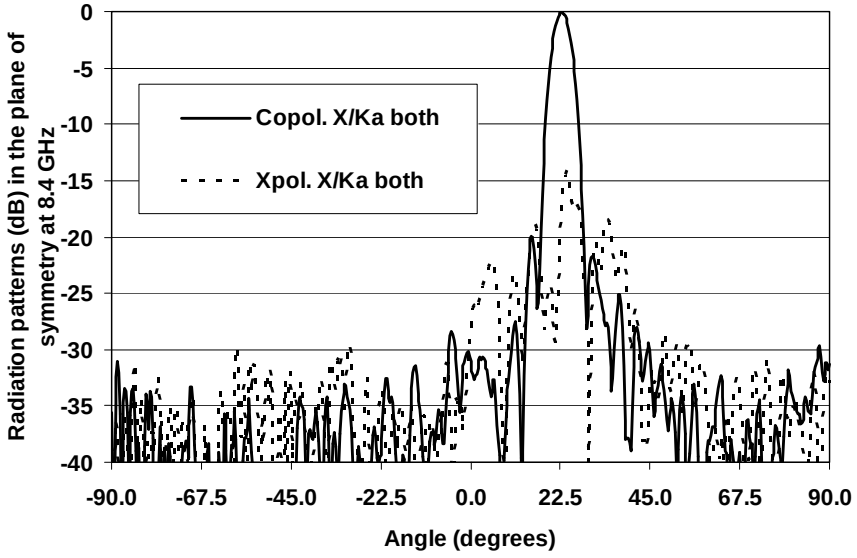

(b)

Fig. B4. Normalized radiation patterns (dB) in the plane of symmetry at X-band: (a) 8.2 GHz; (b) 8.4 GHz; (c) 8.5 GHz; (d) 8.9 GHz.

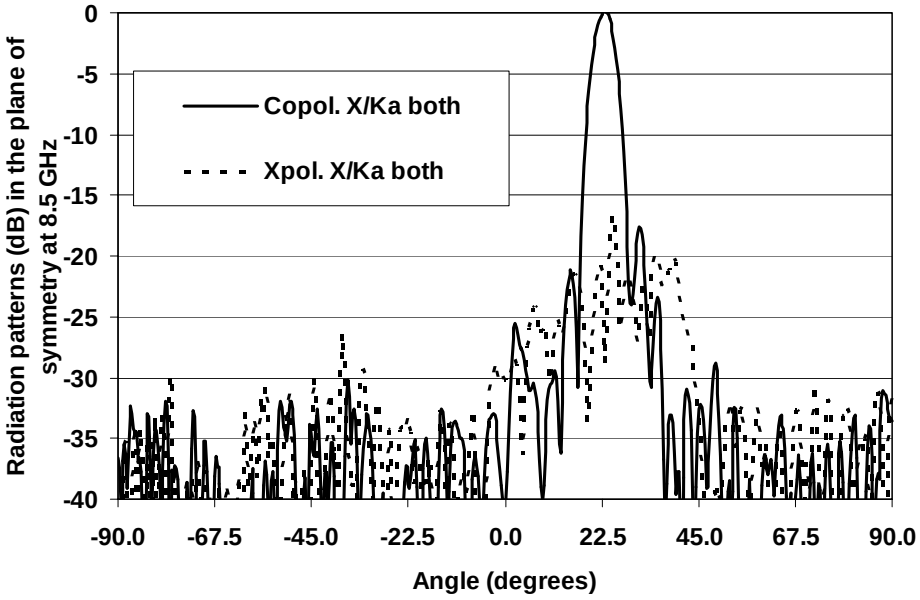

(c)

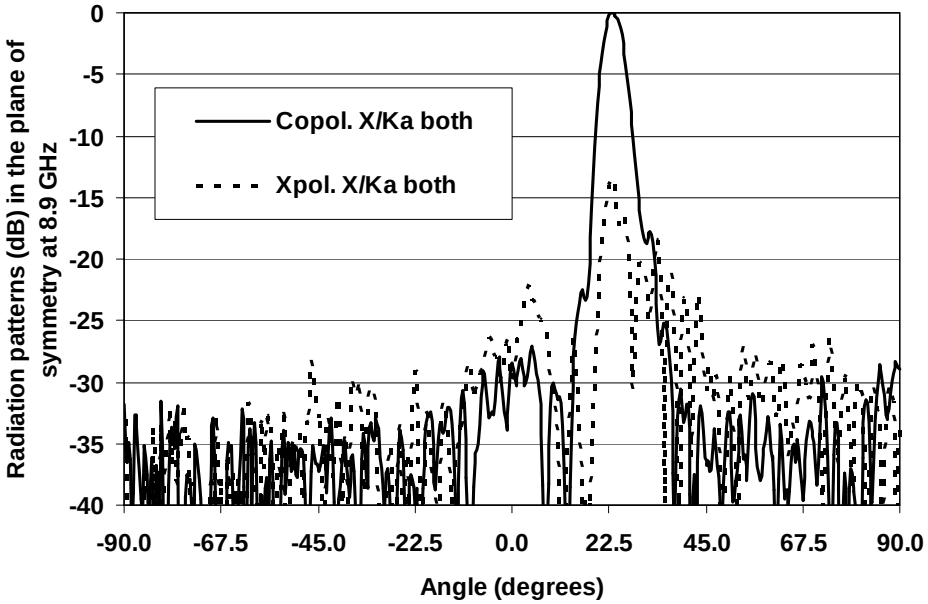

(d)

Fig. B4. Continued.

APPENDIX C

C1. X-band measurement results

Normalized radiation patterns in the plane of asymmetry are provided at 8.2 GHz, 8.3 GHz, 8.5 GHz, and 8.6 GHz with the corresponding cross-polarization patterns. Normalized radiation patterns in the offset plane (in the plane of symmetry) are provided at 8 GHz, 8.3 GHz, 8.5 GHz, and 8.7 GHz respectively.

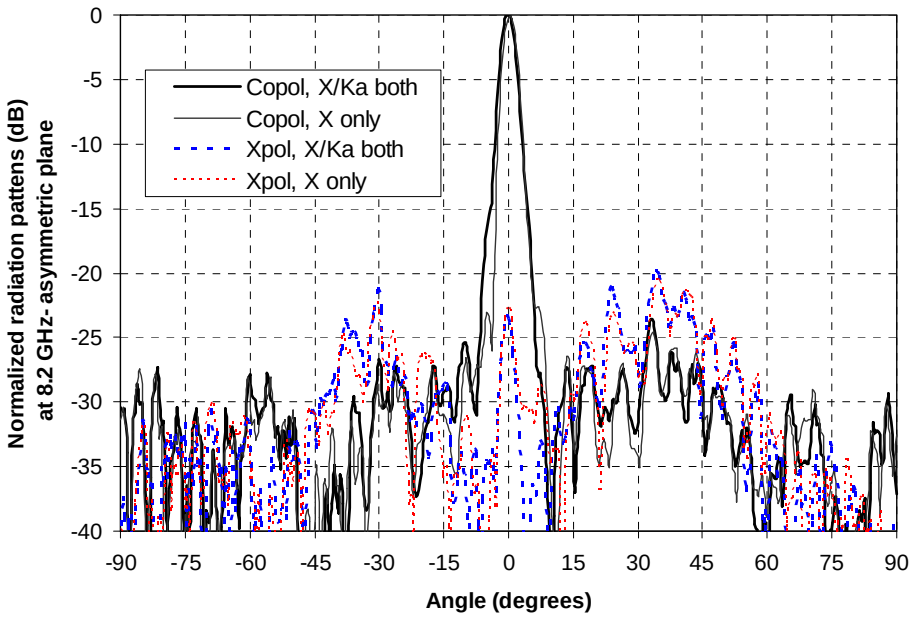

(a)

Fig. C1. Normalized radiation patterns (dB) in the asymmetric plane at X-band: (a) 8.2 GHz; (b) 8.3 GHz; (c) 8.5 GHz; (d) 8.6 GHz.

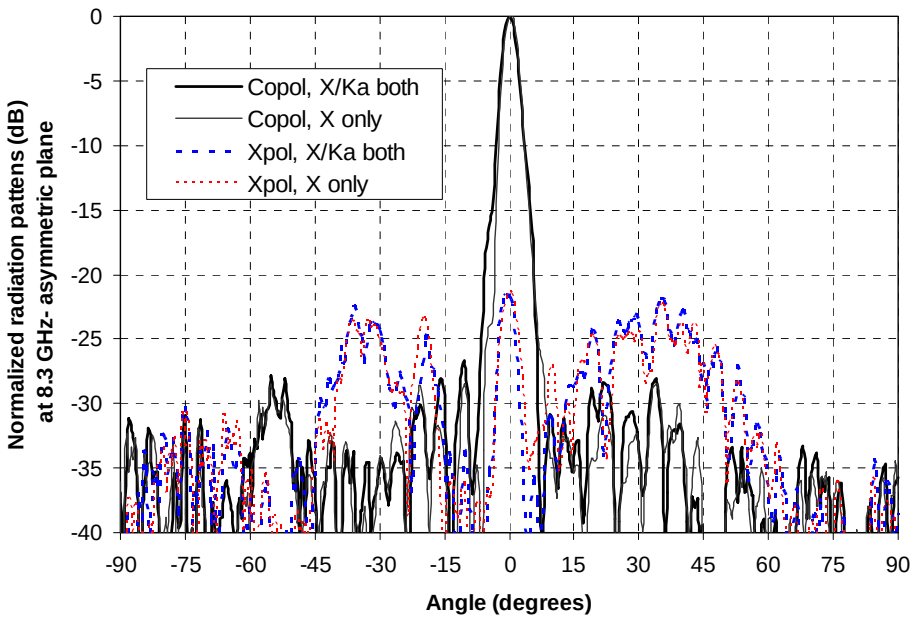

(b)

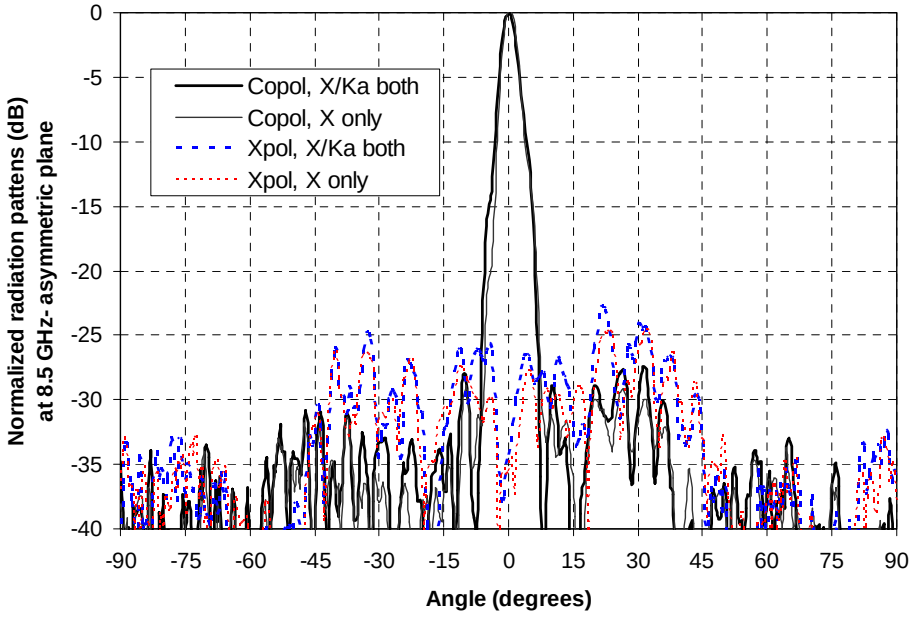

(c)

Fig. C1. Continued.

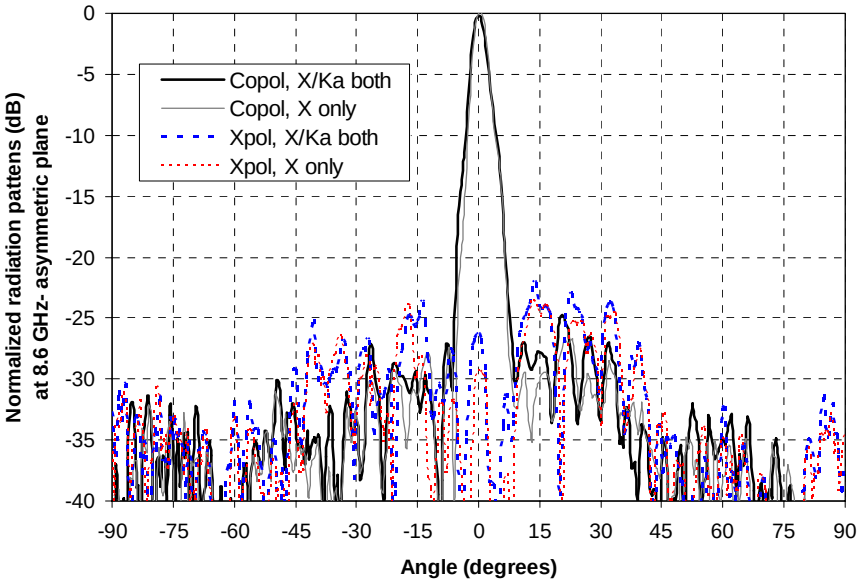

(d)

Fig. C1. Continued.

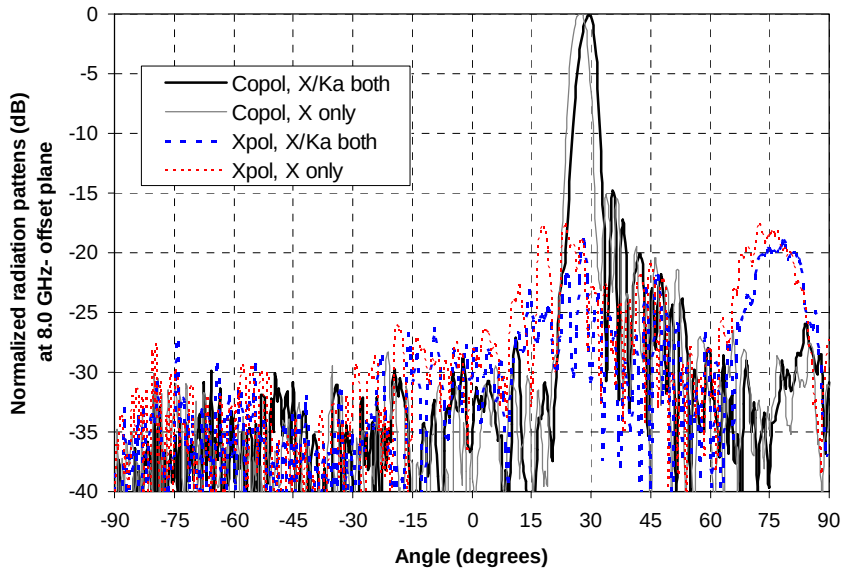

(a)

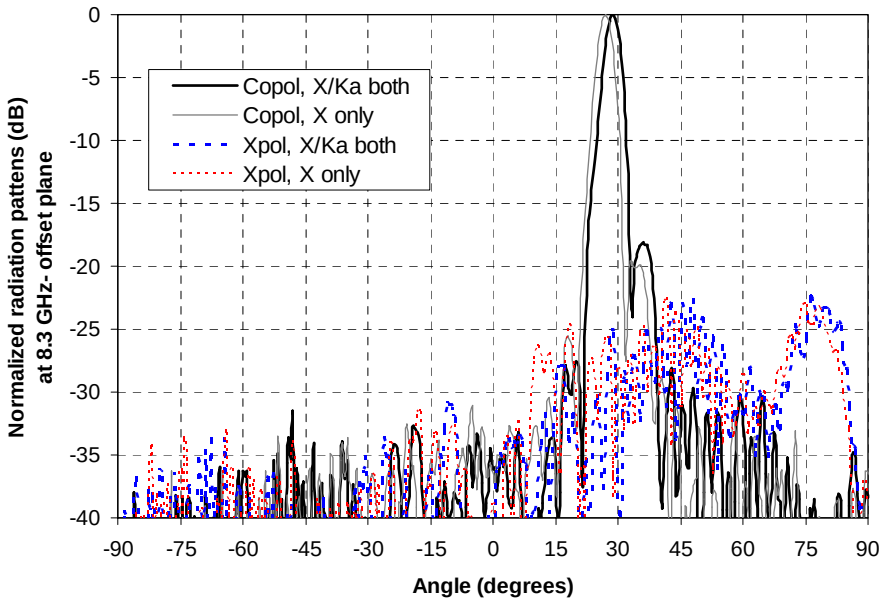

(b)

Fig. C2. Normalized radiation patterns (dB) in the offset plane at X-band: (a) 8.0 GHz; (b) 8.3 GHz; (c) 8.5 GHz; (d) 8.7 GHz.

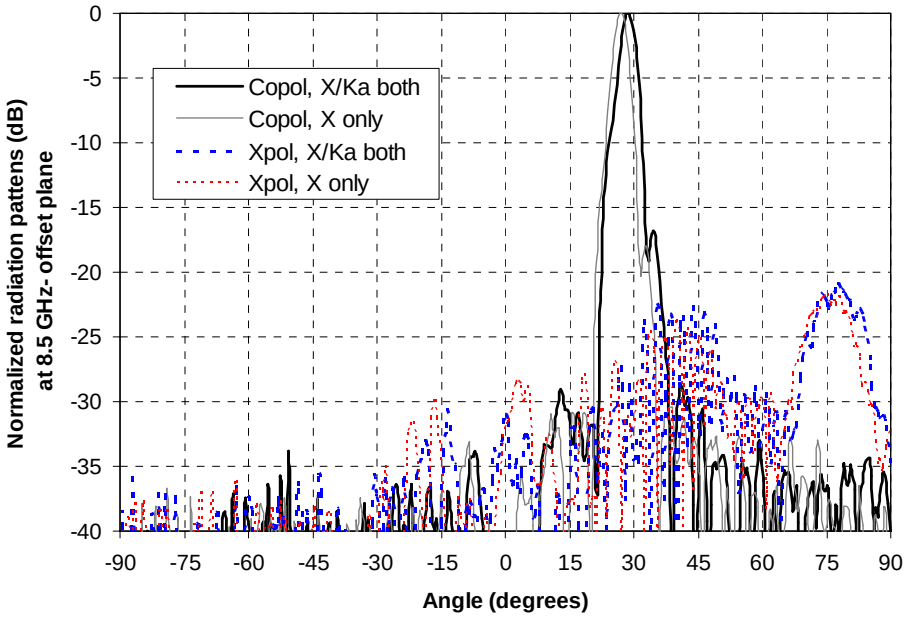

(c)

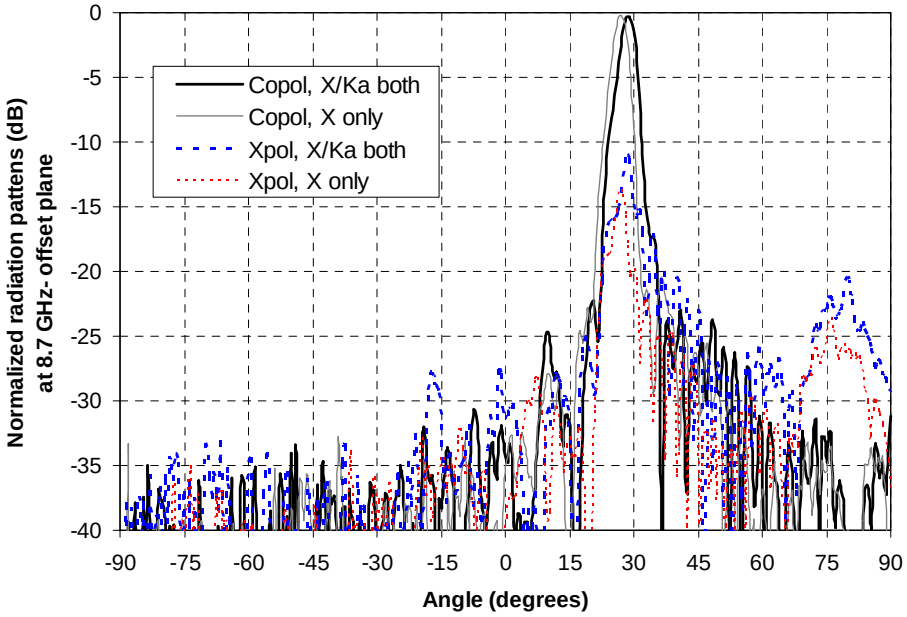

(d)

Fig. C2. Continued.

C2. Ka-band measurement results

Normalized radiation patterns in the plane of asymmetry are provided at 31 GHz, 31.4 GHz, 32 GHz, 32.6 GHz and 33 GHz with the corresponding cross-polarization patterns. Normalized radiation patterns in the offset plane (in the plane of symmetry) are provided at 31 GHz, 31.6 GHz, 32 GHz, 32.4 GHz and 33 GHz respectively.

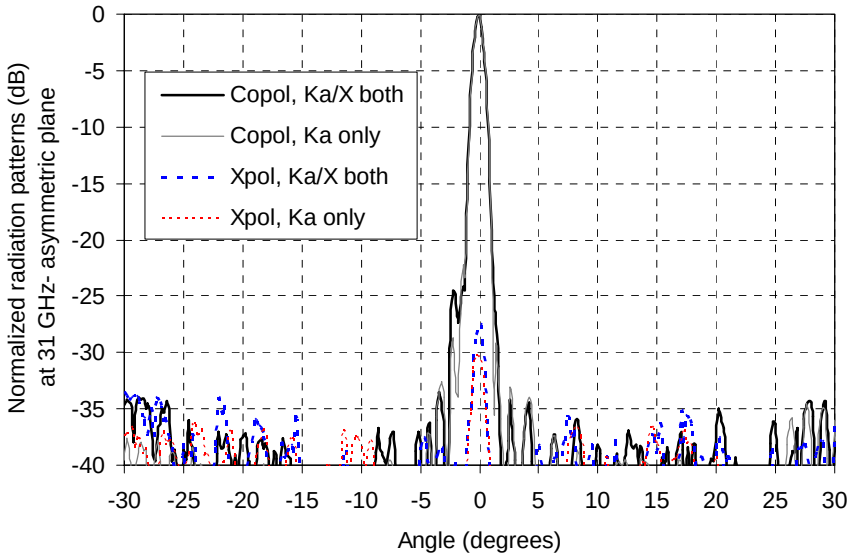

(a)

Fig. C3. Normalized radiation patterns (dB) in the asymmetric plane at Ka-band: (a) 31 GHz; (b) 31.4 GHz; (c) 32 GHz; (d) 32.6 GHz; (e) 33 GHz.

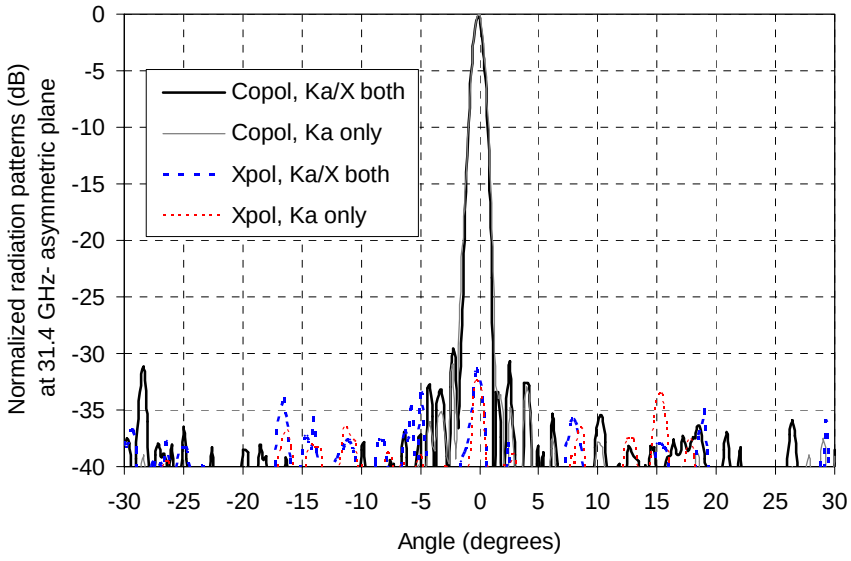

(b)

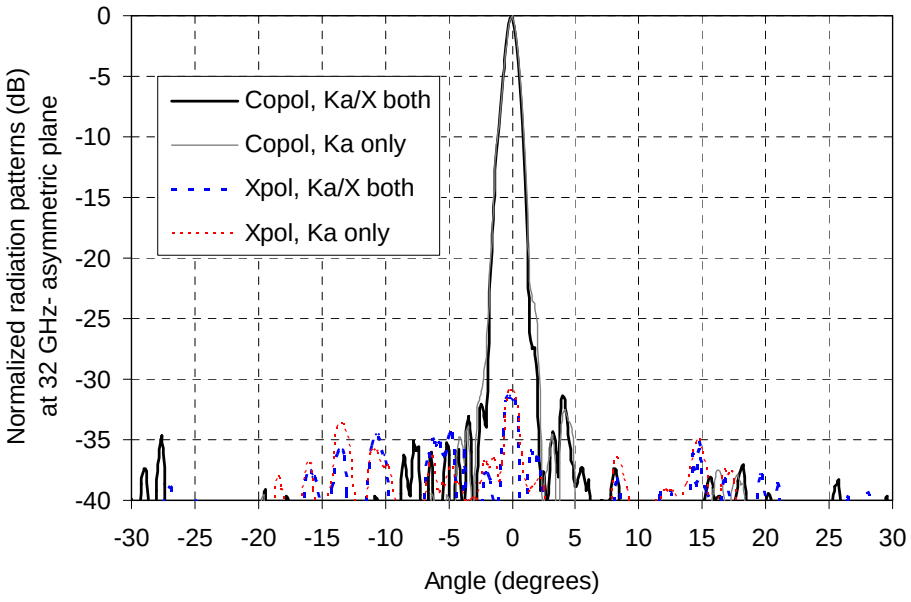

(c)

Fig. C3. Continued.

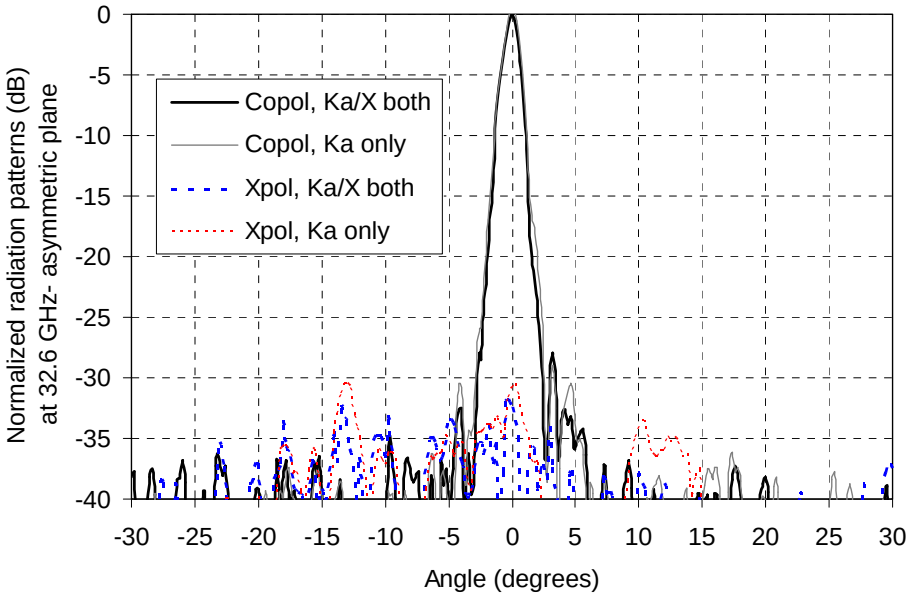

(d)

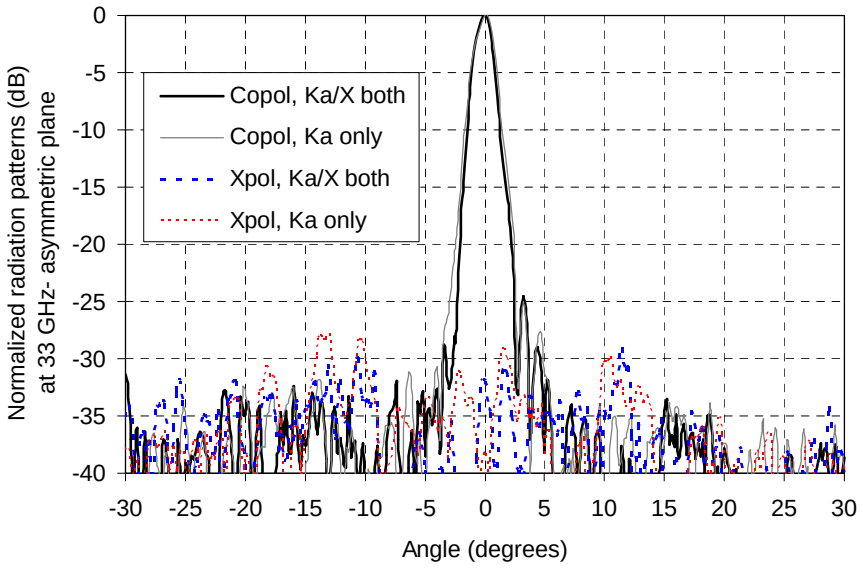

(e)

Fig. C3. Continued.

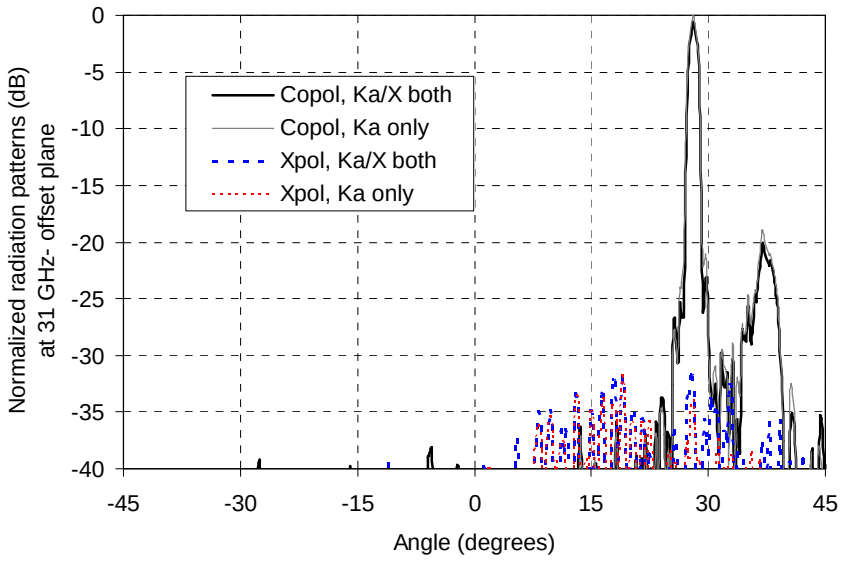

(a)

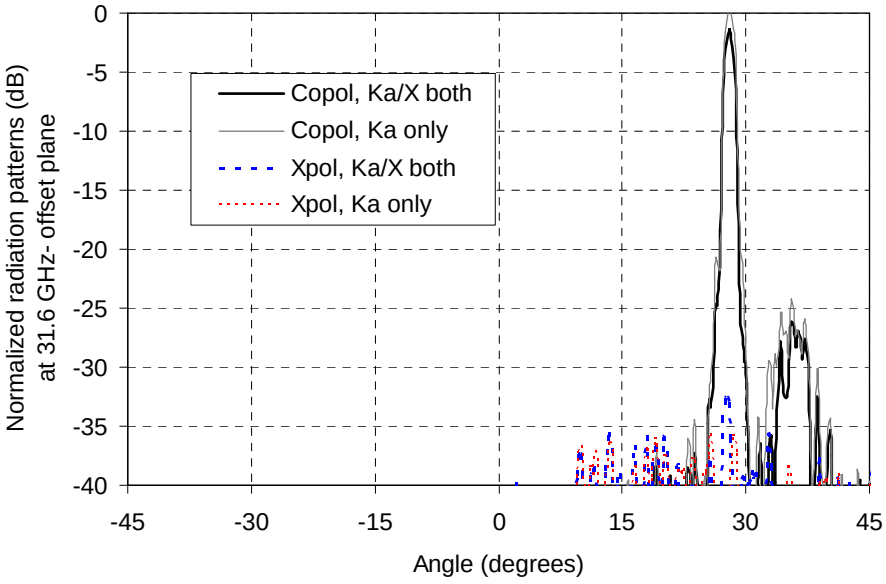

(b)

Fig. C4. Normalized radiation patterns (dB) in the offset plane at Ka-band: (a) 31 GHz; (b) 31.6 GHz; (c) 32 GHz; (d) 32.4 GHz; (e) 33 GHz.

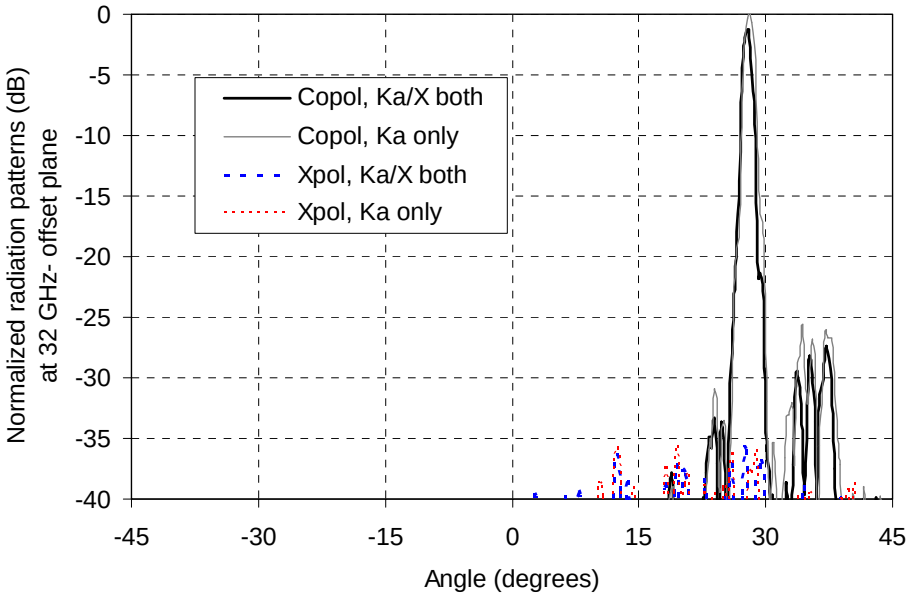

(c)

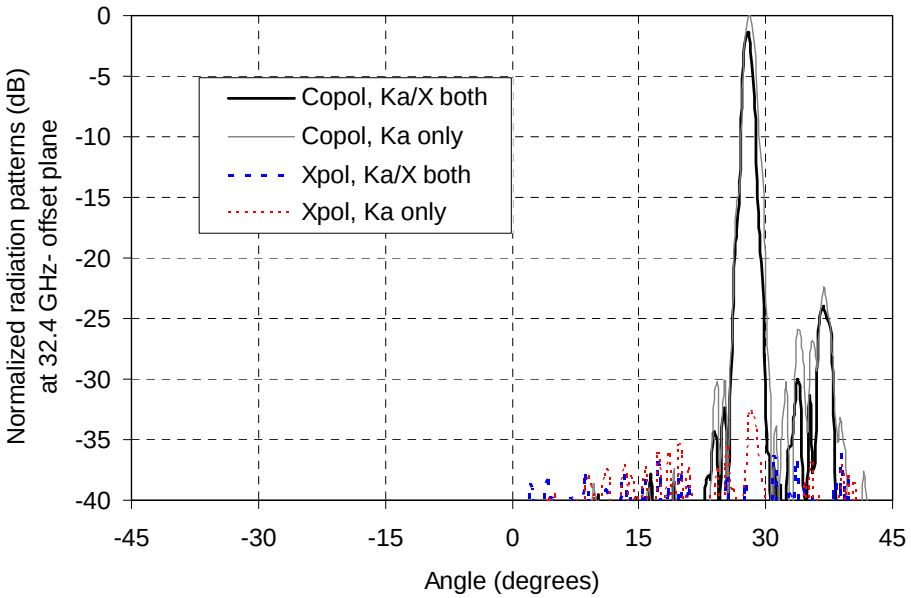

(d)

Fig. C4. Continued.

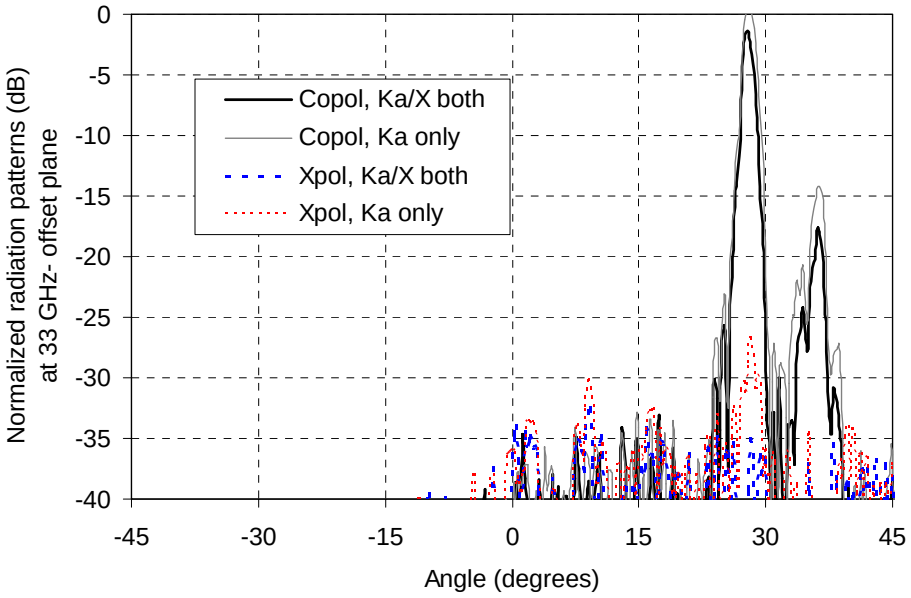

(e)

Fig. C4. Continued.

VITA

Chul Min Han was born in Jun-Ju, Republic of Korea on Jan. 18, 1972. He received his B.S. in electronics engineering from Korea University in Aug. 1997. In 2000, he started his Ph.D. degree in electrical engineering at Texas A&M University, College Station, Texas and was guided by Dr. Kai Chang in the Electromagnetics and Microwave Laboratory. He is a grateful recipient of the Ebens-berger Gaduate Fellowship in the Department of Electrical Engineering in 2005. During the summer months of 2001, he was employed by Mimix Broadband Inc. in Houston as an engineering intern working on active biasing circuits for microwave monolithic circuits. His graduate research projects have been supported by grants from the NASA Jet Propulsion Laboratory. He can be reached through Professor Kai Chang, Department of Electrical Engineering, Texas A&M University, College Station, TX 77843-3128.